Dissertations, Master's Theses and Master's Reports

2019

ESTIMATION OF MULTI-DIRECTIONAL ANKLE IMPEDANCE AS A FUNCTION OF LOWER EXTREMITY MUSCLE ACTIVATION

Lauren Knop
Michigan Technological University, lknop@mtu.edu

Recommended Citation

ESTIMATION OF MULTI-DIRECTIONAL ANKLE IMPEDANCE AS A FUNCTION OF LOWER EXTREMITY MUSCLE ACTIVATION

By

Lauren N. Knop

A DISSERTATION

Submitted in partial fulfillment of the requirements for the degree of

DOCTOR OF PHILOSOPHY

In Mechanical Engineering-Engineering Mechanics

MICHIGAN TECHNOLOGICAL UNIVERSITY

2019

© 2019 Lauren N. Knop

This dissertation has been approved in partial fulfillment of the requirements for the Degree of DOCTOR OF PHILOSOPHY in Mechanical Engineering-Engineering Mechanics.

Department of Mechanical Engineering – Engineering Mechanics

Dissertation Co-Advisor: *Mo Rastgaar*

Dissertation Co-Advisor: *Ye Sun*

Committee Member: *Nina Mahmoudian*

Committee Member: *Timothy Havens*

Department Chair: *William Predebon*

Table of Contents

List of figures

vii

List of tables

Preface

This work presents the exploration into the relationship between the mechanical impedance of the human ankle as a function of lower extremity muscle activation. The work was completed in the Human Interactive Robotics Laboratory at Michigan Technological University, under the advisement of Dr. Mo Rastgaar. In addition, the research presented was completed by the author in collaboration with Dr. Mo Rastgaar, Dr. Evandro Ficanha, Dr. Houman Dallali, Guilherme A. Ribeiro, and Leslie Castillo. All work was supported by the National Science Foundation, under grant numbers 1350154 and 1830460.

This dissertation is divided into five chapters. A summary of each chapter is shown below:

- Chapter 1. Provides an introduction and background information on established methods for estimating ankle impedance, using electromyography to understand muscle function, and implications for this work.

- Chapter 2. A novel method that applies Artificial Neural Networks (ANN) to relate the non-loaded, multi-directional ankle impedance to lower-leg muscle co-contraction levels in the DP, IE, and ML directions. The materials in this chapter were published in two journal articles in the *International Journal of Intelligent Robotics and Applications.*

- Chapter 3. The work presented expands upon the results from the previous chapter to explore the ankle impedance and muscle co-contraction activity during standing. The work in this chapter was presented in four conference publications; including the 1) *Design of Medical Devices (2018),* 2) *International Conference on NeuroRehabilitation (2018)*, 3) *7th IEEE International Conference on Biomedical Robotics and Biomechatronics (2018)*, and 4) *Design of Medical Devices (2019).*

- Chapter 4. The methods used in Chapter 2 and Chapter 3 are used to further explore the relationship between standing ankle impedance and muscle activity at varying levels of the center of pressure and ankle angle.

- Chapter 5. This final chapter summarizes the main conclusions and contributions of this work and describes future implications for modeling an EMG – ankle impedance relationship and applications in control of robotic medical devices

Acknowledgments

I cannot express enough how thankful I am for all of the people who have made an impact in my life and have helped to make this dream into a reality. This work would not have been made possible without your support. I would first like to express my deepest thanks to my advisor Dr. Mo Rastgaar, who has provided me the opportunity to work as a member of the lab, grow as a professional, attend numerous conferences, and provide guidance throughout my career.

I would also like to thank the following mentors who I have looked up to throughout my time as a student. You have taught me many technical, professional, and interpersonal skills that have helped build my confidence as an engineer. These people include Dr. Craig Friedrich, Dr. Nina Mahmoudian, Dr. Jason Blough, and Dr. Craig Goehler. You have all influenced my life in more ways than I can give credit for.

In addition, I am grateful to all of my colleagues and friends that I have had the pleasure of working with throughout the past four years. Many hours have been spent completing coursework projects, studying for exams, teaching and troubleshooting practice labs, running experimental tests, writing and presenting papers, and so much more! The community that we created and shared at Michigan Tech has helped to shape the person I am today, and is something I will forever cherish.

Last, this journey could not have been made possible without the love and support of my family and friends. I am so thankful for all of you. I especially want to thank my Mom, Dad, and my two siblings, Allison and Evan, for all the encouragement, support, and patience you have given me throughout the years. You've helped me to believe I can do anything I set my mind to.

List of abbreviations

DOF	Degree(s) of freedom
EMG	Electromyography
ADL	Activities of Daily Living
DP	Dorsiflexion – Plantarflexion
IE	Inversion – Eversion
ML	Medial – Lateral
ROM	Range of Motion
TA	Tibialis Anterior
PL	Peroneus Longus
SOL	Soleus
GAL	Gastrocnemius Lateral
GAM	Gastrocnemius Medial
MU	Motor Unit
MVC	Maximum Voluntary Contraction
VAF	Variance Accounted For
ANN	Artificial Neural Network
LTI	Linear, and Time Invariant
NMSE	Normalized Mean Squared Error
RMS	Root-Mean-Square
mse	Mean Squared Error
TD	Time Domain
MAV	Mean Absolute Value
ZC	Zero Crossings
SSC	Number of Slope Sign Changes
CL	Cumulative signal Length

Abstract

The purpose of this research is to investigate the relationship between the mechanical impedance of the human ankle and the corresponding lower extremity muscle activity. Three experimental studies were performed to measure the ankle impedance about multiple degrees of freedom (DOF), while the ankle was subjected to different loading conditions and different levels of muscle activity. The first study determined the non-loaded ankle impedance in the sagittal, frontal, and transverse anatomical planes while the ankle was suspended above the ground. The subjects actively co-contracted their agonist and antagonistic muscles to various levels, measured using electromyography (EMG). An Artificial Neural Network (ANN) was implemented to characterize the relationship between the EMG and non-loaded ankle impedance in 3-DOF. The next two studies determined the ankle impedance and muscle activity during standing, while the foot and ankle were subjected to ground perturbations in the sagittal and frontal planes. These studies investigate the performance of subject-dependent models, aggregated models, and the feasibility of a generic, subject-independent model to predict ankle impedance based on the muscle activity of any person. Several regression models, including Least Square, Support Vector Machine, Gaussian Process Regression, and ANN, and EMG feature extraction techniques were explored. The resulting subject-dependent and aggregated models were able to predict ankle impedance with reasonable accuracy. Furthermore, preliminary efforts toward a subject-independent model showed promising results for the design of an EMG-impedance model that can predict ankle impedance using new subjects. This work contributes to understanding the relationship between the lower extremity muscles and the mechanical impedance of the ankle in multiple DOF. Applications of this work could be used to improve user intent recognition for the control of active ankle-foot prostheses.

1 Introduction

1.1 Motivation

The role of the human ankle is imperative to performing tasks such as balance, gait, and other activities of daily living (ADLs) [1]. With the help of the muscles synergy of the lower leg, the ankle is capable of absorbing shock as the foot comes in contact with the ground, accelerating the body forward during locomotion, changing speed and direction during gait maneuvers, and maintaining a stable balance to prevent from falling. An able-bodied person has the ability to control their ankle angles and torques by contracting and relaxing the antagonistic and agonistic muscles of the lower leg, resulting in a desired ankle motion.

Unfortunately, many individuals are afflicted by a disability, such as lower-leg amputation, stroke, musculoskeletal diseases, or other neurological injuries, that has prevented normal ankle function. It is estimated that 2 million people in the United States have undergone limb amputation, resulting in approximately 185,000 amputations performed each year [2]. Roughly 60 - 70% (nearly 1.2 million people) of these amputations were performed on the lower-limb, with the majority being below-knee, transtibial amputation [3]. The leading causes of lower-limb amputations are due to diabetes mellitus and other diseases associated with it, such as peripheral vascular disease, cardiovascular disease, and obesity [3]–[5]. It is estimated that the number of amputations caused by these vascular diseases could double by the year 2050 [2]. Other reasons for lower-limb and transtibial amputation include, but are not limited to, traumatic accidents, cancer, and congenital limb defects [6], [7].

Consequently, lower-limb amputation has an immense impact on the quality of life, both physically and emotionally, because the individual has lost some degree of mobility to be able to perform ADLs. The use of conventional passive prostheses provides a simple and relatively low-cost solution to recover lost mobility; however, the amount of metabolic energy required by a transtibial amputee using a passive prosthesis increases up to 30% when compared to a healthy person walking at the same speed [8], [9]. Likewise, the preferred walking speed of the amputees are typically 30-40% slower than that of a non-amputee [4], [8]. Transtibial amputees usually have an altered gait strategy or compensatory mechanism to account for the loss of mobility and mechanical power at the ankle [10]–[14]. Often this leads to secondary musculoskeletal injuries,

such as chronic disorders of the lower back, hips, and knees on both the amputated and non-amputated limbs [15], [16].

Recent advancements in active lower extremity prostheses and assistive devices have demonstrated the ability to generate mechanical power during the push-off phase of gait, which is comparable to the power generated by the healthy ankle. Several state-of-the-art active prostheses, including both transtibial and transfemoral, have been designed, clinically tested, or have become commercially available within the past 20 years [17]–[21]. These prostheses can actuate the foot and knee joints to help restore power loss in the sagittal plane of motion; which is something that is advantageous during the push-off phase of straight walk, ascending or descending stairs, or walking up and down a sloped surface [22]–[25]. In fact, one study showed that the use of a single-degree-of-freedom (DOF) active prosthesis decreased metabolic cost during straight, level walking by approximately 14% when compared to a traditional passive prosthesis [26].

However, the ankle range of motion (ROM) is not limited to rotations only in the sagittal plane. The ankle modulates about multiple degrees of freedom during ADLs [27]–[29]. Active transtibial prostheses that are capable of generating motion in the frontal and transverse planes are currently being researched and can contribute to a more natural ankle function. Ficanha et al. developed a 2-DOF active prosthesis that is actuated in the sagittal and frontal planes, corresponding to ankle motion in dorsi-plantarflexion (DP) and inversion-eversion (IE), respectively [30], [31]. In addition, Olson and Klute designed a transtibial prosthesis with active control in the transverse plane, corresponding to medial-lateral (ML) ankle rotation (also referred to as External-Internal rotation), to aid turning steps and reducing shear stress acting on the socket during locomotion [32]. The ability to actuate multiple DOF may better resemble the biomechanical features of the ankle, when compared to the single-DOF active designs, and can facilitate turning maneuvers or walking on uneven ground.

While the mechanical design and development of active ankle-foot prostheses can provide substantial benefits to an amputee during ADLs, there are still many obstacles regarding how to control the device to include the biomimetic properties of a healthy ankle and how these devices interface with the user's motion intentions [9], [14]. Understanding how the human ankle functions via an individual's neuromuscular system is necessary for addressing these challenges. One

technique used to quantify ankle dynamics is the study of the mechanical impedance of the ankle. This property can be defined mathematically as a transfer function relating the ankle reaction torque to an input ankle perturbation, and has been shown to resemble a linear, second-order system [33]. By quantifying the ankle impedance parameters, we can improve the design and control of ankle-foot prostheses.

This chapter includes the following: Section 1.2 describes the anatomy and function of the ankle, including the ankle axes of rotation and the surrounding muscles. Next, Section 1.3, Section 1.4, and Section 1.5 provide a description of previous work that quantified the mechanical impedance of the ankle during non-loaded, standing, and walking scenarios. Section 1.6 explains the use of electromyography (EMG) to study muscle activity. Lastly, Section 1.7 describes the applications of EMG for user intent recognition in prostheses control.

1.2 Human Ankle Behavior

The dynamic capabilities of the human ankle and the corresponding neural control and muscle activity have been widely studied within the fields of engineering and kinesiology. Understanding the kinematic, kinetic, and musculoskeletal information of the ankle provides essential information for improving the design of several medical devices; including passive and powered ankle-foot prostheses, exoskeletons, orthoses, and other assistive devices. The following section explains the ankle anatomy and the function of the musculoskeletal system surrounding the ankle.

The ankle joint complex is comprised of the talocrural, subtalar, and talocalcaneonavicular joints that are interconnected by a variety of tendons and ligaments and are actuated by surrounding muscles [1]. The geometry and orientation of each joint create oblique axes of rotation, which allow the ankle to rotate in multiple directions. The combined function of these joints provide stability and allow for motion in the sagittal, frontal, and transverse anatomical planes, shown in Figure 1-1. The subtalar joint is the largest of the three joints and allows for the majority of the ankle motion in inversion-eversion (IE) [1], [34]. The primary role of the talocrural joint contributes to movement in dorsiflexion and plantarflexion (DP) and, because of its unique geometry, also provides stability to motion in eversion [1], [34]. Lastly, the talocalcaneonavicular, which shares the same axes of rotation with the subtalar joint, also contributes to inversion and

15

eversion (IE) rotation of the ankle. Medial-lateral (ML) motion in the transverse plane is generated from a combination of rotation axes about the talocrural and subtalar joints [34], [35].
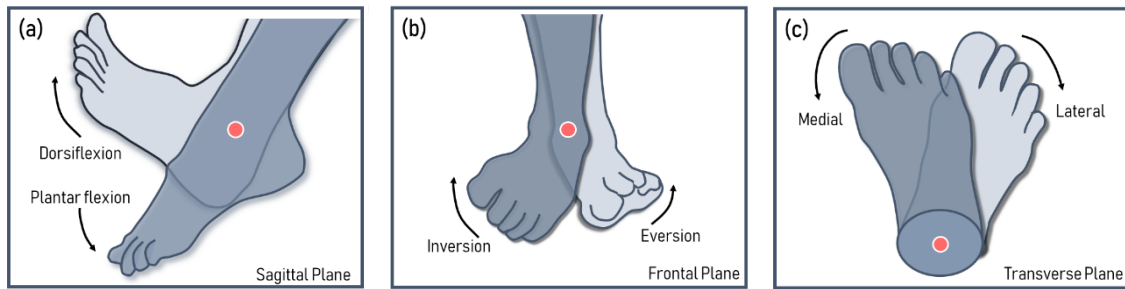
Figure 1-1. Foot and ankle rotation schematic in the sagittal, frontal, and transverse planes. (a) Ankle rotation in dorsi-plantarflexion (DP), (b) Ankle rotation in inversion-eversion (IE), and (c) Ankle rotation in the medial-lateral (ML) directions. The red circle denotes the ankle center of rotation.

The lower-leg muscles are used to control ankle motion in DP, IE, and ML directions [1]. Five of the 13 muscles in the lower leg are referenced throughout this paper due to their contribution to ankle motion and superficial location. These muscles include: 1) Tibialis Anterior (TA), which contributes to movement in dorsiflexion and inversion of the foot; 2) Peroneus Longus (PL), which contributes to plantarflexion and eversion of the foot; and the 3) Soleus (SOL) and 4) Gastrocnemius Medial (GAM) and Lateral (GAL), which all contribute to plantarflexion [36], [37]. Majority of the research to study the ankle and muscle contribution to ankle motion has focused on DP rotation; however, quantifying the ankle dynamics in DP, IE, and ML is essential be better understand the interdependence of ankle dynamics.

1.3 Non-loaded Ankle Impedance

Early work by Hunter and Kearney [38], [39] and Weiss et al. [40]–[42] quantified the passive and active ankle impedance in the DP direction using a stochastic system identification approach. To estimate the impedance parameters, they applied perturbations to the ankle and measured the resulting reaction torques and muscle activity of the TA and GA muscles. A notable conclusion drawn from these works was that the impedance parameters increased as the mean ankle torque and muscle activity increased, regardless of the ankle angle [38], [41], [42]. The stiffness and mean ankle torque are dependent on the size of the ankle perturbation and decreased as the amplitude of the angular perturbation increased [39]. Additionally, the damping and stiffness increased as the

ankle was rotated away from its neutral angle; resulting in the maximum impedance at the limits of the DP range of motion [40], [42]. Lastly, the inertia remained relatively constant across all experiments.

As a continuation of these studies, it was determined that the total impedance is equal to the summation of the intrinsic response of the muscles and tendons and the reflexive response of the neuromuscular system, as measured by Sinkjaer [43] and Kearney [44]–[46]. The reflex contribution to ankle torque was determined to have a transport delay of approximately 40-50 ms from the start of the muscle stretch due to a perturbation. The resulting reflex ankle impedance values were described using more complex dynamics, where the parameters were dependent on the velocity, amplitude, and contraction level of the stretch perturbation; while the intrinsic ankle impedance parameters more closely resembled a linear, second-order system. Together, the intrinsic and reflexive components are used to describe the total ankle impedance [44]. While many studies have separated the intrinsic and reflexive components of the impedance, the work presented in this dissertation studied the total impedance, without dividing it into two parts.

Furthermore, the multi-variable ankle impedance was determined with passive and active muscle activity in DP, IE, and ML while the ankle was not loaded [47]–[54]. Anklebot, a wearable robotic device designed for stroke rehabilitation, was repurposed to estimate the multi-variable ankle impedance. This device is composed of two hydraulic linear actuators that apply stochastic perturbations to the foot. Depending on the orientation of the actuators, ankle motion was generated in the sagittal, frontal, or transverse planes and the resulting ankle torque and angle due to perturbations were measured. The ankle impedance was determined during static and dynamic perturbation conditions while subjects were seated with their ankle and foot raised above the ground, as described in the following paragraphs.

Using the Anklebot, the ankle impedance in DP and IE were determined simultaneously by applying perturbations in both the sagittal and frontals planes. The Anklebot actuators were placed parallel the shin of the subject and were actuated in phase or out of phase with one another to generate a torque DP and IE, respectively. Using quasi-static perturbations in the sagittal and frontal planes, the multi-variable static ankle impedance was determined while muscles were completely relaxed [47]. It was determined that the ankle torque-angle relation is direction-dependent, showing higher impedance in the sagittal plane than in the frontal plane. This study

17

was repeated while the lower-extremity muscles were co-contracted, and the resulting static impedance increased with muscle activity [48]. Expanding upon the quasi-static experiments, the dynamic ankle impedance was measured using a stochastic frequency-domain system identification methods for both relaxed and actively contracted muscles [49], [50]. These studies determined that the ankle impedance was greater in DP than IE, and both directions increased when muscles were actively contracted.

To study the ankle impedance in ML, Anklebot was perpendicular to the shin so that it generated motion in the frontal plane [51], [52]. Similar to the DP/IE experiments, the subjects were in a seated position with their foot suspended above the ground and leg fixed in place. Quasi-static and stochastic perturbations were applied to the ankle in the ML direction, and the ankle angles and torques were measured. The resulting impedance also showed behavior that closely resembled a linear, second-order system and was slightly smaller than the ankle impedance parameters determined for DP and IE directions.

1.4   Standing Ankle Impedance

Next, the mechanical impedance of the ankle during quiet standing has been investigated in DP and IE directions. These works contribute to understanding the ankle mechanisms used to maintain an upright balance. Early work focused on determining the critical stiffness of the ankle, which is the stiffness required to maintain a stable upright posture and is based on a 'human inverted pendulum' model [55], [56]. The ankle stiffness was determined by measuring the ankle angles and torques resulting from either the small perturbation due to the sway of the body's center of mass (COM) or by small external perturbations applied to the ankle in the DP direction [55]–[59]. These works determined that the intrinsic ankle stiffness (due to inherent properties of the muscle, tendon, and other tissues surrounding the ankle) is not enough to maintain a stable balance and additional contributions from surrounding neuromuscular modulation are required [60]–[65].

Furthermore, the intrinsic ankle impedance was also studied as a function of the body's natural sway using the center of pressure (COP) in the DP direction. Sakanaka et al. asked subjects to consciously shift their COP forwards or backward by modulating their ankle torque against a force plate while standing with parallel feet [66]. It was determined that intrinsic ankle impedance

significantly changed when the COP moved forward or behind the neural COP position. Similarly, the muscular activity of the TA and GA muscles changed depending on the location of the person's COP. Similar results were presented by Kearney et al., who found that the intrinsic impedance and GA muscle activity increased as the subject's COP moved forward during standing sway [67].

The influence of ankle stiffness and impedance in the IE direction has been studied, mainly to understand how a person maintains a stable balance during standing. The study of this DOF is essential because it has the most number of reported ankle injuries due to lack of stability [68], [69]. Zinder et al. quantified the ankle stiffness in IE by applying perturbations with a swaying cradle device [68]. Additionally, other studies found that ankle stiffness increased when the ankle was inverted or everted (IE) using a wedged platform [70], [71].

To estimate impedance in both DP and IE, Ficanha et al. developed a 2-DOF instrumented platform [72]–[75]. This platform consisted of two linear actuators connected to a force plate module via Bowden cables and surrounded by a motion capture camera system. The actuators applied a torque perturbation to the subject's foot in both DP and IE. The resulting ankle rotations and torques were measured, and a variety of system identification methods have been developed to estimate the ankle impedance [72], [75], [76]. Similar to the non-loaded impedance, the stiffness and damping parameters were more significant in the sagittal plane than in the frontal plane during standing.

1.5 Time-Varying Ankle Impedance during Gait

Last, the study of the ankle mechanical impedance was analyzed during walking scenarios. The gait cycle is divided into the stance phase, which includes heel-strike, mid-stance, terminal-stance, and toe-off, and the swing phase, which includes initial swing, mid-swing, and terminal swing. A few groups have looked to quantify how the impedance modulates throughout the stance and swing phases of the gait cycle during straight walk and turning maneuvers. Initial work by Lee et al. quantified the impedance during the swing phase with the use of the Anklebot and found that the stiffness and damping in both DP and IE increased just before heel-strike and decreased around the toe-off and initial swing stages [77]. During the stance phase, various vibrating platforms were used to perturb the ankle and estimate the ankle impedance [78]–[82]. Rouse et al. determined that impedance in DP increased linearly between 20% - 70% of the stance phase

[78]. Using the 2-DOF instrumented platform described in the previous section, Ficanha et al. estimated the time-varying impedance in both the sagittal and frontal planes during the stance phase of straight walk and a turning maneuver [72], [80], [81], [83]. Similar changes in the ankle impedance were found throughout the gait cycle in both DP and IE directions. Additionally, there were notable differences in the stiffness and damping when comparing the straight walk and turning steps. These works provide a characterization of how the impedance changes throughout the gait cycle and provide the foundation for improving the control of active ankle-foot prostheses during ADLs.

1.6 Electromyography and Joint Dynamics

In addition to studying the mechanical impedance of the ankle, it is also essential to understand how the lower extremity muscle signals reflect the mechanisms surrounding the ankle. Electromyography has been studied for more than a century. Much of the research has focused on either 1) explaining the underlying structure and neuromuscular properties that cause the muscle to flex and extend, or 2) studying ways to utilize the muscle signals, such as in movement analysis, disease diagnoses, ergonomics, rehabilitation, and for use in the control of prostheses, exoskeletons and other orthopedic devices [84]. The work presented in this paper focuses on the latter.

It is common to describe a muscle as a collection of motor units (MU), which are composed of motor neurons connected to the spinal cord and the corresponding muscle fibers. The MUs are considered the smallest functional unit within a muscle that allows for its contraction [85]. The number of MUs found in a muscle is dependent on its size, and the amount of force the muscle can generate [86]. Early work determined that as the number of recruited MUs increased, there were also increasing trends in the resulting EMG signal amplitude, power spectrum, mean frequency, and generated force by the muscle [87], [88]. One study showed that as subjects increased their biceps muscle contraction level from rest to 80% of the Maximum Voluntary Contraction (MVC) the EMG amplitude and mean power frequency significantly increased, supporting the idea that EMG signals can provide information about the relative change in muscle force generation [87]. Furthermore, the effects of muscle fatigue, individual muscle fiber potential, and muscle synergies have also been shown to impact the EMG signal measurement [89]–[91].

The relationship between the muscle activation amplitude and the corresponding muscle force and joint torques has been widely studied. Both invasive and non-invasive techniques are used to understand how muscle force relates to musculoskeletal loading and joint dynamics. Preliminary work predicted the muscle forces generated by the biceps brachii (elbow flexion) and triceps brachii (elbow extension) using surface EMG measurements during isometric, static contractions [85], [92]–[94]. Similarly, EMG signals were used to model the relationship between the upper extremity muscles activity and the corresponding joint kinematics and kinetics. Numerous studies have developed linear and nonlinear models to relate surface EMG signals to the torques and positions of the elbow [95]–[98], wrist [99]–[101], and fingers [102]. In a similar way, models relating the lower extremity muscle activity to the ankle kinematics and kinetics have also been studied; however, not as extensively as the upper extremity. Early work determined the relationship between EMG and ankle torque using a second-order least-squares fit [103], [104]. More recent work developed a model using wavelet neural networks to predict ankle torque during walking when provided with the EMG and ground impact force information [105].

Less commonly, understanding the neuromuscular activity as a function of joint impedance has been studied. This idea differs from the relationship between EMG and joint torque because, unlike from the torque modulation, the impedance can be modulated by co-contracting the muscles surrounding the joint [106]. Recent work by Dai et al. developed a model to relate EMG of the biceps and triceps muscles to the corresponding impedance of the elbow across a range of joint torques [106]. In addition, the ankle impedance and corresponding muscle contraction of the lower extremity muscles has been studied. Early work used stochastic system identification methods to determine the ankle impedance in DP over a range of muscle contraction level from resting to MVC [38], [39]. These studies used linear regression to fit the ankle stiffness and damping properties to EMG as the mean ankle torque increased. The linear regression showed correlation values ranging between 0.39 and 0.99 across five subjects [38]. More recent work implemented nonlinear models to relate the isometric contraction of the ankle plantar flexor muscles and non-parametric ankle impedance while subjects were lying in a supine position [107]. The models were able to determine the intrinsic and reflexive contributions of the muscle between 0% and 40% MVC and could predict ankle torque based on EMG with 92 ± 3% variance accounted for (VAF) across five subjects.

The relationship between EMG and ankle impedance provides a new perspective in understanding the function of the human neuromuscular system. However, the relationship between EMG and ankle impedance has only been quantified in the DP direction during non-loaded activities, while subjects were either lying flat on their back or placed in a seated position. Likewise, the muscle activation measurements were typically from isometric contractions of a single muscle. Little work has been done to explore the relationship between ankle impedance and muscle co-contractions of the agonistic and antagonistic muscles surrounding the ankle, especially during weight-bearing activities such as standing and walking. To address some of these gaps, the work presented in this paper explored the development of EMG-impedance models that can predict ankle impedance in DP, IE, and ML directions [108], [109]. Additionally, these models use predictors from multiple muscles of the lower extremity, as opposed to a single muscle, and examine both non-loaded and various standing scenarios [110], [111]. Lastly, implications toward a generalized model that can predict ankle impedance from any subject were tested [111].

1.7 User Intent Recognition

To further enhance the control of active prostheses, the prostheses must generate the necessary power at the correct time and be able to adapt to the user's motion intentions. Classification, pattern recognition, regression, and other machine learning techniques have demonstrated the ability to transform EMG measurements into a functional signal to control prostheses [112]–[114]. Tucker et al. divided these control methods into two generalized groups; including (1) activity mode recognition, which identifies finite behavioral states, such as walking or going upstairs, that are used to control discrete events, and (2) direct volitional control, where the user can freely modulate the kinematics or kinetics of the prosthetic device [9]. The main goal for active prostheses control is to use a combination of the activity mode recognition and volitional control; such that the device can observe the user's motion intention, and respond accordingly in a way that mirrors the motion of a healthy, intact limb. The information from EMG signals has the potential to improve prostheses control based on a user's intentions [115]. The following section includes an overview of these techniques for the control of upper and lower extremity active prostheses.

Activity mode recognition uses techniques such as classification and pattern recognition to detect a specific, discrete event in time. These techniques have been widely used to classify joint motion and in prostheses control, especially for powered upper extremity prostheses. Numerous studies have used pattern recognitions techniques to classify movement of the elbow, wrist, and thumbs to control prostheses [116]–[118]. Furthermore, a surgical procedure called targeted muscle reinnervation (TMR) has been used to improve the EMG signal measurements of upper extremity amputees [119], [120]. The resulting EMG signals after TMR surgery has shown to improve the classification accuracy of shoulder, elbow, wrist, or hand motions, which can be used to enhance the control of powered prostheses.

Furthermore, pattern recognition and classification techniques have also been used for the control of lower extremity prostheses, specifically during locomotion. Huang et al. used EMG and pattern recognition to identify seven different locomotion modes throughout the gait cycle, including level walking, avoiding an obstacle, stair ascent, and descent, turning, and standing [121]. The classification accuracy ranged between 75% - 100%, depending on the task performed. Other studies have looked to use lower extremity EMG to classify ramp ascent and descent, and terrain identification during walking for above-knee amputees [122]–[124]. However, for these techniques to be used in practical applications, the classification error and update time needs to be improved in order to create safe prostheses.

Volitional and proportional control techniques of prosthetic devices using surface EMG have been studied since the 1960s [112]. In some cases, these methods of control have shown to perform better than pattern recognition counterparts [125]. Wang et al. used proportional control to activate the DP motion of an active ankle-foot prosthesis using the residual muscle of an amputee [126]. In this study, the amputee was able to control the push-off angle and the prostheses power generation at varying speeds of walking by modulating the EMG activity of their calf muscle. Other related work has implemented proportional control using EMG to control a powered ankle-foot orthosis and additional types of active prostheses [25], [127], [128].

Some volitional control techniques have utilized complex musculoskeletal dynamic models to relate the muscle signal information to the desired prosthesis motion [129]. These models often make many assumptions about the muscle's dynamic properties. To avoid the need for a complex dynamic model of the system, linear and nonlinear regression models have also been studied for

prostheses control. Smith et al. used linear regression to improve the volitional control for upper extremity hand and wrist prosthesis [130]–[132]. These studies determined that a combination of linear and nonlinear regression methods can improve the control of wrist motion in a single-DOF, as well as multiple-DOFs simultaneously.

This chapter reviews the current methods used to quantify the multivariable mechanical impedance of the healthy human ankle in the sagittal, frontal, and transverse planes and how it is related to muscle function. The use of surface EMG has potential to predict the ankle torque and impedance requirements for a given locomotion task. Limited work has been done to explore lower extremity muscle activity as a function of ankle impedance. The purpose of the work described in this dissertation is to investigate the relationship between the mechanical impedance of the human ankle in multiple DOF based on lower extremity muscle activity during non-weight bearing and weight-bearing ADLs.

2 Relationship between Muscle Co-Contraction and Unloaded Ankle Impedance in three Degrees-of-Freedom

2.1 Motivation

This chapter describes the non-loaded ankle impedance in DP, IE, and ML directions as a function of increasing levels of muscle co-contraction. Previous work used the wearable rehabilitation robot called Anklebot to characterize the mechanical impedance of the ankle during quasi-static and dynamic conditions while subjects were seated and their leg was suspended above the ground [47]–[50], [52], [53]. The resulting impedance was defined as a function of the ankle angle and torque due to an applied input perturbation. Frequency domain analysis techniques were used to quantify the impedance, which closely resembled the response of a second-order dynamic system for all three directions. In addition, these works investigated the influence of increased levels of lower extremity muscle activity on the impedance parameters in the DP and IE directions. The experimental results showed that the stiffness and damping parameters of the ankle impedance increased with muscle activity. The relationship between muscle activation of the TA and SOL muscles with the corresponding ankle impedance could be described using two separate linear models, with R^2 values close to one for some subjects [50]. However, this was not the case for all subjects. Other subjects from these trials exhibited relationships that could not be described using linear regression; suggesting that modeling techniques to account for nonlinear dynamics and the effects of more than two of the lower-extremity muscles should be explored.

This chapter examines the influence of using artificial neural networks (ANN) to account for both linear and nonlinear models of ankle dynamics. There are four sections: Section 2.2 provides an overview of the Anklebot, used for experiments in DP, IE, and ML, Section 2.3 describes the characterization of ankle impedance in DP and IE as a function varied muscle activation levels using ANN, and Section 2.4 expands upon the process to create a model for the ML DOF. To our knowledge, the ankle impedance in ML as a function of muscle activity has not been studied previously. Last, Section 2.5 includes concluding remarks from both experimental studies. This work is important in understanding the ankle dynamics, and has the potential to be used for rehabilitation, injury prevention, and the improved control of ankle-foot prostheses. The results presented in this chapter have been published previously [109],[108].

2.2 Anklebot Description

An in-depth description of the Anklebot mechanical design specifications is described in Roy et al [133]. As shown in Figure 2-1, the orientation of Anklebot was placed either parallel to the subject's shin (DP/IE) or perpendicular to the shin (ML). Anklebot is designed with two, back-drivable linear actuators that are positioned nearly-parallel to each other. The ends of each actuator are fixed to a custom shoe bracket, on both sides of the ankle, and the weight of the device is suspended by a custom knee brace, supporting straps, and a frame. With the Anklebot orientation in Figure 2-1a, a DP torque was produced when the actuators moved in the same directions, and an IE torque was produced when the actuators moved in opposite directions. To generate torque in ML, Anklebot was placed parallel to the ground (Figure 2-1b), and the actuators moved in different directions with equal amplitudes.
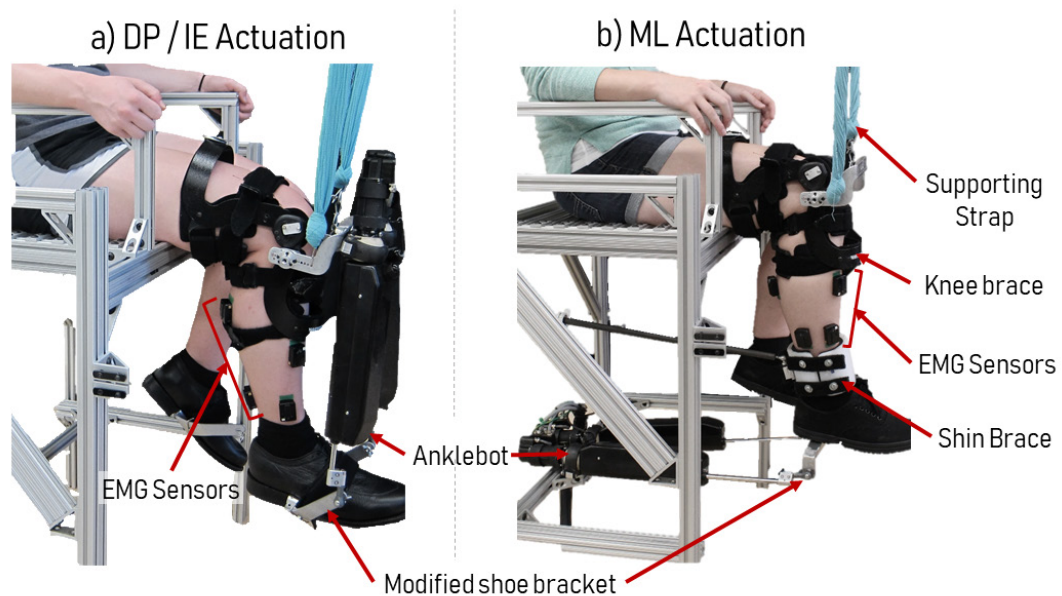
Figure 2-1 Experimental setup, including Anklebot and EMG sensor placement, to estimate ankle impedance in a) DP/IE and b) ML directions.

The maximum torques capable of being generated in DP, IE, and ML were 23 Nm, 15 Nm, and 15 Nm, respectively. The root-mean-squared (RMS) of the angles during the experiment were 2.48°, 2.70°, and 3.72° for DP, IE, and ML, respectively. In addition, the motor torques and actuator positions were measured with current sensors (Burr-Brown 1NA117P) and linear encoders (Reinshaw), respectively. The resolution of the torque measurements are 2.59 x 10^{-6} Nm, and the linear encoders have a resolution of 5x10^{-6} m.

To prevent the displacement of the actuators from drifting, an active impedance control was used with an active stiffness gain of 10 Nm/rad and 12.8 Nm/rad for the DP/IE and ML tests, respectively, and zero damping for all tests. At the beginning of an experiment, the ankle angle was placed such that the foot and shank formed approximately 90°, and the neutral position for each actuator was defined. The controller gains were determined previously through trial and error so that the ankle remained within the neutral position for the duration of the experiment [51], [53]. During the ML experiments, a shin brace (Figure 2-1b) was also used to prevent the knee from translating in the transverse plane.

2.3 DP/IE Experiment

All subjects had no previously reported musculoskeletal injury to the ankle and gave written consent of participation through the Michigan Technological University Institutional Review Board. The following biometric information for all subjects is presented in Table 2-1.

Table 2-1. Subject biometric information for DP/IE Anklebot experiments

Gender	Age*	Mass (kg)*	Height (cm)*
9 males	24.4 ± 1.1	74.1 ± 16.7	174.7 ± 8.2

* mean ± standard deviation across population

2.3.1 Procedure

First, EMG sensors (Delsys Trigno Wireless System) were placed on the TA, PL, SOL, and GAL muscles to measure muscle activity and provide visual feedback of the subject's EMG signal from the TA muscle during the test, as shown in Figure 2-1a. Before placing the sensors, the skin was cleaned with rubbing alcohol, and excess hair was removed. All EMG signals were sampled at 1925 Hz, and the Delsys software used motion artifact suppression to reduce the effects of low frequency noise throughout the experiment. The first step during the experiment was to determine the subject's maximum voluntary contraction (MVC). The subjects were instructed to co-contract all four muscles to their maximum level without moving the ankle, and the highest voltages were determined. The maximum voltage of the TA muscle was recorded and used as a reference for the remainder of the experiment.

The experimental procedure for ankle impedance estimation was similar to the methods used in [50]. Anklebot applied pseudo-random torque perturbations to the ankle for 70 seconds

with a frequency bandwidth up to 100 Hz. As the perturbations were applied, the ankle reaction torques and angles were recorded with a sampling rate of 200 Hz. There were a total of 15 trials, where the subjects controlled their muscles to be relaxed or maintained at a constant muscle co-contraction of 10% MVC or 20% MVC for the duration of the trial. Each activation level was repeated five times. Real-time visual feedback of the TA EMG signal and the desired voltage level were provided so that the subject could adjust their activation level accordingly. Afterward, the initial 10 seconds of data were removed to reduce the transient effects present at the beginning of each trial.

2.3.2 System Identification of DP/IE Ankle Impedance

The previously proposed method of stochastic system identification was used to estimate the ankle impedance in [49], [50], [53]. First, the mechanical admittance of the ankle (defined as Y) is described as the ratio between the measured output rotational angles, Θ, and the applied input torque, T. This can be expressed in the frequency domain (f) as:

$$\Theta = Y(f)\text{T}. \qquad\qquad 2.1$$

Assuming that the perturbations generated a small ankle angle and the system was linear and time-invariant (LTI), the mechanical impedance is calculated as the inverse of the mechanical admittance:

$$\text{T} = Y^{-1}(f)\Theta = Z(f)\Theta \qquad\qquad 2.2$$

where Z denotes the ankle impedance. Because the Anklebot excited the ankle in the DP and IE DOF simultaneously, a matrix is defined to relate the input ankles and output torques in DP, IE, and any coupling between the two DOF. The following matrix is used to describe the impedance calculation:

$$\begin{bmatrix} \text{T}_{DP} \\ \text{T}_{IE} \end{bmatrix} = \begin{bmatrix} Z_{DP}(f) & Z_{DP,IE}(f) \\ Z_{IE,DP}(f) & Z_{IE}(f) \end{bmatrix} \begin{bmatrix} \Theta_{DP} \\ \Theta_{IE} \end{bmatrix} \qquad\qquad 2.3$$

where the torque and ankle measurements in DP and IE are T_{DP}, T_{IE}, Θ_{DP}, and Θ_{IE}, in the frequency domain, respectively. When solving for Z, the influence of the Anklebot impedance controller must be removed from the estimate. Because the human ankle and the Anklebot form a closed-loop system, the active control stiffness can be subtracted from the total impedance. The resulting impedance is equivalent to:

$$Z_i(f) = \frac{\mathrm{T}_i(f)}{\Theta_i(f)} - k_i \qquad\qquad 2.4$$

where the controller stiffness k is defined as a diagonal gain matrix of the Anklebot controller, where $i = \{DP, IE\}$. The resulting impedance can be substituted Eq. 2.3 to solve for Z_{DP} and Z_{IE}.

Next, the foot and shoe shared the same motion during perturbations. As a result, the torques used in Eq. 2.3 and Eq. 2.4 are equal to the torque of the human ankle impedance plus the torque due to the dynamics of the Anklebot and the acceleration of the shoe inertia. An additional test was performed using only the Anklebot and shoe to estimate the combined impedance of the Anklebot and shoe ($Z_{Anklebot+shoe}$). Accordingly, the impedance of the ankle is equal to the total impedance of the system ($Z_{ankle+Anklebot+shoe}$) minus the combined impedance of the Anklebot and shoe (Eq. 2.5).

$$Z_{ankle} = Z_{ankle+Anklebot+shoe} - Z_{Anklebot+shoe} \qquad\qquad 2.5$$

For this analysis, the impedance Z_{ankle} was described as the magnitude and phase across a desired frequency range. These results were later used as the target data to generate an ANN model.

Last, the impedance was estimated using the *tfestimate* function in MATLAB. This method implemented the Welch's averaged, modified periodogram algorithm to calculate the auto-power and cross-power spectral densities between the ankle angle and ankle torque for the DP and IE directions. The parameters included a 512 length Hamming window, 50% overlap, sampling frequency of 200 Hz, and an FFT length of 1024 samples. The partial coherence of the transfer function estimates were also determined using the MATLAB *mscohere* function. The partial coherences were used to justify that the torque perturbations added enough energy to the ankle to perform system identification, after removing the effects of the other input directions. Additional information about the impedance transfer function matrices and partial coherence calculations can be found in [53], [134].

2.3.3   Ankle Impedance in DP and IE

For each subject, the ankle impedance was estimated in DP and IE directions across 15 trials. Figure 2-2 shows the DP and IE Bode plots for the ankle mechanical impedance of a representative subject at the muscle co-contraction levels of relaxed, 10% MVC, and 20% MVC within the frequency range of $0.78 - 8$ Hz. Each muscle activation level was averaged across five trials, and

the standard deviation is shown by the shaded regions. The frequency region was selected to be approximately less than the break frequency of the second-order system, where the magnitude remains relatively constant, and the effects of the inertia are minimal [53]. This bandwidth range will be used for the ANN models, as described in the next section. Additionally, Table 2-2 shows the magnitude averaged across five trials and frequency for each muscle activation level. The standard deviation was calculated across the frequency range of 0.7 – 8 Hz.

For all of the trials, the resulting magnitude in DP was greater than in IE at all frequencies for their respective muscle activation levels. This is consistent with previous work where the stiffness in the DP direction was greater than the stiffness in IE by at least a factor 2 [53]. The average magnitudes and standard deviation across nine subjects were 24.6 ± 13.2 Nm/rad, 61.5 ± 32.9 Nm/rad, and 74.0 ± 27.6 Nm/rad for the relaxed, 10% MVC, and 20% MVC in the DP direction, and 12.3 ± 6.1 Nm/rad, 20.0 ± 11.2 Nm/rad, and 25.2 ± 12.0 Nm/rad for the relaxed, 10% MVC, and 20% MVC in the IE direction, respectively (Table 2-2). Interestingly, Subject 4 in Table 2-2 did not show an increase in the average magnitude from 10% MVC to 20% MVC, but rather the magnitude remained relatively the same.

Table 2-2. Average DP and IE impedance magnitudes ± standard deviation with relaxed muscles, 10% MVC, and 20% MVC. Total mean and standard deviation across nine subjects are included.

Subject	DP			IE		
	Relaxed [Nm/rad]	10% MVC [Nm/rad]	20% MVC [Nm/rad]	Relaxed [Nm/rad]	10% MVC [Nm/rad]	20% MVC [Nm/rad]
1	13.5 ± 8.6	29.4 ± 15.1	40.9 ± 23.4	6.4 ± 2.1	8.0 ± 2.7	10.2 ± 3.1
2	13.9 ± 5.8	45.7 ± 13.2	61.6 ± 18.3	10.1 ± 2.3	18.0 ± 3.0	24.2 ± 3.7
3	40.9 ± 12.5	114.2 ± 25.5	121.7 ± 28.6	18.9 ± 4.6	39.3 ± 7.5	48.0 ± 9.5
4	51.6 ± 14.4	118.1 ± 44.9	117.7 ± 37.2	25.5 ± 7.7	36.8 ± 8.7	40.0 ± 9.1
5	15.7 ± 3.5	42.5 ± 7.6	64.1 ± 11.0	8.9 ± 2.6	13.4 ± 3.9	19.4 ± 5.2
6	24.6 ± 10.9	41.2 ± 16.5	74.7 ± 38.4	8.8 ± 2.4	11.5 ± 3.0	17.1 ± 3.9
7	15.5 ± 4.4	38.7 ± 10.1	56.7 ± 12.6	9.1 ± 2.8	11.3 ± 2.8	16.3 ± 3.6
8	23.1 ± 6.4	55.2 ± 37.7	57.5 ± 37.0	11.0 ± 3.0	19.9 ± 5.8	26.6 ± 8.7
9	22.4 ± 6.2	68.3 ± 15.8	71.4 ± 17.3	11.5 ± 3.3	22.1 ± 5.2	24.6 ± 6.3
Mean	24.6	61.5	74.0	12.3	20.0	25.2
stdev	13.2	32.9	27.6	6.1	11.2	12.0
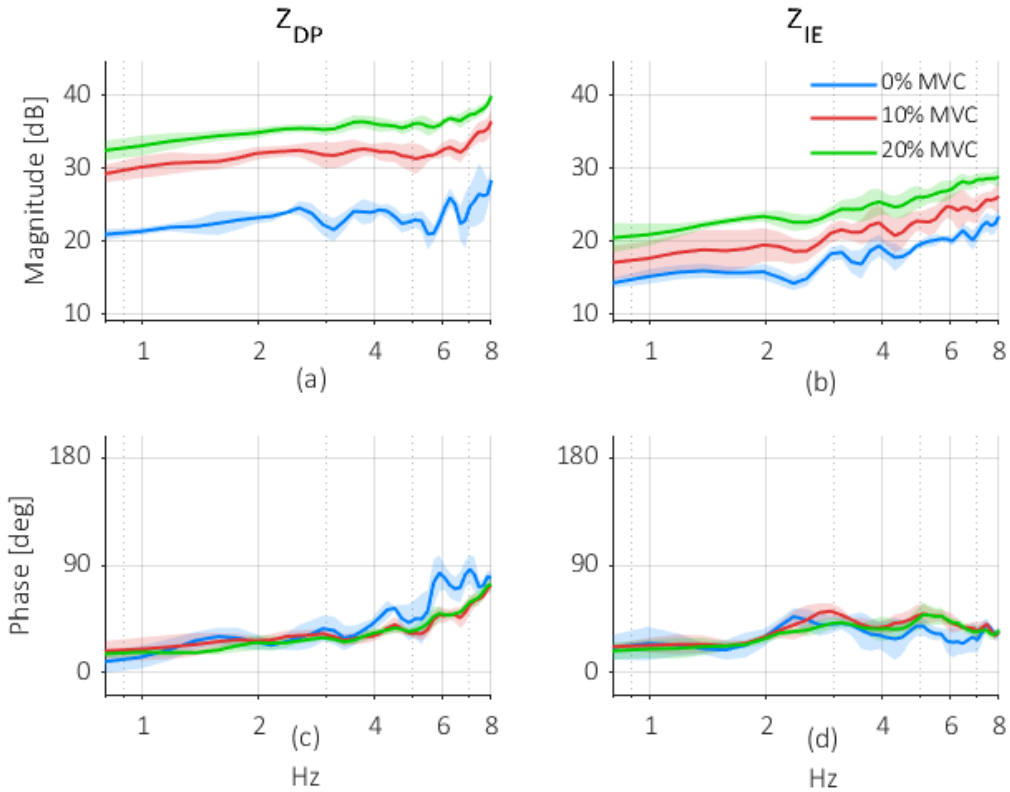
Figure 2-2 Average (solid line) ± standard deviation (shaded) of the ankle impedance magnitude [dB] and phase [°] for a representative subject (#5). The blue, red, and green lines correspond to relaxed, 10% MVC, and 20% MVC trials, respectively. (a) and (b) show the average magnitude in DP and IE. (c) and (d) shows the average phase in DP and IE, respectively.

The partial coherences for each muscle activation level were determined to validate that the selected system identification method can estimate the impedance between the selected frequency bandwidth of 0.7 to 8 Hz. Figure 2-3 shows the partial coherences between joint angles, Θ and joint torques, T for the Anklebot plus shoe plus ankle between 0.5 to 30 Hz for each muscle activation level. The diagonal components show the coherence in the sagittal (Figure 2-3a) and frontal (Figure 2-3d) planes, independent from one another. The averaged partial coherence for the representative subject was 0.91 in DP and 0.92 in IE, validating the impedance results in these directions. Furthermore, the coherences in the off-diagonal components (Figure 2-3 b & c) were on average less than 0.27, indicating that minimal coupling occurred between DP and IE DOF. The average partial coherence for the diagonal components across nine subjects was always greater than 0.89, as shown in Table 2-3.

Table 2-3. Average (± standard deviation) partial coherence across the total population for each muscle activation level in the DP and IE between 0.7 − 8 Hz.

	0% MVC	10% MVC	20% MVC
DP	0.89 ± 0.02	0.89 ± 0.02	0.89 ± 0.01
IE	0.90 ± 0.01	0.90 ± 0.02	0.89 ± 0.01
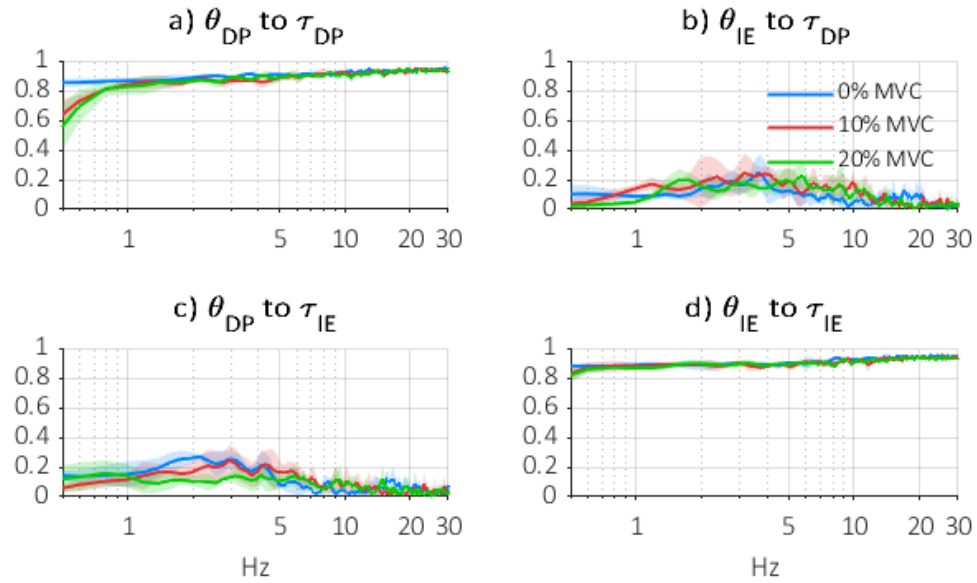
Figure 2-3. Partial coherence for the Anklebot + ankle +shoe system for a representative subject (#5) at relaxed, 10% MVC, and 20% MVC. The diagonal elements correspond to the DP (a) and IE (d) directions, respectively. The shaded region shows the standard deviation across five trials.

2.3.4 EMG Analysis

The EMG signals were recorded while the subject's lower-leg muscles were relaxed, or co-contracted to 10% MVC and 20% MVC. The RMS of the resulting EMG signals were calculated across each 60-second trial. In addition, all muscle signals were normalized with respect to the RMS value of the relaxed muscle trials. Normalization increased the scale of the EMG signal and was used to construct the input for the ANN models. The averaged EMG RMS across all subjects is presented in Figure 2-4 for each muscle and activation level. An increasing trend across all four muscles is shown between relaxed, 10% MVC, and 20% MVC co-contraction levels. The standard error was calculated using

$$SE = \frac{\sigma}{\sqrt{N}} \qquad\qquad 2.6$$

32

where σ is the standard deviation across the subjects and N is the total number of subjects.
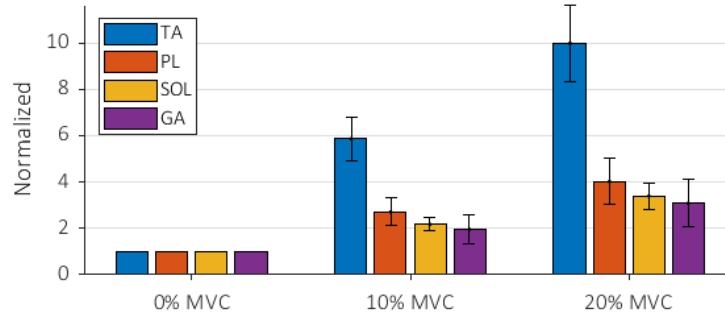
Figure 2-4. Average (± standard error) normalized RMS across nine subjects for the TA, PL, SOL, and GAL muscles.

2.3.5   Artificial Neural Network Design

A feedforward ANN was selected for regression, and used the EMG signals of four muscles to predict the ankle impedance in the DP and IE. The model design consists of five input neurons, a single hidden layer with 50 neurons, and an output layer of neurons that generate the magnitude and phase of the ankle impedance in either DP or IE. As shown in Figure 2-5 and Eq. 2.7, the neural network model is described as the linear combination of the inputs (x) and a series of weights (w), biases (b, b'), nonlinear sigmoid activation functions (φ), and linear activation functions (β); all resulting in the model output (y).

$$y_k(\boldsymbol{x}, \boldsymbol{w}, \boldsymbol{b}, \boldsymbol{b}') = \beta \left(\sum_{j=1}^{50} w_{kj}\, \varphi \left(\sum_{i=1}^{5} w_{ji} x_i + b_j \right) + b'_k \right) \qquad 2.7$$

The input matrix in Eq. 2.7 contains x_i neurons, where $i = 1{:}5$; including the four RMS EMG signals across 15 trials and the select frequency range, f across all subjects. The input neurons are connected to all neurons in the hidden layer by a series of weights, w_{ji} and biases, b_j, where $j = 1, \dots, 50$. The number of hidden layer neurons was selected by initially testing the performance of the ANN models with a hidden layer size between $10 - 200$ neurons. The models with the smallest error between the target and predicted impedance had 50 neurons. The summation at each of the hidden layer neurons is transformed by a tan-sigmoid activation function φ, which is a commonly used activation function from the MATLAB Neural Network toolbox [135]. Next, the resulting values from the 50 hidden layer neurons are again summed together at each of the output neurons y_k where $k = 1, 2$. Each operation is multiplied by weights

33

w_{kj} summed by a bias b'_k and again are transformed by the linear activation function β. An illustration of this process can be found in Figure 2-5.
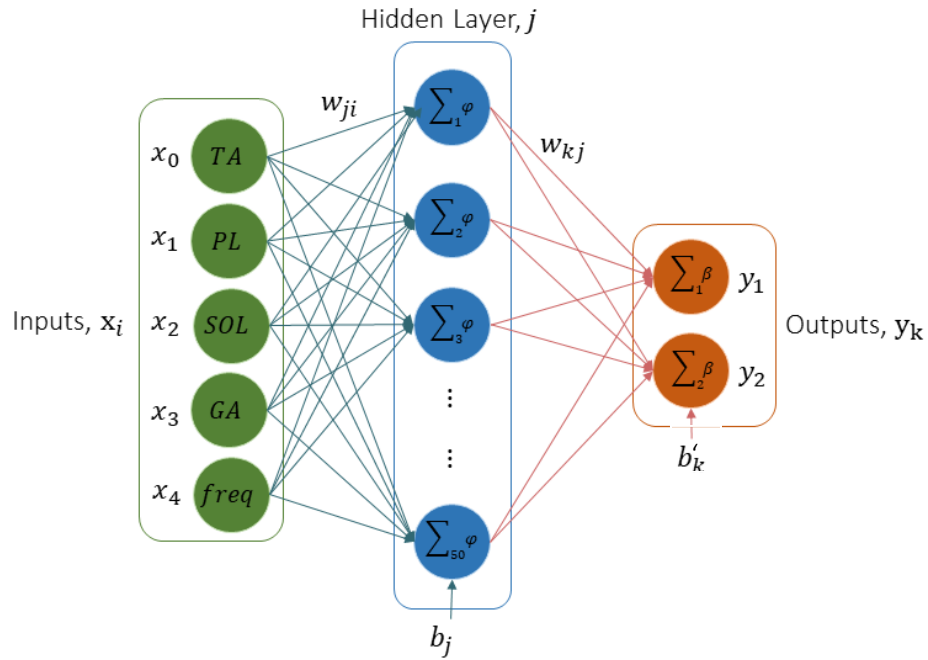
Figure 2-5. The feedforward ANN design, composed of five inputs, 50 hidden layer neurons, and two outputs.

2.3.5.1 Input matrix design

The input matrix contains the normalized RMS of the EMG signals across 15 trials. Additionally, the desired frequency range of $0.7 - 8$ Hz the impedance magnitude and phase were used as input. This frequency vector contained a total of 38 frequencies points, so the RMS of each EMG signal was reshaped to a vector of size 1x38. The resulting input matrix r_m for an individual trial took the form:

$$r_m = [x_0(TA);\ x_1(PL);\ x_2(SOL);\ x_3(GA);\ x_4(freq)]_{5x38} \qquad 2.8$$

Where $m = 1, \dots, 15$, corresponding to 15 trials per subject. All the trials were concatenated into a single overall input matrix, resulting in a matrix with size 5x570 to be used for both the DP and IE models, as described in Eq. 2.9.

$$R = [r_1, r_2, \dots r_{15}]_{5x570} \qquad 2.9$$

www.manaraa.com

2.3.5.2 *Target matrix design*

The target matrix is used during ANN supervised learning and consists of the desired ankle impedance values that were determined experimentally in Section 2.3.3. Similar to the input matrix, the target matrix for a single trial took the form:

$$y_m = \begin{bmatrix} Mg_i \\ Ph_i \end{bmatrix}_{2x38} \qquad\qquad 2.10$$

where Mg_m and Ph_m are the impedance magnitude and phase within the select frequency range for 15 trials. Each submatrix was concatenated to create the overall target matrix Y used to train the ANN models. A single matrix of size 2 x 570 was generated for the ankle impedance results in DP, and another for the ankle impedance in IE.

$$Y = [y_1, y_2, \dots, y_{15}]_{2x570} \qquad\qquad 2.11$$

2.3.5.3 *ANN Supervised Learning*

The input and target matrices were used during a process called supervised learning to train and validate each ANN model. This process ensures the proper weights and biases were selected so that the model does not overfit to the training data. First, the input and target matrices are divided randomly into three groups: 1) 70% training, 2) 15% validation, and 3) 15% testing. The training dataset is used to update the weights and biases between each of the network neurons using the Levenberg-Marquardt algorithm. To check that appropriate model weights were chosen, the validation dataset, which does not contain data used during training, determines the mean-squared-error (mse) between the validation target and output data. The iterative process of using the training data to update weights and the validation data to determine the mse continues until the mse converges to a minimum. Next, the remaining 15% of the data is used to test the overall performance of the ANN model. If the performance was desirable, the model was saved and used for future analysis.

2.3.6   ANN Performance

After training, it was necessary to verify that the supervised learning process was able to successfully generate a model that explains the relationship between the inputs and outputs. Two techniques were used to assess the training, validation, and testing performance of each ANN model. The first technique was to check that the mse of each model converged to a minimum value

and never showed any increasing trends throughout the learning process. If the mse for the validation or testing datasets increased, it is likely that the weights and biases were overfitting to the training data and the model was not used for analysis. The mse for all the models selected for this analysis converged to a minimum value.

The second technique determined the correlation coefficient R between the target and output impedance for the training, validation, and testing datasets. The correlation coefficient is a measure of the linear dependence between the target and predicted impedance, with $R = 1$ being a perfect correlation. If any of the groups showed substantially lower R values, it is again likely that the model overfits to the data, and the model was not selected. Table 2-4 shows the R values for the training, validation, and testing performance between the target and output data in DP and IE for all the subject models. The R values ranged between 0.945 and 0.997 for the DP direction and 0.895 and 0.980 for the IE direction. The high performance across training, validation, and testing confirmed that the selected models were successfully trained.

Table 2-4. Training, Validation, and Testing correlation coefficients (R) for each ANN models during supervised learning. The overall average ± standard deviation across subjects is included.

	DP			IE		
Subject	Training	Validation	Testing	Training	Validation	Testing
1	0.946	0.945	0.959	0.942	0.942	0.916
2	0.961	0.963	0.956	0.944	0.950	0.938
3	0.997	0.994	0.993	0.979	0.980	0.971
4	0.995	0.991	0.991	0.977	0.958	0.952
5	0.969	0.963	0.970	0.951	0.936	0.941
6	0.993	0.976	0.978	0.916	0.913	0.895
7	0.964	0.961	0.965	0.960	0.951	0.937
8	0.994	0.991	0.990	0.975	0.945	0.964
9	0.988	0.974	0.977	0.967	0.960	0.950
Mean	**0.979**	**0.973**	**0.975**	**0.957**	**0.948**	**0.940**
(Stdev)	**(0.02)**	**(0.02)**	**(0.01)**	**(0.02)**	**(0.02)**	**(0.02)**

2.3.7 ANN Impedance Prediction Accuracy

Figure 2-6 describes the average impedance predicted by the DP and IE ANN models for the representative subject, indicated by the dashed line. The target impedance used to train the models is also included in the figure for visual comparison, and is shown by the solid line. The average relative error for the subject (Figure 2-6) across all trials and frequencies was 5.0 ± 5.4% for the DP model and 4.9 ± 4.4% for the IE model, respectively. One observation from Figure 2-6 is

that the ANN predicted impedance had a smoother response than the target impedance for the selected frequency range. This also supports the claim that the ANN models did not overfit to noise in the experiment, which could be useful for future implications such as model generalization across subjects or for prostheses control.

In addition, the boxplots in Figure 2-7 show the range of errors between the target and predicted impedance magnitude for all subjects. The average errors for the magnitude and phase across all subjects were 2.6 ± 0.5 Nm/rad and 4.3 ± 1.4° for the DP models and 1.1 ± 0.2 Nm/rad and 3.3 ± 0.9° for the IE models, respectively. When compared to the range of the magnitude and phase, the errors were very small.
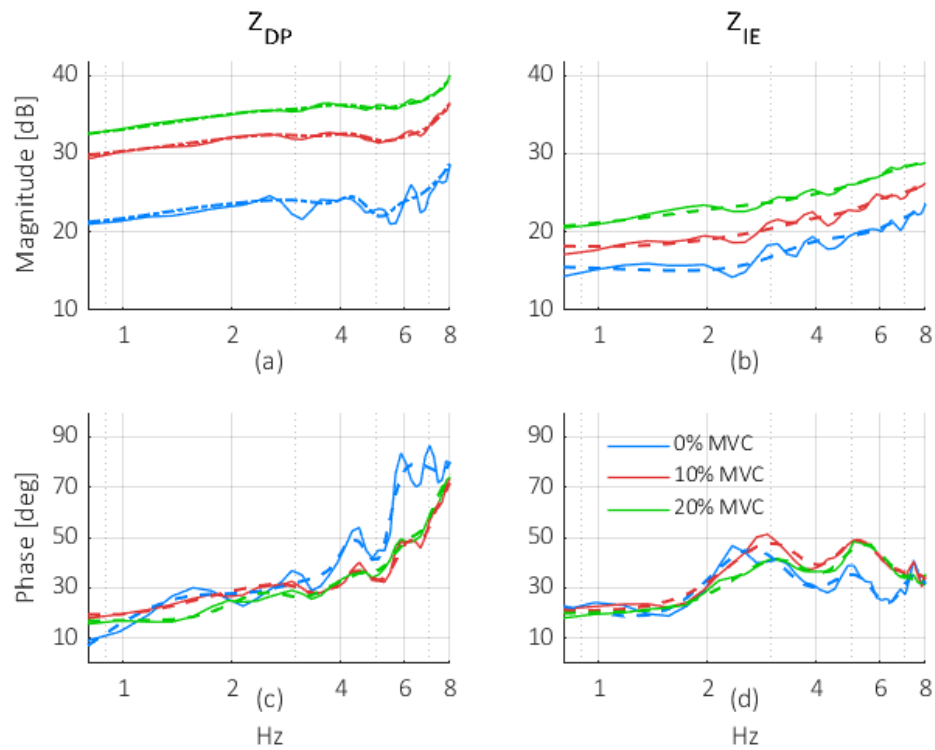
Figure 2-6. Average target (solid) and predicted (dashed) impedance for a representative subject (#5) with relaxed muscles (blue), and co-contraction at 10% MVC (red) and 20% MVC (green). The average magnitudes are presented in (a) and (b), and the average phases are shown in (c) and (d).
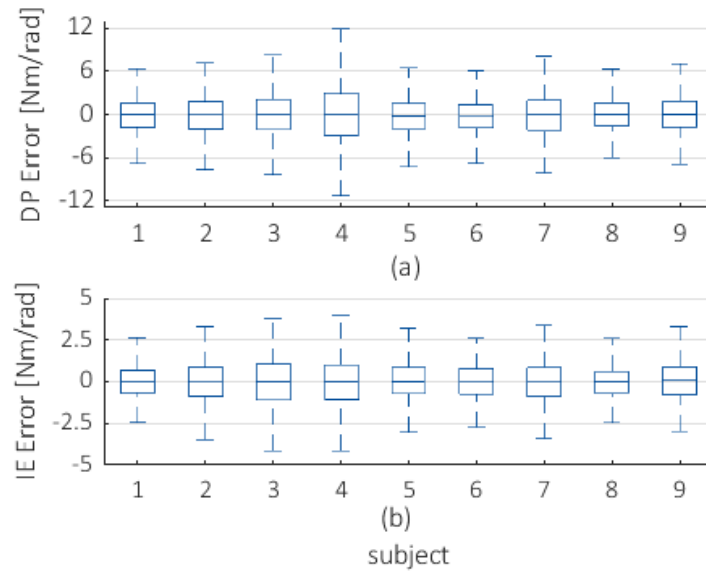
Figure 2-7. The error between the predicted and target impedance magnitude for each subject. The results for DP are shown in (a) and IE in (b). As reference, the average impedance was 53.4 Nm/rad and 19.1 Nm/rad for DP and IE, respectively.

2.4 ML Experiment

In addition to the study of ankle impedance and muscle activity in DP and IE, these methods were expanded to the transverse plane to examine the ML direction. The following section describes the experimental procedure, ankle impedance characterization, the ANN model design, and ANN results in the ML direction. Analysis of this DOF provides additional insights into how the lower extremity muscles influence the ankle dynamics, something that has not been studied before to the author's knowledge. Altogether, the exploration of the ML direction allows for comparison and conclusions about all three anatomical DOF of the ankle. The experimental setup, procedure, and model design are mirrored from the previous section in DP and IE, with the minimal differences explained below.

For the ML experiments, a new subject database was recruited. The subjects had no previously reported musculoskeletal injuries and gave written consent to participation as approved by the Michigan Technological University Institutional Review Board. The biometric information for the ML experiment subjects can be found in Table 2-5. The experimental procedure was repeated from the DP/IE experiments (Section 2.3.1); however, the Anklebot apparatus was rotated so that the actuators were perpendicular to the shin, as shown in Figure 2-1b.

38

Gender	Age*	Mass (kg)*	Height (cm)*
5 male, 5 female	25.2 ± 4.7	71.9 ± 18.2	172.7 ± 8.8

* mean ± standard deviation across population

2.4.1 Procedure

First, four EMG sensors were placed on the TA, PL, SOL, and GA muscles and the TA muscle signal was used as visual feedback to the subject during each trial. The MVC was determined while the subject co-contracted their lower-leg muscles, and the maximum TA signal was used as the reference voltage. Next, 15 trials were performed while the subject kept their muscles relaxed, or actively co-contracted their muscles to 10% MVC and 20% MVC. Each activation level was repeated five times. During each 70-second trial, Anklebot applied pseudo-random perturbations to the ankle in the transverse plane, and the resultant ankle angles and ankle torques were measured. The first 10 seconds of each trial were removed to reduce the transient effects, and the data was used to estimate the ankle impedance in the ML direction.

2.4.2 System Identification of ML Ankle Impedance

Based on Eq. 2.1 and Eq. 2.2, the impedance in ML, Z_{ML} is determined using the measured ankle torques and angles in the transverse plane. Assuming an LTI system, this relationship can be described as

$$\mathrm{T}_{ML} = Z_{ML}(f)\Theta_{ML} \tag{2.12}$$

where T_{ML} and Θ_{ML} are the respective ankle torques and angles across the frequency range, f.

The same system identification procedure from the DP/IE experiment was used, except the transfer function matrix only contained a single-DOF. The *tfestimate* function implemented Welch's averaged-modified periodogram algorithm. The parameters selected to estimate the transfer function were: a 512 length Hamming window, 50% overlap, sampling frequency of 200 Hz, and an FFT length of 1024 samples. The coherence was also determined across all trials to confirm that the assumption of a linear relation between ankle torques and angles were valid.

The active stiffness from the Anklebot controller was subtracted from the impedance as in Eq. 2.13, where the stiffness $k = 12.8$ Nm/rad.

$$Z_{ML}(f) = \frac{T_{ML}(f)}{\Theta_{ML}(f)} - k_{ML} \qquad\qquad 2.13$$

Additionally, when the actuators were applying perturbations, the shoe and the ankle shared the same motion. The resulting impedance of the Anklebot and ankle were in parallel, and the impedance of the Anklebot and shoe could be subtracted from the total impedance. The resulting impedance of only the ankle, as described in Eq. 2.14, was used in the target matrix to train the ANN models.

$$Z_{ML,ankle} = Z_{ML,ankle+Anklebot+shoe} - Z_{ML,Anklebot+shoe} \qquad\qquad 2.14$$

2.4.3 Ankle Impedance in ML

The upper frequency range selected to train the ANN models was determined to be 4.1 Hz for all subjects, which is less than the average break frequency of the ankle in the ML direction [51]. In addition, the low-frequency components (< 0.5 Hz) were also not selected due to low coherence. The resulting bandwidth chosen for this analysis was 0.7 − 4.1 Hz and contained 18 samples for each trial.

The impedance results for a representative subject can be found in Figure 2-8. The mean and standard deviation (shaded regions) of the magnitude and phase at each frequency were determined across five trials. Coinciding with the results in DP and IE, the magnitude of the impedance in ML increased with muscle activation level. Table 2-6 shows the average magnitude at each muscle activation level for the rest of the subjects. The overall mean and standard deviation of the magnitude across the total population was 5.1 ± 1.9 Nm/rad, 15.1 ± 4.6 Nm/rad, and 19.8 ± 6.3 Nm/rad for the relaxed, 10% MVC, and 20% MVC trials, respectively.

The resulting ankle impedance in ML was comparable to the results presented in previous work, where the ML ankle impedance was determined for relaxed muscles [52]. These results found an average impedance magnitude to be 6.0 ± 0.9 Nm/rad (< 4.4 Hz) for relaxed muscles. In addition, previous work determined the average impedance magnitude for co-contraction at 10% MVC to be approximately 27 Nm/rad (< 9.1 Hz) [51]. The slight increases from the magnitude presented in the literature for both relaxed and 10% MVC experiments are likely because the average was determined over a larger bandwidth. Last, the impedance magnitude at 20% MVC has not been reported in the literature.

Table 2-6. Average magnitude ± standard deviation for the relaxed, 10% MVC and 20% MVC Co-contraction levels across all subjects

Subject	0% MVC [Nm/rad]	10% MVC [Nm/rad]	20% MVC [Nm/rad]
1	2.4 ± 0.9	9.4 ± 1.1	14.1 ± 1.7
2	2.4 ± 0.5	14.3 ± 1.5	22.1 ± 2.6
3	6.0 ± 0.8	16.3 ± 1.1	23.5 ± 3.0
4	5.5 ± 0.7	12.4 ± 0.7	14.9 ± 0.5
5	6.2 ± 2.3	15.9 ± 2.7	19.0 ± 4.2
6	4.5 ± 0.6	16.2 ± 0.7	17.8 ± 0.9
7	7.1 ± 3.3	17.9 ± 3.3	20.8 ± 2.5
8	8.2 ± 0.6	25.6 ± 1.7	35.1 ± 2.7
9	4.7 ± 0.4	10.5 ± 0.6	14.8 ± 0.7
10	4.2 ± 0.8	13.2 ± 1.4	15.3 ± 2.0
Mean	5.1	15.1	19.8
Stdev	1.9	4.6	6.3
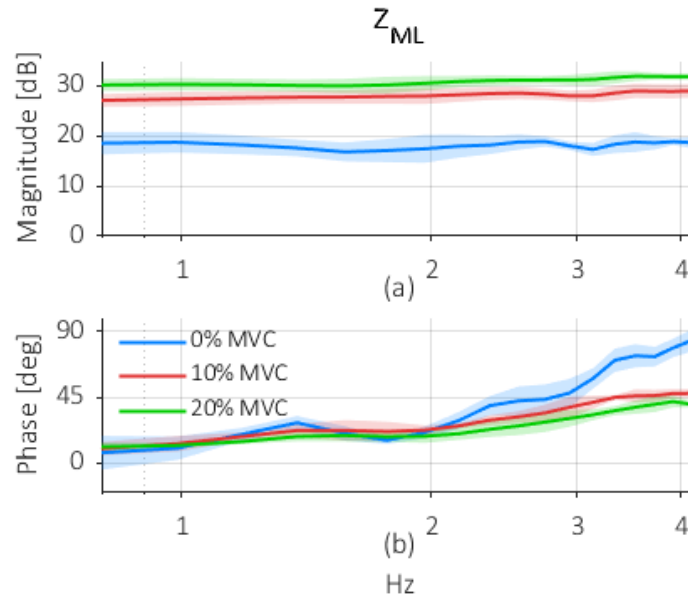
Figure 2-8. Average ankle impedance magnitude [dB] and phase [°] in the ML direction for a representative subject (#8). The muscle activation levels are denoted by the blue (relaxed), red (10% MVC), and green (20% MVC) curves. The shaded regions show the standard deviation.

Furthermore, the coherences were determined for all trials using the *mscohere* function in MATLAB. Table 2-7 shows that the average coherence of the whole system (Anklebot + shoe +

41

ankle) across the total population was always greater than 0.88 for all trials, with the maximum average coherence reaching 0.91. The high coherence verifies that the system identification method could accurately estimate the ankle impedance in the ML direction.

Table 2-7. Average and standard deviation coherence across the 10 subjects for each muscle activation level in the ML direction between 0.7 – 4.1 Hz.

	0% MVC	10% MVC	20% MVC
Mean	0.89	0.89	0.88
Stdev	0.009	0.01	0.03

2.4.4   EMG Analysis

The RMS of the EMG for four muscles was determined across each 60 second trial. Each set of three trials (relaxed, 10% MVC, and 20% MVC) were normalized by the passive trial of that set. Figure 2-9 shows the average of the normalized RMS EMG signals across all subjects. An increasing trend across all the muscles for the three levels.
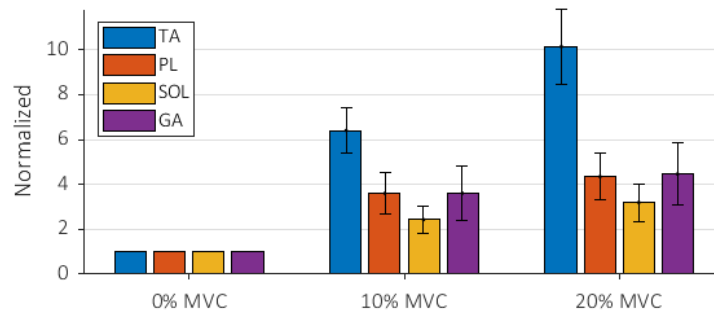
Figure 2-9. Average (± standard error) normalized RMS across all trials for the TA, PL, SOL, and GA muscles for ML experiment.

2.4.5   ANN Design

An in-depth description of the ANN model parameters and training and validation techniques used for this experiment can be found in Section 2.3.5. As depicted in Figure 2-5, the ANN models had five input neurons, containing the normalized EMG RMS for each contraction level and a frequency value, 60 hidden layer neurons, and two output layer neurons for the predicted ankle impedance. Furthermore, the models were trained using the same supervised learning cross-validation techniques. The input and target matrices were divided randomly into training, validation, and testing datasets, and the model weights and biases were updated until the highest

performance was achieved. A brief description of the input matrix and the target matrix design used to generate a model for each subject can be found in this section.

2.4.5.1 *Input matrix design*

The input matrix contains the RMS of the EMG signals that were normalized by the passive trials and a vector of the desired frequency range between $0.7 - 4.1$ Hz. The size of the vector for each trial was 18 samples. Equation 2.16 explains the input matrix r_m for an individual trial:

$$r_m = [x_0(TA); \ x_1(PL); \ x_2(SOL); \ x_3(GA); \ x_4(freq)]_{5x18} \qquad 2.15$$

where $m = 1, \dots, 15,$ for the 15 trials. All the trials were concatenated into a single overall input matrix of size 5 x 270 and was used for the ML model training, as described in Eq. 2.16.

$$R = [r_1, r_2, \dots r_{15}]_{5x270} \qquad 2.16$$

2.4.5.2 *Target matrix design*

The target matrix was composed of the desired ankle impedance values for each frequency. The target matrix for a single trial took the form:

$$y_m = \begin{bmatrix} Re_m \\ Im_m \end{bmatrix}_{2x18} \qquad 2.17$$

Where Re_m and Im_m are the real and imaginary components of the impedance in the complex form and $m = \{1, 2, \dots, 15\}$. Unlike the DP and IE models where the magnitude and phase of the ankle impedance were used to populate the target matrix, the complex form of the impedance resulted in higher model performance for the ML direction. For analysis purposes, the ANN models predicted the complex impedance, and the results were transformed back to the magnitude and phase in the frequency domain. The overall target matrix Y was created by concatenating each submatrix, y_m. The total matrix was used to train the ANN models for the ML ankle impedance.

$$Y = [y_1, y_2, \dots, y_{15}]_{2x270} \qquad 2.18$$

2.4.6 ANN Performance

To determine if the ANN models were adequately trained it was necessary to determine that the mse for the training, validation, and testing datasets decreased during model training and that the regression performance between the target and predicted impedance for each dataset was high. This process is used to verify that the model weights did not overfit or underfit to the

selected dataset. When overfitting occurs, the model does not respond well to new or unseen input data. If any of these three training, validation, or testing steps performed poorly, the model training process was repeated with new parameters. The best performing models were selected for this analysis.

Table 2-8 contains the correlation coefficient R values for each of the three steps during model cross-validation. For 10 subjects, the correlation coefficients were always greater than 0.980 for the training, validation, and testing datasets. The high R across all datasets demonstrates that the models can predict ankle impedance based on new input data that was not used to train the models. During the cross-validation, the mse for the training, validation, and testing datasets always decreased for each iteration until a minimum error was achieved. This also supports the claim that none of the models overfit to the data during training, and the models can be used to predict ankle impedance based on the EMG signal information.

Table 2-8. The correlation coefficient (R) for the Training, Validation, and Testing datasets during supervised learning for all subject models. The overall average ± standard deviation across all subjects is provided.

	ML		
Subject	Training	Validation	Testing
1	0.993	0.989	0.984
2	0.998	0.991	0.989
3	0.996	0.991	0.984
4	0.992	0.983	0.985
5	0.997	0.991	0.989
6	0.996	0.991	0.983
7	0.998	0.989	0.984
8	0.996	0.989	0.990
9	0.995	0.980	0.981
10	0.995	0.991	0.986
Mean (stdev)	0.996 ± 0.002	0.989 ± 0.004	0.986 ± 0.003

2.4.7 ANN Impedance Prediction Accuracy

Figure 2-10 displays the average impedance magnitude and phase predicted from the ANN model (dashed) and the corresponding target (solid) impedance for a representative subject. The average relative errors between the target and predicted impedance magnitude for the representative subject (Figure 2-10) were 7.0 ± 10.2%, 2.5 ± 3.2%, and 2.3 ± 2.5% for the 0% MVC, 10% MVC, and 20% MVC trials, respectively. Similar to the observation of the ANN impedance

prediction in the DP and IE directions (Section 2.3.7), the predicted impedance typically followed a smoother curve than the experimentally determined impedance.

The range of errors between the target and ANN predicted impedance across the ten subjects are presented with boxplots in Figure 2-11. The average error for the magnitude and phase across all subjects were 0.47 ± 0.1 Nm/rad and 4.7 ± 2.5°, respectively. The small error is acceptable, considering the range of the magnitude and phase across the three levels of muscle activation. Interestingly, the representative subject impedance, shown in Figure 2-8 and Figure 2-10, had the highest error across all subjects with a maximum amount of 2.5 Nm/rad. The larger error can be justified by the fact that this subject also had the highest average impedance magnitude across all subjects, with a value of 35.1 Nm/rad.
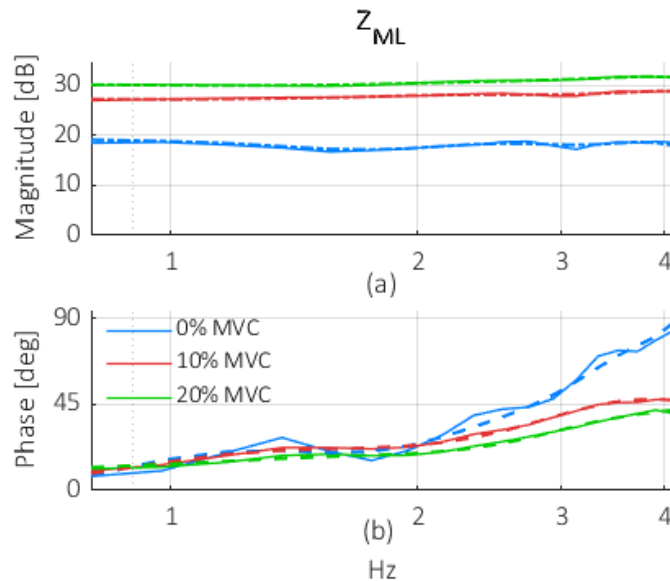
Figure 2-10. Average target (solid) and predicted (dashed) impedance from the ANN model for a representative subject (#8) with relaxed muscles (blue), and co-activation at 10% MVC (red) and 20% MVC (green).

45
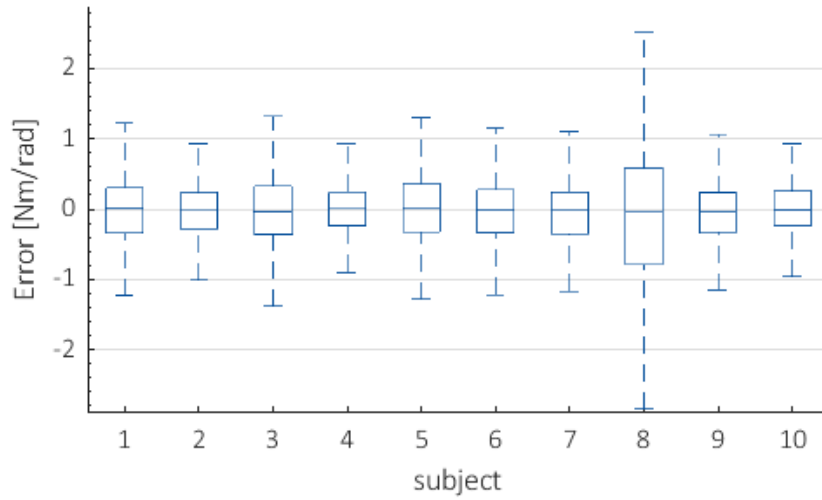
Figure 2-11. The range of error between the predicted and target impedance magnitude across all trials for ten subjects. As reference, the average impedance was 13.4 Nm/rad for ML.

2.5 Discussion

The goal of this study was to model the relationship between the non-loaded ankle impedance in the DP, IE, and ML directions with lower extremity muscle co-contraction using ANN. The DP/IE and ML experiments were performed during two separate studies. Using Anklebot, the ankle impedance was determined with an established stochastic identification method. During all trials, subjects maintained their muscles relaxed or co-contracted to 10% and 20% MVC. The relationship between muscle activity and ankle impedance was determined by training the ANN model for each subject.

Comparing the ankle impedance results for the DP, IE, and ML directions, the DP direction had the highest overall magnitude, with an overall average value of 53.4 ± 25.7 Nm/rad, followed by the IE direction, which had an average of 19.1 ± 6.5 Nm/rad, and then ML, with a mean of 13.4 ± 7.5 Nm/rad. These results agree with the findings in the literature, which used the Anklebot to study ankle impedance in DP and IE [47]–[50]. Furthermore, the impedance magnitude for all three directions with the level of muscle activation, which is also in agreement with previous findings [38], [41], [48], [50].

In addition, the individual models for each subject could accurately predict the ankle impedance, when presented with EMG information. The average relative errors across the subjects

46

for the DP, IE, and ML directions were 7.9 ± 16.8%, 7.5 ± 8.1%, and 6.6 ± 13.1%, respectively. The predicted impedance almost always had a smoother response compared to the experimentally estimated impedance, possibly removing noise that was present during estimation process. This model property could be useful for the possibility of implementation into a control system.

One limitation of this study is that a separate ANN model is required to predict a subject's ankle impedance in DP, IE, and ML. Not only does this require valuable time to train three separate models, but the models can only predict the impedance of that individual subject. Preliminary tests showed that using the EMG information from a different subject would not perform well in predicting ankle impedance. To eliminate the need to experimentally determine a subject's ankle impedance and train an ANN model for them, a subject-independent or a "generalized" model may be considered. Once developed, this model has the potential to predict impedance solely from the measurements of muscle activity.

Using EMG to estimate a user's motion intention has shown to be promising in recent years. To the author's knowledge, a model relating the ankle impedance in 3-DOF to lower extremity co-contraction levels has not been determined. The results of this study provide preliminary models that can accurately use EMG data to predict ankle impedance. However, these experiments explore this relationship while the ankle is not bearing any weight. To determine a model potentially more suitable in predicting a user's motion intention for active ankle-foot prostheses, a better understanding of how the muscle activity relates to ankle impedance during weight-bearing activities, such as standing and walking, is required. This work provides a "proof-of-concept" model toward the work described in proceeding chapters.

3 Relationship between Muscle Co-Contraction and 2-DOF Standing Ankle Impedance

3.1 Motivation

The work presented in this chapter expands upon the techniques used in Chapter 2 to investigate the EMG-ankle impedance relationship during standing. Previous work determined that the ankle impedance varies during quiet standing while a person maintains an upright posture [55]. The standing ankle impedance differs from the non-loaded ankle impedance because the ankle must compensate for the weight of the subject and external ground reactions.

Additionally, the lower extremity muscle activities play a key role in the control of ankle impedance modulation during standing [63]. One group suggested that the agonistic and antagonistic muscles of the lower extremity use a ballistic-like position control to prevent a person from falling using both intrinsic and active contractions [61]–[63]. Furthermore, similar observations of ballistic-like muscle activation patterns were measured from the residual ankle muscles of transtibial amputees [128]. As a result of these findings, a model that relates the EMG and standing ankle impedance may be significant for applications in the control and design of ankle-foot prostheses.

Furthermore, the experiments from Ch. 2 developed user-specific models that were dependent on the inherent properties of each subject. Only a few groups have looked into the feasibility of developing a generalized, or subject-independent, model that can use new or unseen subject EMG data to predict ankle impedance. Recently, Pan et al. developed a subject-independent model that could predict the motion of the wrist and fingers from both able-bodied and amputee subjects using EMG signals [136]. This work used a musculoskeletal dynamic model of the wrist and hand and showed that the subject-independent model had comparable results with a user-specific model. In particular, the subject-independent model reported fewer overshoots across three target positions. The work presented in this chapter explores the feasibility of a subject-independent model that can predict standing ankle impedance based on different levels of muscle co-contraction. In addition, this work proposes to characterize this relationship using a regression-based model, without the need for a complex musculoskeletal dynamic model of the ankle, as described previously.

This chapter is organized as follows: Section 3.2 and Section 3.3 describe the experimental procedure and results to determine the standing ankle impedance in DP and IE at varying levels of muscle co-contraction. Section 3.4 explores the correlation between the EMG from four muscles to the corresponding impedance parameters. The motivation for studying a simple linear correlation was to determine if there was a need for more robust regression techniques, such as ANN. Section 3.5 implements ANN to model the relationship between EMG and ankle impedance for individual subject models and an aggregated model. Section 3.6 expands upon these results to examine the feasibility of creating a subject-independent predictor for standing ankle impedance using the EMG measurements. Lastly, Section 3.7 provides concluding remarks, limitations, and future implications for the results found in this study. The results presented in this chapter are published in [76], [110], [111], [137].

3.2 Experimental Study

3.2.1 Setup

A total of 15 male subjects were recruited for the standing experiments with muscle co-contraction. All subjects had no history of musculoskeletal injuries or disorders, and gave written consent to participate in the study approved by the Michigan Technological University Institutional Review Board. Three subjects during the experiments were removed due to sensor issues and failure to complete the procedure requirements. The biometric information for the 12 inlier subjects is available in Table 3-1.

Table 3-1. Subject biometric information for standing co-contraction experiment

Age*	Mass (kg)*	Height (cm)*
27.9 ± 3.5	92.3 ± 27.6	180.3 ± 6.7

* mean ± standard deviation across population

The experiment employed an instrumented platform designed to estimate the ankle impedance in the sagittal and frontal planes while standing or walking. The platform consisted of a vibrating force plate (Kistler 9260AA3) module and a motion capture camera system (eight cameras - Optitrack Prime 17W) that were used to measure the kinetics and kinematics of the subject's ankle. A description of the vibrating force plate module can be found in [72]–[75].

Additionally, four wireless EMG sensors (Delsys Trigno Wireless System) were placed on the subject's TA, PL, SOL, and GAL muscles to measure muscle activities (Figure 3-1). Proper procedures were implemented to clean the surface of the skin before placing the sensor; including shaving excess leg hair and wiping the skin with rubbing alcohol to remove body oils. Muscle palpation was used to carefully place the sensor on the belly of each muscle. After placing the EMG sensors, a test was performed to make sure a signal was generated when each of the four muscles were contracted.
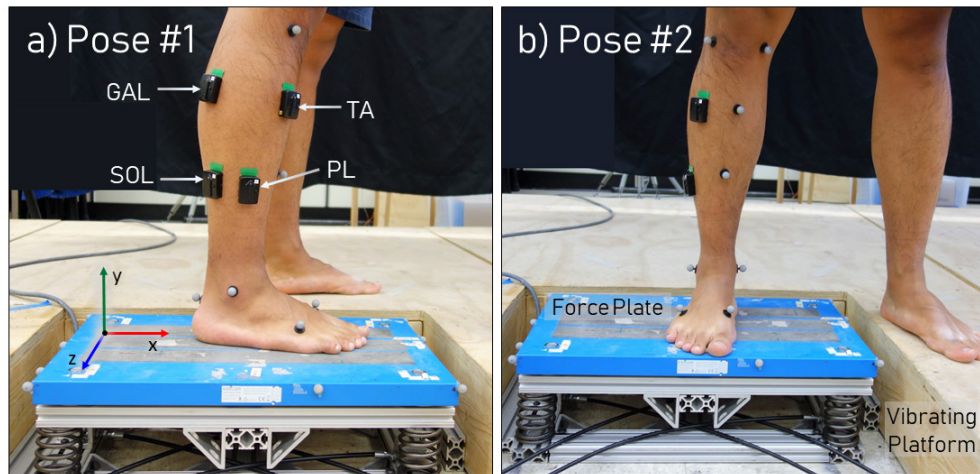
Figure 3-1. Experimental setup while subjects stood (a) with their heading oriented w.r.t the x-axis and (b) with their heading aligned with the z-axis. The setup included a vibrating platform, force plate, motion capture camera system, and four EMG sensors.

3.2.2 Procedure

At the beginning of each experiment, the MVC of the muscles were determined while the subjects were in a normal standing position. The subjects co-contracted their muscles to the maximum level in approximately 1-second bursts. They repeated the bursts between 5 to 10 times, and the highest voltage of the TA muscle was selected to be the reference MVC. During the trials, subjects were asked to maintain, to the best of their abilities, a constant muscle co-contraction at a percentage of the MVC voltage.

During a trial, the vibrating platform applied pseudorandom perturbations with a bandwidth up to 33 Hz to the right ankle in both DP and IE directions, simultaneously, for 70 seconds. While the ankle was being perturbed the subjects performed one of five tasks: stand normally with no active contraction of the lower extremity muscles (this is often referred to as 'relaxed' or '0% MVC')

50

or stand with muscles actively co-contracted to 10%, 20%, 30%, and 40% MVC. To maintain a constant co-contraction level, real-time visual feedback of the subject's TA EMG voltage and the target EMG voltage were provided. For visualization purposes, this signal was displayed as the root-mean-square (RMS) of a moving 20-milliseconds window. For the duration of the 70-second trial, the subject controlled their muscles to maintain a constant voltage around the target voltage level.

The five contraction levels (relaxed, 10%, 20%, 30%, and 40% MVC) were performed once while the foot was oriented parallel to the x-axis coordinate frame (Figure 3-1a) and once while the foot was rotated to be parallel to the z-axis (Figure 3-1b): for a total of 10 trials per subject. To reduce the effects of muscle fatigue the order of the trials were selected randomly, and the subjects were required to rest between each trial. The purpose of repeating the trials with two heading orientations was to validate the ankle impedance estimation; however, the trials in which the heading was parallel to the z-axis were not considered for this study. The analysis in this chapter focused solely on the five trials where the heading oriented parallel to the x-axis of the force plate.

3.2.3   Data Acquisition

The kinematic and kinetic data were collected with a sampling rate of 350 Hz, and were bandpass filtered at 1-40 Hz, using a 501st order finite impulse response filter. An example of the external torques and the ankle angle measurements in both DP and IE can be found in Figure 3-2. The maximum ranges of the external torques and ankle rotations generated from the pseudo-random input were ± 21.4 Nm and ± 3.9° in the DP direction and ± 3.1 Nm and ± 1.8° in the IE direction, respectively. The resulting ground reaction forces, ground reaction torques, and the ankle rotations were used to estimate the standing ankle impedance in DP and IE.

All EMG data were recorded with a sampling rate of 2000 Hz and were synchronized to the kinematic and kinetic data. An example of a raw TA EMG measurement from a representative subject is presented in Figure 3-3. This figure shows how the amplitude and frequency content of the EMG signal increased as the muscle co-contraction level increased. In addition, the solid black line indicates the moving RMS with a window size of 20 milliseconds across the time frame. This line is an example of the visual feedback of the EMG signal that was provided to the subjects during each trial.
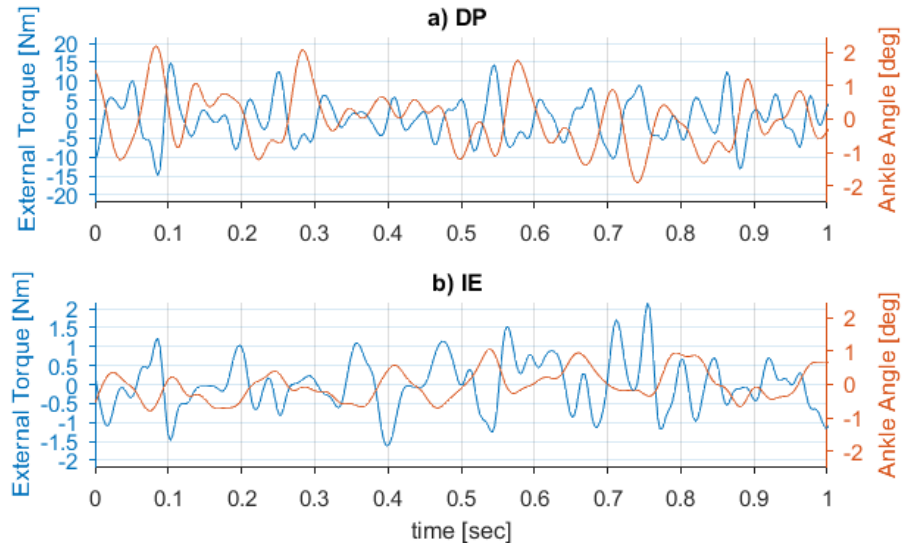
Figure 3-2. External torque (blue) applied to the foot by the force plate module and the resulting ankle angle (red) from a sample trial. The upper plot a) shows the measurements in DP and b) shows the measurements in the IE direction, respectively.
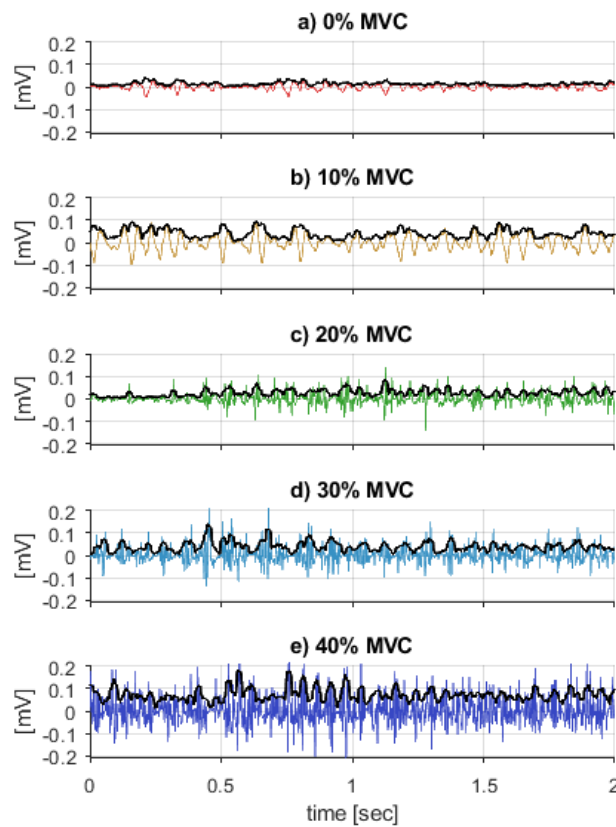
Figure 3-3. TA EMG signal of representative subject for 0% - 40% MVC co-contraction levels (a – e). The solid black line on each figure shows the moving 20 ms RMS window, which represents the signal that was visible to the subject during each trial.

52

The EMG signals were bandpass filtered between $65 - 150$ Hz using a 2000th order, finite impulse response filter. This filter bandwidth was selected because the most dominant and energy-rich region of the signal is between 50-150 Hz [138]. Additionally, this filter removed the lower frequency artifacts caused by the human and vibrating force plate ($0 - 33$ Hz), instability in the signal ($0 - 20$ Hz), and ambient noise (60 Hz).

Next, the first and last five seconds of each trial were cropped to remove any transient data. The collected data, including the kinematic, kinetic, and EMG data, were then separated into 5-second windows with 4.9 seconds overlap. The corresponding ankle impedance and RMS of the EMG for all muscle channels were determined for each window, resulting in a total of 24060 samples across the 12-subject population. Before being used for analysis, the RMS of the EMG muscle signals were z-score normalized using

$$\bar{x}_i = \frac{x_i - \mu_{x_i}}{\sigma_{x_i}} \qquad\qquad 3.1$$

where x_i is the subject data for each muscle $i = \{TA, PL, SOL, GAL\}$, and μ_{x_i} and σ_{x_i} are the mean and standard deviation across five trials for each particular muscle, respectively. Normalization of EMG signals is necessary when using the change in amplitude to compare across other muscles and the EMG signals of different subjects. An example of the z-score normalization of the EMG signals across four muscles and five co-contraction levels is shown in Figure 3-4 for a representative subject.
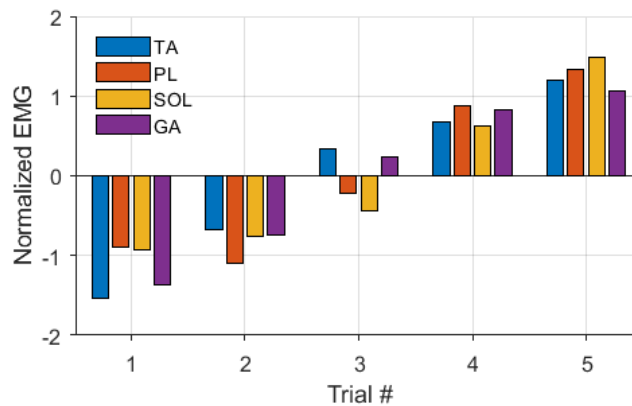
Figure 3-4. The z-score normalized RMS EMG of the TA, PL, SOL, and GAL muscles across five muscle contraction levels for a representative subject #5.

53

3.3 Standing Ankle impedance

The first method for calculating the standing ankle impedance used an ordinary least squares optimization to solve for each impedance parameter. This model assumed the shank and the foot are connected via a revolute joint with a spring and damper. In addition, only the inertial properties of the foot and force plate were accounted for because 1) the actuator dynamics could be disregarded due to the platform design [72], and 2) the dynamics above the ankle can be accounted for by the ankle angle deflection. To solve for the impedance parameters, the sum of the external torques acting on the ankle τ, determined from the experimental data, were set equal to the sum of the internal torques. Equation 3.2 describes the external ground reaction torques T_F and forces F_F of the foot, measured by the force plate, and the average moment arm between the center of the force plate and the ankle center $\overline{r_{PA}}$, measured by the motion capture system. Equation 3.3 describes the internal ankle torque, where the parameters K, B, J_F, and J_P are the ankle stiffness, ankle damping, foot inertia, and the force plate inertia, respectively.

$$\tau(t) = T_F(t) + \overline{r_{PA}} \times F_F(t) \qquad\qquad 3.2$$

$$\tau(t) = K\theta_A(t) + B\dot{\theta}_A(t) + J_F\ddot{\theta}_F(t) + J_P\ddot{\theta}_P(t) \qquad\qquad 3.3$$

The variables $\theta_A(t)$, $\dot{\theta}_A(t)$, $\ddot{\theta}_F(t)$, and $\ddot{\theta}_P(t)$ correspond to the ankle angle, ankle angular velocity, foot angular acceleration, and the force plate angular acceleration. The derivatives of the angle measurements were calculated using a Savitzky-Golay 15th order filter and an 11th order polynomial. Lastly, the unknown ankle impedance parameters in both DP and IE directions were estimated using an ordinary least squares optimization to minimize the residual of the Equation 3.3:

$$(K, B, J_F, J_P) = \operatorname{argmin}_{(K,B,J_F,J_P)} \left\| K\theta_A + B\dot{\theta}_A + J_F\ddot{\theta}_F + J_P\ddot{\theta}_P - \tau \right\|. \qquad\qquad 3.4$$

This method for estimating the ankle impedance eliminated the need to solve for the dynamics above the ankle, including the effects of the shank and upper body.

The results from the least-square optimization of the ankle impedance parameter estimations are described in Figure 3-5. The results show the average (± standard deviation) of the a) stiffness, b) damping, c) foot inertia, and d) % NMSE across 12 subjects for the five co-contraction levels. This figure shows that the stiffness in DP and IE had increasing trends as the muscle

activation levels increased. Additionally, the damping in DP also had a slight increase with muscle activity; however, the damping in IE remained relatively constant across the trials. The overall average stiffness and damping in DP were 258.2 ± 83.0 Nm/rad and 0.79 ± 0.10 Nms/rad, respectively, and in IE were 126.3 ± 22.9 Nm/rad and 0.31 ± 0.07 Nms/rad. Additionally, the inertia remained relatively small throughout all trials, as expected, with average values of 8.7 x 10^{-3} ± 2.9 x 10^{-3} kgm^2 and 4.6 x 10^{-3} ± 1.1 x 10^{-3} kgm^2 in the DP and IE directions, respectively. Last, the percent Normalized Mean Squared Error (NMSE) of the impedance estimation had average values between 77% - 92% in DP and 72% - 83% in IE across all muscle levels and subjects. The large NMSE across all trials verifies that the optimization method was able to estimate the impedance parameters sufficiently.
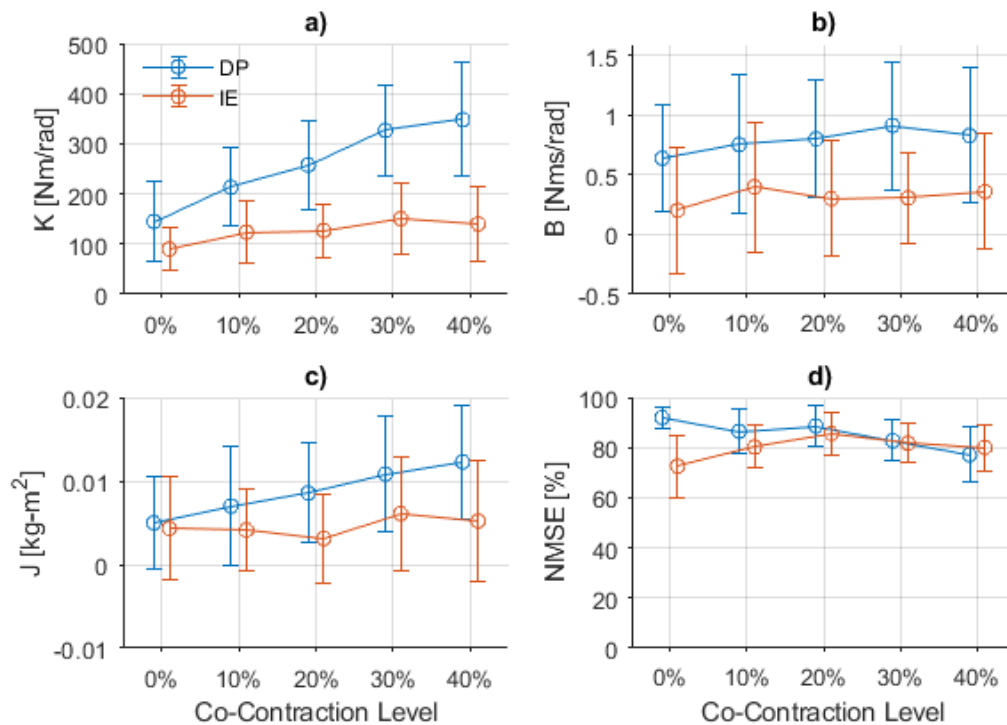
Figure 3-5. Average (± standard deviation) ankle a) stiffness, b) damping, and c) inertia across five muscle co-contraction levels. The results in d) show the average NMSE across all the 12 subjects.

3.4 Correlation between Standing Ankle Impedance and EMG signals

3.4.1 Linear Correlation

A linear model was developed to relate the EMG signals with the ankle stiffness and damping parameters. First, the median of the ankle impedance parameters Z_i and normalized RMS of the muscle signals EMG_j were calculated for each trial, where $i = \{K_{DP}, K_{IE}, B_{DP}, B_{IE}\}$ and $j = \{TA, PL, SOL, GA\}$. As shown in Eq. 3.5, all combinations i and j samples were fitted with the linear model

$$Z_i = \beta_1 EMG_j + \beta_0. \hspace{3cm} 3.5$$

This was repeated to fit 16 equations for every subject. The significance of the slope coefficient β_1 was determined for every fit equation using Analysis of Variance (ANOVA) for linear models. A linear correlation was determined with p-values less than or equal to 0.05.

Figure 3-6 shows an example of the fit equation for two representative subjects that explored the correlation between the DP stiffness and the SOL muscle. The small filled and unfilled circles represent the inlier data, within 10 and 90 percentiles, and the outlier data, respectively. Additionally, the center of the larger circles denotes the median for the corresponding impedance and EMG parameters across the five co-contraction levels. The colors represent 0% MVC (relaxed muscles) up to 40% MVC, as shown by the legend. The size of the larger circles is fixed to the same size for all trials, with the center of the large circle placed at the median.
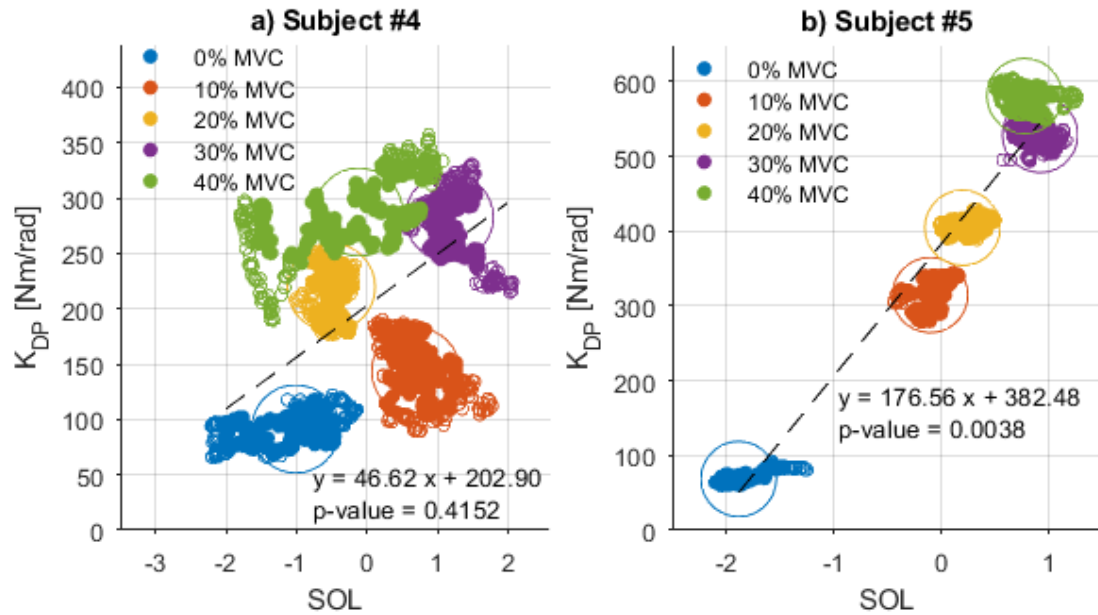
Figure 3-6. Example of linear fit between the ankle stiffness in DP and the normalized RMS of the SOL muscle for two subjects (#3 and #4). The colored circles denote the median for the 0% (blue), 10% (red), 20% (yellow), 30% (purple), and 40% (green) MVC. The fit equation and p-values of the slope coefficients are shown on each figure.

Figure 3-6a is an example of a fitted equation that did not display a linear correlation. The resulting *p*-value was equal to 0.4152, showing no significant linear correlation between the SOL and stiffness in DP. While there is no linear correlation, this does not imply that no relationship exists. It is possible that nonlinear or higher-order models could describe this relationship. Conversely, Figure 3-6b is an example of a subject that exhibited a linear relationship between the impedance and EMG parameters. The resulting *p*-value for the slope coefficient was equal to 0.0038, which shows that the parameters were significantly linearly correlated to one another.

Similar trends resembling the results in both Figure 3-6a and Figure 3-6b were determined across all subjects. Interestingly, most subjects showed linear correlation for some combinations of parameters but not for other combinations. Other subjects did not show any linear correlation across all 16 fitted equations. Table 3-2 describes the percentage across 12 subjects that exhibited a significant linear correlation (*p*-value ≤ 0.05) between the impedance and EMG signal parameters. The acronyms KDP, KIE, BDP, and BIE correspond to the stiffness and damping in DP and IE, respectively.

www.manaraa.com

Table 3-2. Percentage of subjects with a significant correlation (p < 0.05) between the ankle impedance parameter and EMG for each muscle. As the number of subjects showing a significant correlation increased, the color of the box became darker in color.

EMG		KDP	KIE	BDP	BIE
	TA	50%	33%	25%	17%
	PL	33%	17%	8%	8%
	SOL	42%	17%	25%	8%
	GAL	33%	17%	17%	8%

3.4.2 Discussion

In some cases, a significant correlation existed between the ankle impedance parameters and the EMG signals; however, these relations were not consistent across the subjects. The impedance parameter that was most correlated to the EMG signals was the ankle stiffness in DP. Table 3-2 shows that 50% of the subjects had a significant correlation between the TA muscle and the stiffness in DP (KDP). Conversely, the damping in the IE had the least number of subjects that exhibited a linear correlation; especially between damping in IE (BIE) and the PL, SOL, and GAL muscles. Similar trends were determined while studying the correlation between the muscles surrounding the knee and the torque about the knee for 28 subjects [139]. This study concluded that while significant correlations do exist, there are many inconsistencies across the results. The resulting regression model could only estimate knee torques with up to 50% Variance Accounted For (VAF) [139].

The results of this study aimed to assess if the relationship between ankle impedance and muscle co-contraction could be represented by a linear model. From the results shown in Table 3-2, only 20% of the total fit equations could be explained with a significant linear correlation. For the remaining 80%, additional methods can explore ways to select the appropriate regression models, improve EMG feature selection, and improve the ankle impedance estimation. These methods will be discussed throughout the remainder of this chapter.

3.5 Using ANN to model EMG-Impedance Relationship for Standing Subjects

To further examine the relationship between the lower extremity muscle co-contraction and the standing ankle impedance in DP and IE, a similar approach to Chapter 2 was implemented. The

function-approximation capabilities of ANN were used to address the experimental trials that did not exhibit a significant correlation between the input and output data. The following section describes the ANN model designs, feature extraction techniques, and standing ankle impedance prediction results using this technique. The findings of this study provide the next steps toward an EMG-Ankle Impedance model during standing.

3.5.1   ANN Procedure

Before training the ANN models, the data was pre-processed. First, all impedance samples with a NMSE less than 0.6 were removed from the dataset, as well as the corresponding EMG samples. This accounted for approximately 10% of total data. Next, the ankle impedance parameters were normalized by the mass of each subject. Then, the impedance and the RMS EMG data were z-score normalized using Eq. 3.1, where $i = \{KDP, BDP, JDP, KIE, BIE, JIE, TA, PL, SOL, GAL\}$, within each subject. The process of z-score normalization assigns a normally distributed score across all data points. The standard score can more easily be compared across subjects because the data are distributed on a similar scale. The normalized data were used to train the ANN models.

Next, two approaches investigated the prediction accuracy of 1) individual ANN models optimized for each subject, and 2) an "aggregated" ANN model that was trained with the data of all subjects. A feedforward ANN model was selected for both approaches, using the MATLAB Neural Network Toolbox. The same cross-validation techniques used in Chapter 2 were chosen for this analysis. The input and target matrices of each model were divided into training (70%), validation (15%), and testing (15%) groups. The weights and biases of each model were updated using a log-sigmoid activation function and the Levenberg-Marquardt algorithm until a minimum mean squared error (mse) was achieved.

The performances of each model were determined by how well the model was able to predict ankle impedance using the testing (15%) dataset. The metrics used to quantify the performances included the goodness of fit between the predicted and actual ankle impedance, which used the normalized mean squared error (NMSE) cost function, as shown in Eq. 3.6 as

$$NMSE = 1 - \frac{\left\| \bar{z}_{predicted} - \bar{z}_{actual} \right\|^2}{\left\| \bar{z}_{actual} - mean(\bar{z}_{actual}) \right\|^2}$$

3.6

59

where ‖ denotes the 2-norm, $\bar{z}_{predicted}$ is the array of predicted ankle impedance (stiffness, damping, and inertia) in DP and IE from the ANN model, and $\bar{z}_{actual}$ is the array of ankle impedance estimated from the parameter estimation in Section 3.3. A perfect fit between the predicted and actual impedance would result in a NMSE = 1.0. In addition, the mean absolute error (MAE) was selected as another metric, which used the mean and absolute values of the difference between the predicted and actual impedance, as

$$MAE = mean(|\bar{z}_{predicted} - \bar{z}_{actual}|)$$

<div align="right">3.7</div>

The MAE results are presented in the standard impedance units by reversing the z-score normalization and multiplying by the respective subject masses. This metric provides a perspective of the model error with respect to the actual ankle impedance range. The following sections describe additional training parameters selected for both modeling approaches, as well as the resulting model performance.

3.5.2   Individual ANN Models

The individual ANN models used the z-score normalized RMS EMG signals as the input matrix to the model, and six normalized ankle impedance parameters as the target matrix for cross-validation. The optimal number of hidden layer neurons for this model type was 40 neurons, determined through trial and error. The weights and biases for each neuron were optimized using cross-validation. The ANN model performances across all subjects can be found in Table 3-3. The stiffness in the DP impedance parameter has the highest overall performance, with an average NMSE of 0.98 ± 0.02. The lowest average NMSE reported was 0.93 ± 0.03 for the IE damping parameter. Interestingly, these results coincide with the parameters that had the highest and lowest number of significantly correlated EMG to impedance parameters, respectively (Table 3-2). However, even though the IE damping parameter had the weakest overall performance, the NMSE still showed that the ANN model could predict this impedance parameter with high accuracy. The total average NMSE error across all impedance parameter and all subjects is 0.96 ± 0.03. Furthermore, the average MAE across all subject models is also presented in Table 3-3. When compared to the range of the results shown in Figure 3-5, the error between the predicted and actual impedance was relatively small.

Table 3-3. Average (± standard deviation) NMSE and MAE results of the standing ankle impedance predictions from the individual subject ANN models.

Metric	DOF	K $\left(\frac{Nm}{rad}\right)$	B $\left(\frac{Nms}{rad}\right)$	J ($kg.m^2$)
NMSE (R²)	DP	0.983 ± 0.02	0.954 ± 0.02	0.956 ± 0.02
	IE	0.963 ± 0.03	0.931 ± 0.03	0.959 ± 0.03
MAE	DP	6.7 ± 1.3	$(36.6 \pm 11.3) \times 10^{-3}$	$(0.8 \pm 2.2) \times 10^{-3}$
	IE	3.6 ± 1.3	$(40.4 \pm 13.9) \times 10^{-3}$	$(4.2 \pm 2.0) \times 10^{-3}$

The results of this study improved slightly when compared to the results obtained in Chapter 2. Using the same ANN model technique, the non-loaded ankle impedance could be predicted with an average NMSE of 0.95 ± 0.05 in DP and 0.86 ± 0.11 in IE. For both non-loaded and loaded ankle impedance, the results of training an ANN model for each subject can predict ankle impedance with very high accuracy. One likely reason for the high performance is that the testing data was from the same subject as the training data, even though it was not used during the model training process. Additionally, the data used to train and test the model performance were collected from the same experiment. If the normalized RMS EMG data from a different subject were evaluated by the trained model, the performance of the impedance prediction decreased. To improve the performance of a model to unseen data, additional techniques were explored in the following sections.

3.5.3   Aggregated ANN Model

This approach tested if a single model could be trained with the data of all subjects. Even though the muscle activation and impedance parameters varied across subjects, the goal was to determine if the model could still maintain a high prediction performance. A single model, referred to as an aggregated model, was developed using the experimental data collected from 12 subjects.

Two types of input matrices were tested using this model. The first input matrix was similar to the individual models and used the z-score normalized RMS EMG data from the four muscles of all subjects. The second input matrix used the subjects' biometric information, including age, height, and weight, in addition to the normalized RMS EMG data, resulting in an input matrix with seven channels. The biometric data were z-score normalized across the population.

The target matrix for both input matrices used four normalized impedance parameters across all subjects, including the stiffness and damping in DP and IE. The inertia parameters were removed from the model training because it remained relatively constant and did not change with muscle activation. Next, using a trial and error technique, a model containing 100 neurons had the highest overall performance and was selected for analysis. Last, 70% of every trial was randomly selected to be the training matrix, 15% was selected for validation, and the remaining 15% was selected for testing. This ensured that all the muscle co-contraction trials and every subject were represented in each group.

Table 3-4 shows the NMSE and MAE performance from a single Aggregated ANN model in predicting the ankle impedance across the entire population. Also, the table includes the results from both types of input matrices. The results showed that the input matrix containing both the EMG and subject biometric information performed better than the input matrix with only the normalized RMS EMG information of all the subjects. The overall average NMSE was 0.79 for the "EMG only" input and 0.91 for the "EMG + Biometric" input, respectively. The latter regression model has a higher fitness likely because it accounts for the subjectivity in the EMG measurements. By adding additional input information that was dependent on each subject, the model could better predict the ankle impedance for each subject. Thus, adding other biometric variables, such as foot length, shank length, percent muscle mass, or percent body fat, could improve the estimation further.

Table 3-4. NMSE and MAE (± standard deviation) results of the standing ankle impedance predictions from the Aggregated ANN models.

Metric	DOF	EMG Input Only		EMG + Biometric Input	
		$K\left(\frac{Nm}{rad}\right)$	$B\left(\frac{Nms}{rad}\right)$	$K\left(\frac{Nm}{rad}\right)$	$B\left(\frac{Nms}{rad}\right)$
NMSE (R^2)	DP	0.896	0.763	0.955	0.897
	IE	0.810	0.688	0.917	0.874
MAE	DP	19.4 ± 4.5	0.09 ± 0.03	12.4 ± 3.6	0.06 ± 0.02
	IE	9.6 ± 4.0	0.10 ± 0.05	5.7 ± 2.1	0.06 ± 0.03

For the EMG and biometric data input model, the highest performance across the impedance parameters was the stiffness in DP, with a NMSE of 0.96 and a MAE of 12.4 ± 3.6 Nm/rad. The lowest-performing parameter, with a NMSE of 0.87 and MAE of 0.06 ± 0.03 Nms/rad, was again the damping in IE. The maximum difference between the average NMSE from the individual models, and the NMSE from the aggregated model was 0.06 for both the damping parameters in DP and IE, respectively. While the model performance was high, the aggregated model performance decreased slightly from the individual models. One explanation for the decreased performance is that there was noise in the ankle impedance estimation process and the RMS EMG signals across the subjects. It is possible that the aggregated model overfitted to some of the noise present in the impedance, which in turn impacted the model's ability to predict ankle impedance from unseen input data.

Overall, the performance of the aggregated ANN model showed that a single model, containing data from a range of subjects, can accurately predict multi-directional ankle impedance based on varying levels of muscle co-contraction. Additional measures to reduce the variance in the ankle impedance estimation and noise in the EMG signal could further improve the model performance. However, the performance of this model is still tested with data from the same subjects that were used during the training process. While the aggregated model can generalize to a wider variety of subject data, it is still unknown how such model would perform when a new subject is presented.

3.6   Investigation toward Subject-Independent Model

The results from the aggregated model prompted new questions toward the idea of generating a "subject-independent" model that is general and can accurately predict the ankle impedance of new subjects. A few of the main questions included: How many subjects are needed to train a model that can predict ankle impedance with a reasonable accuracy using unseen subject data? Will additional EMG features improve the generalizability of a model? Should biometric information about the subject be included? Is ANN the best regression option to use for a subject-independent model? The following section investigates some potential solutions to these questions.

3.6.1 Preliminary Investigation: Leave-one-subject-out Cross Validation

The individual and aggregated ANN models described in Section 3.5 tested the prediction accuracy of the model using the EMG data of subjects also used for training. Alternatively, the leave-one-subject-out technique reported in this section tested the prediction accuracy on subjects that were not used during training (unseen subjects). Specifically, the goal of this approach was (1) to determine if an ANN model can accurately predict ankle impedance using the muscle activity of an unseen subject and (2) to investigate how the model generalization improves with an increasing number of subjects used for training. The details of this process are described in Algorithm 3-1.

Algorithm 3-1: "Leave-one-subject- out" Technique for Varied ANN Model Sizes

1	Total number of subjects, $N_{sub} = 12$
2	for $ANN_{modelsize} = 2$ to $(N_{subj} - 1)$
3	for $S_{test} = 1$ to N_{sub}
4	$\mathbb{P} = \{ x \in \mathbb{N}^+ \mid x \leq N_{sub} \} - \{ S_{test} \}$
5	$r_{combo} = $ all combinations of size $ANN_{modelsize}$ from set $\mathbb{P}$
6	if $r_{combo} < 30$
7	Repeat r_{combo} until 30
8	else
9	Randomly select 30 of the total combinations
10	end
11	for $t = 1$ to 30 combinations
12	$NET = $ Generate ANN model using the subject data of $r_{combo}(t)$
13	Perform cross-validation (70% train – 15% validation – 15% test)
14	$Z_{predict}(S_{test}) = NET(EMG(S_{test}))$
15	end
16	end
17	$NMSE(ANN_{modelsize}) = $ goodnessoffit($Z_{predict}, Z_{target}$)
18	end

First, the total number of subjects used for this process N_{subj} was defined as 12 (line 1). Then, the number of subjects used to train an ANN model, defined as $ANN_{modelsize}$, was selected

to range from 2 subjects to 11 subjects (line 2). Within each model size, a second loop iterated through the leave-one-subject-out method (lines 3- 17), which sets aside the data of a single subject S_{test} from the entire population set, $\mathbb{P}$ (line 4). The S_{test} subject is later used as an unseen test subject for the ANN models. Next, the other 11 subjects of set $\mathbb{P}$ are used to determine all subset combinations of subjects with the size $ANN_{modelsize}$ (line 5). For example, for $ANN_{modelsize} = 2$ the total number of subset combinations of subjects from set $\mathbb{P}$ is equal to $\binom{11}{2} = 165$. If the total number of subset combinations (r_{combo}) is less than 30, the existing subsets are repeated until a total of 30 subsets are generated (lines 6-7). If the total number of subset combinations (r_{combo}) is greater than 30, 30 subsets are randomly selected (lines 8-10).

Next, an ANN model was generated for each of the 30 selected subject combinations (r_{combo}) (lines 11 − 15). Each ANN model was composed of four input neurons (normalized RMS EMG), a single hidden layer neuron, and four output neurons (stiffness and damping). The purpose of selecting only 30 subsets was to limit computational requirements (line 12). Additionally, a single hidden layer neuron was selected because it had the highest performance. Cross-validation was performed by dividing the selected subset data (out of the 30 subsets) into 70% training, 15% validation, and 15% testing (line 13). The resulting model was tested against the input EMG of the subject that was set aside (S_{test}). Last, the resulting overall NMSE was determined between the predicted and actual impedance for each model size and was saved for further analysis. This process was repeated for all 10 model sizes (1 vs. 2, 1 vs. 3, …, 1 vs. 11).
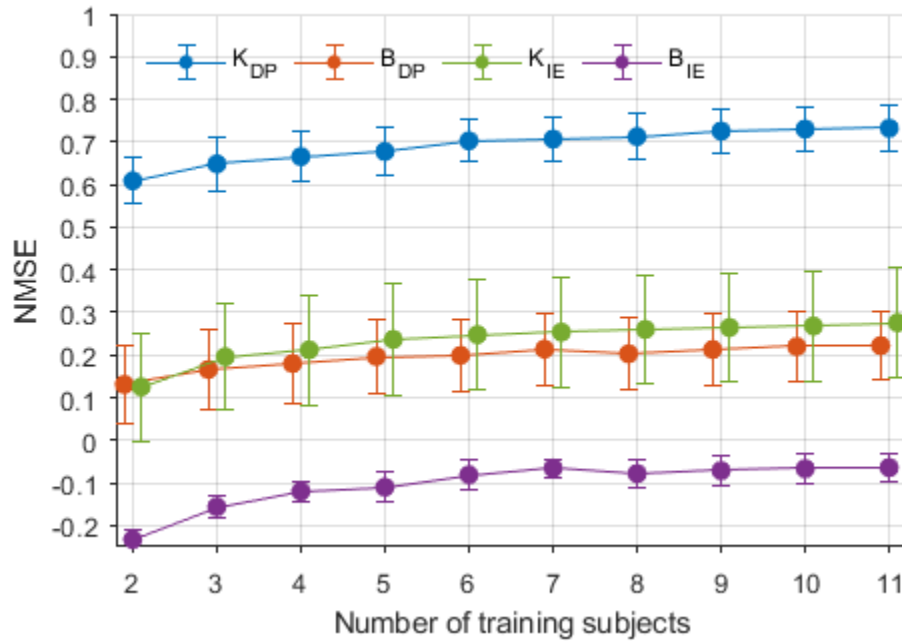
Figure 3-7. Average ± standard error NMSE for models with a subject-size between 2 to 11 subjects and unseen testing data. Results taken across 12 subjects.

Figure 3-7 shows the average NMSE for the ANN model sizes between 2 subjects up to 11 subjects, while each of the 12 subjects was used as the unseen testing data. The error bars represent the standard error of the 12 subjects. As the number of subjects used for model training grew, the average NMSE increased. Overall, the models that contained 11 subjects had the highest overall average NMSE. These models had an average (± standard deviation) of 0.69 ± 0.04 for KDP, 0.23 ± 0.05 for KIE, 0.19 ± 0.03 for BDP, and -0.10 ± 0.05 for BIE. A negative NMSE means that no relationship was determined between the EMG and ankle impedance.

When compared to the results from the individual and aggregated models, the average NMSE for the leave-one-subject-out technique decreased overall. However, as suggested by the increasing trend in Figure 3-7, the performance of the subject-independent models increased as more subjects were used during training. In fact, a few subjects reported NMSE values greater than 0.987 for the stiffness in DP and 0.814 for the stiffness in IE. These results suggest that if more subject data (> 12 subjects) were used to create a model, the prediction accuracy may continue to increase. The subject-independent model could have the potential to predict the ankle impedance from EMG measurements of subjects that did not have their ankle impedance experimentally characterized in a prior test.

66

Noticeably, the NMSE results for the damping parameters were less than the stiffness parameter results; with a poor NMSE overall. However, the damping parameters had very high NMSE for the individual and aggregated ANN models. A few reasons for the decreased performance could be that the change in damping parameters with muscle activity had very different trends across subjects. For example, some subjects had an increasing trend in the damping in IE with muscle activation level, while others had a decreasing or constant trend. Additionally, the ranges for the non-normalized damping parameters across all subjects were only 0.94 Nms/rad and 1.64 Nms/rad for the DP and IE directions, respectively. It is possible that the damping parameters in DP and IE did not change enough in amplitude, making it difficult for the model to differentiate changes in impedance using contraction levels. Last, the RMS features extracted from the EMG might not have been able to explain the damping parameters.

The results of the leave-one-subject-out tests showed potential for improvements in the EMG-impedance model. Other methods, in addition to ANN, should be considered to explore the feasibility of developing a generalized relationship between EMG and ankle impedance. Next, this chapter will explore the effects of additional EMG feature selections and examine additional regression modeling algorithms.

3.6.2   Feature Extraction and Regression

The signal processing techniques were updated from the methods described in Section 3.2.3. First, approximately 10% of the data were removed as outliers. As opposed to removing outliers based on only the impedance estimation performance, the outliers were selected based on both the EMG and impedance data for each trial. As described in Eq. 3.14, the standard deviation and mean of the EMG signals for each window of data were selected, as well as the corresponding impedance parameters. All vectors of m_i were z-score normalized to remove the mean value, and the distance squared of each row was determined (Eq. 3.15). Last, 10% of the rows with the largest distance squared within each trial i were removed.

$$m_i = \left[EMGSTD_{1-4}, EMGAVE_{1-4}, K_{DP,IE}, B_{DP,IE} \right]_{401x12} \qquad 3.8$$

$$(dist_i)^2 = \sum \left(\frac{m_i - \mu_{m_i}}{\sigma_{m_i}} \right)^2 \qquad 3.9$$

67

3.6.2.1 *EMG Feature Selection*

Next, the EMG features were extracted from each EMG channel. In the previous section, the RMS of the EMG signals were the only feature selected to train each ANN model. It is possible that the RMS does not contain all the relevant information within the EMG signal. This section investigated additional features, and determined if the model prediction accuracy could improve for a subject-independent model. Selecting the most relevant features has been known to simplify the dimensionality of the model, improve training time, increase generalization, and prevent the model from overfitting to the training data [135].

Table 3-5. The mathematical definitions of each EMG feature.

Feature	Equation	
Mean (AVE)	$\mu = \dfrac{1}{N} \sum\limits_{i=1}^{N} x_i$	*3.10*
Standard Deviation (STD)	$\sigma = \sqrt{\dfrac{1}{N-1} \sum\limits_{i=1}^{N} |x_i - \mu|^2}$	*3.11*
Mean Absolute Value (MAV)	$\bar{x} = \dfrac{1}{N} \sum\limits_{i=1}^{N} |x_i|$	*3.12*
Zero Crossings (ZC)	Number of occurrences where ($\{x_i > 0 \ \& \ x_{i+1} < 0\}$ or $\{x_i < 0 \ \& \ x_{i+1} > 0\}$) and $|x_i - x_{i+1}| \geq 1e-6$	*3.13*
Number of Slope Sign Changes (SSC)	Number of occurrences where ($\{x_i > x_{i-1} \ \& \ x_i > x_{i+1}\}$ or $\{x_i < x_{i-1} \ \& \ x_i < x_{i+1}\}$) and $|x_i - x_{i-1}| \geq 1e-6$ and $|x_i - x_{i+1}| \geq 1e-6$	*3.14*
Cumulative Signal Length (CL)	$len = \sum\limits_{i=1}^{N} |x_i - x_{i-1}|$	*3.15*

* Where x_i is the ith **sample of the** original EMG signal and N is the number of samples per window.

Six time-domain (TD) EMG features were selected to determine if their characteristics contained relevant information about the signal. The features chosen for this study include the

mean (AVE), standard deviation (STD), mean absolute value (MAV), number of zero crossings (ZC), number of slope sign changes (SSC), and the cumulative length of the signal (CL). These features are commonly used for EMG analysis [114], [116], [140]–[142]. Extraction of these features provides information about both the amplitude and frequency content of the EMG signals and could improve the ability of the model to distinguish the varying levels of muscle co-contraction. Table 3-6 contains the mathematical expression used to calculate each feature vector, where the EMG signal for each muscle is expressed as x.

Lastly, after the outliers were removed and the input feature vectors were generated, the EMG and ankle impedance were z-score normalized within each subject. The resulting input and output vectors for each subject had 1800 samples. When all the subjects were combined into a single matrix, the resulting dataset had 21600 samples for each feature.

3.6.2.2   *Regression Algorithm Selection*

In addition to the ANN model, the performance of additional regression techniques were explored. The purpose of this study was to determine if the prediction accuracy of the ankle impedance using the EMG signals from an unseen subject would perform better than the ANN results presented in Figure 3-7. The models ranged from simple, parametric least-squares linear regression to more complex, nonparametric models, such as Gaussian Process Regression. In addition, the ANN performance was also re-examined to understand the effects of the added EMG features. This work utilized the MATLAB Regression Learner App, *fitrlinear* function, and the Neural Network Fitting App to train and test the models across 12 subjects. The five regression models selected for this study included:

1.   Least Squares Linear Regression (LSQ)
2.   Least Squares linear regression with Lasso Regularization (LSQ + Reg)
3.   Medium Gaussian Support Vector Machine (SVM)
4.   Gaussian Process Regression with Matern 5/8 Kernel (GPR)
5.   Artificial Neural Network with 40 hidden layer neurons (ANN40)

3.6.2.3   *Performance Evaluation*

To understand the effects of the EMG features selection and the regression models, two tests were performed. First, the sensitivity of the model performance to the number of EMG feature vectors was examined. Four different sized input vectors were tested, including: 4 – STD

features, 8 – STD + AVE features, 16 – MAV + ZC + SSC + CL features, and 24 – STD + MEAN + MAV + ZC + SSC + CL features. Each feature was extracted four times, once for each muscle channel. Furthermore, the second test used the input vectors containing 4, 8, 16, and 24 features to test the performance of the five regression models (LSQ, LSQ + Reg, SVM, GPR, and ANN40). To limit the computational expense, the input and target matrices were down sampled by a factor of 10 to train the GPR models.

Both the feature extraction and regression model selection tests were implemented using the aggregated and Leave-one-subject-out validation techniques. For the aggregated model, 5-fold cross validation was performed across the data of the entire population. This process randomly selected 80% of the data to train a regression model and 20% to test the performance. Next, this process was repeated five times. Additionally, for the Leave-one-subject-out technique the models were generated using the data of 11 out of 12 subjects. The 12th subject was used to test the model performance. A total of 12 models for each regression algorithm were generated so that all the subjects were used as the unseen input. The performance for each model was quantified using the NMSE between the predicted and experimentally determined impedance across the entire population. Additionally, the MAE was also determined for each individual subject.

3.6.3   Model Performance

3.6.3.1   *Aggregated Regression Models*

Figure 3-8 presents the MAE ± standard deviation and NMSE between predicted and actual ankle impedance for an aggregated regression model. The x-axis of each subplot contains the results for each input matrix size, where the Roman numeral I denotes 4 features, II denotes 8 features, III denotes 16 features, and IV denotes 24 features. As a reference for the MAE, the average and standard deviation across all five activation levels and across all subjects were 258.2 ± 83.0 Nm/rad for KDP, 126.3 ± 22.9 Nm/rad for KIE, 0.79 ± 0.10 Nms/rad for BDP, and 0.31 ± 0.07 Nms/rad for BIE, respectively.
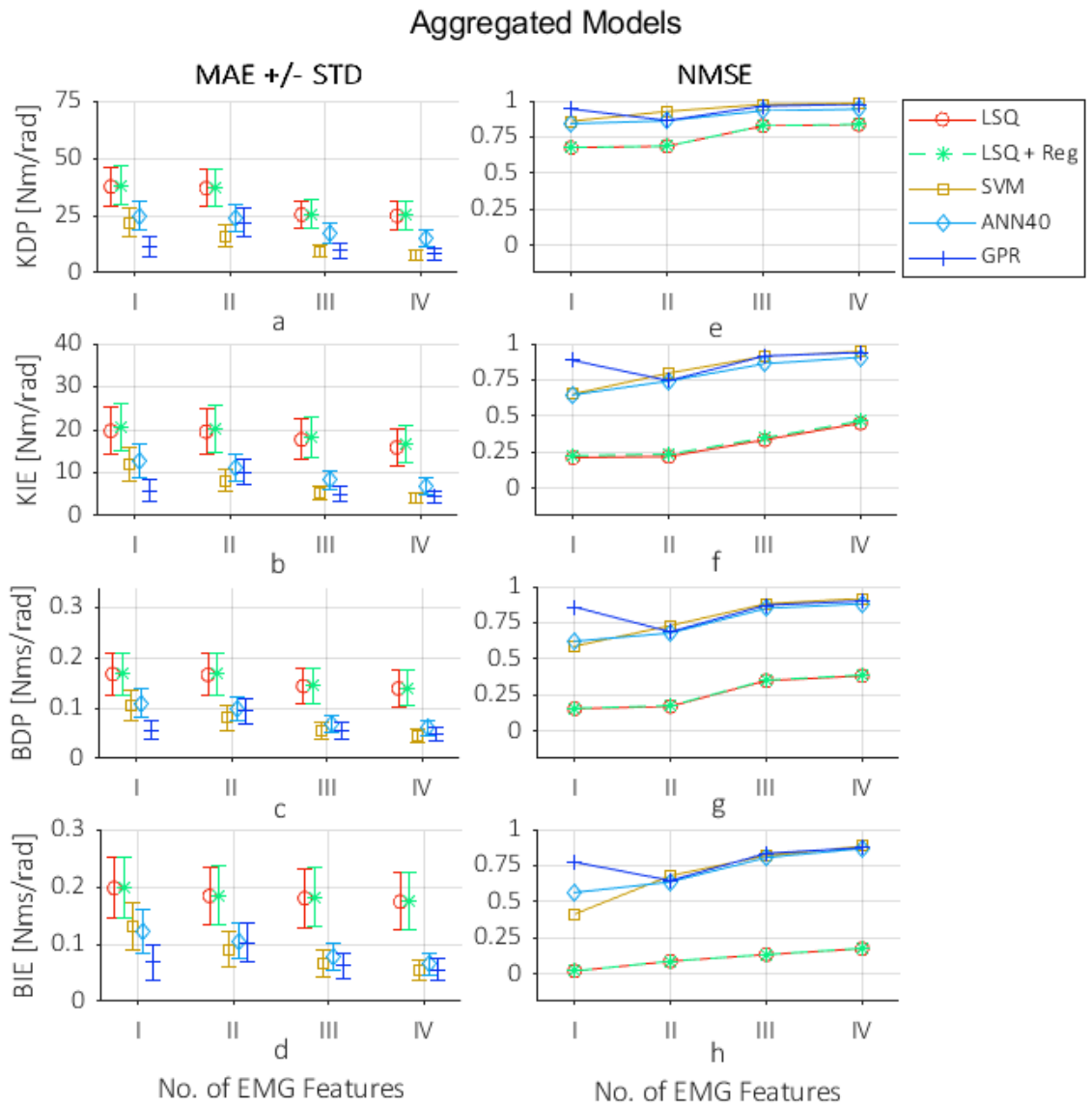
Aggregated Models

Figure 3-8. The MAE ± standard deviation (a – d) and NMSE (e – h) performances of the aggregated regression models for varied number of EMG feature inputs and regression models. The Roman numerals I – IV correspond to input matrices of size 4 – 24.

First, as the number of the TD input feature vectors grew, the performance of the regression algorithms generally improved. The model input matrix containing 24 vectors (4 muscles x 6 TD features) had the highest overall performance for the SVM model, with NMSE of 0.98, 0.95, 0.92, and 0.88 for the KDP, KIE, BDP, and BIE predictions, respectively. In addition, this model reported the smallest MAE with values of 7.9 ± 7.4 Nm/rad, 4.1 ± 4.3 Nm/rad , 0.05 ± 0.05 Nms/rad and 0.05 ± 0.06 Nms/rad for the KDP, KIE, BDP, and BIE parameters, respectively.

71

Additionally, the results from the GPR and ANN algorithms performed similar to the SVM algorithm, where the performance increased as the input matrix used more EMG features. Due to extensive training time requirements, the GPR model was trained with a down sampled dataset. It is possible that the performance of this method could increase further when trained with the total dataset. Furthermore, the ANN model, trained with a hidden layer with 40 neurons, showed increased performance from the preliminary tests found in Section 3.6.3.1. When compared to the RMS EMG input matrix results, all four impedance parameters showed an increase in NMSE.

The algorithms with the worst overall performances were LSQ and LSQ + Reg. While these models did show an increasing performance as the input matrix added more features, the highest NMSE for these features were only 0.84 for KDP, 0.47 for KIE, 0.39 for BDP, and 0.18 for BIE, respectively. The performance for KDP was reasonably high; however, the ability for the models to predict the stiffness in IE, and damping parameters were not as successful. For these parameters, the LSQ and LSQ + Reg were not able to find a strong relationship with varying levels of muscle co-contraction. Similar to the results from the linear correlation test, it is possible that a more complex regression model is needed to determine the relationship between impedance and muscle co-contraction, when presented with the data of multiple subjects.

3.6.3.2   *Leave-one-subject-out Regression Models*

Next, the resulting NMSE and MAE for each regression algorithm using the Leave-one-subject-out training technique is presented in Figure 3-9. This method used 12-fold cross validation, where each subject was used as the testing dataset, and was repeated for all the regression algorithms. Interestingly, the highest NMSE for all impedance parameters was found using the Least Squares with Lasso Regularization model, even though this model showed the worst performance for the Aggregated model. A NMSE of 0.78 and a MAE of 29.1 ± 23.3 Nm/rad were reported for the KDP direction. These results were slightly higher than the performance of the LSQ for KDP, with a NMSE of 0.77. When compared to the preliminary leave-one-subject-out test from Figure 3-7, the NMSE performance improved by an increase of almost 0.1. Furthermore, for the KDP impedance parameter, all five regression algorithms increased the NMSE and decreased the MAE as the number of EMG features increased from 4 features to 24 features; suggesting that the additional features improved the generalizability for this particular parameter.

Surprisingly, the model performance for the KDP was the only parameter to show a relatively high NMSE across the four inputs. The other parameters showed very poor performance for the leave-one-subject-out method, with a NMSE less than 0.25 for KIE, and less than or equal to zero for both damping parameters. The low performance could be explained by differences in the way that the impedance parameters changed with muscle activity across subjects. When new subject information was entered to the model, it was not able to accurately predict the impedance. Another possible reason for the low performance is that these ankle impedance parameters did not vary enough with muscle activity for some subjects, and the model was not able to predict the unchanging or small trends.

Last, the ANN model performance was lower than the other algorithms. When compared to the ANN results presented in Figure 3-7, the NMSE for the stiffness in DP decreased slightly, with a maximum NMSE of 0.66 for the 16 input features model. It could be possible that the ANN models were too complex, resulting in a model overfitting to the training data. When the model is presented with new subject data, the prediction accuracy of the model decreases. For this reason, it is possible that the least-squares algorithm was advantageous because it was not able to fit the additional noise.
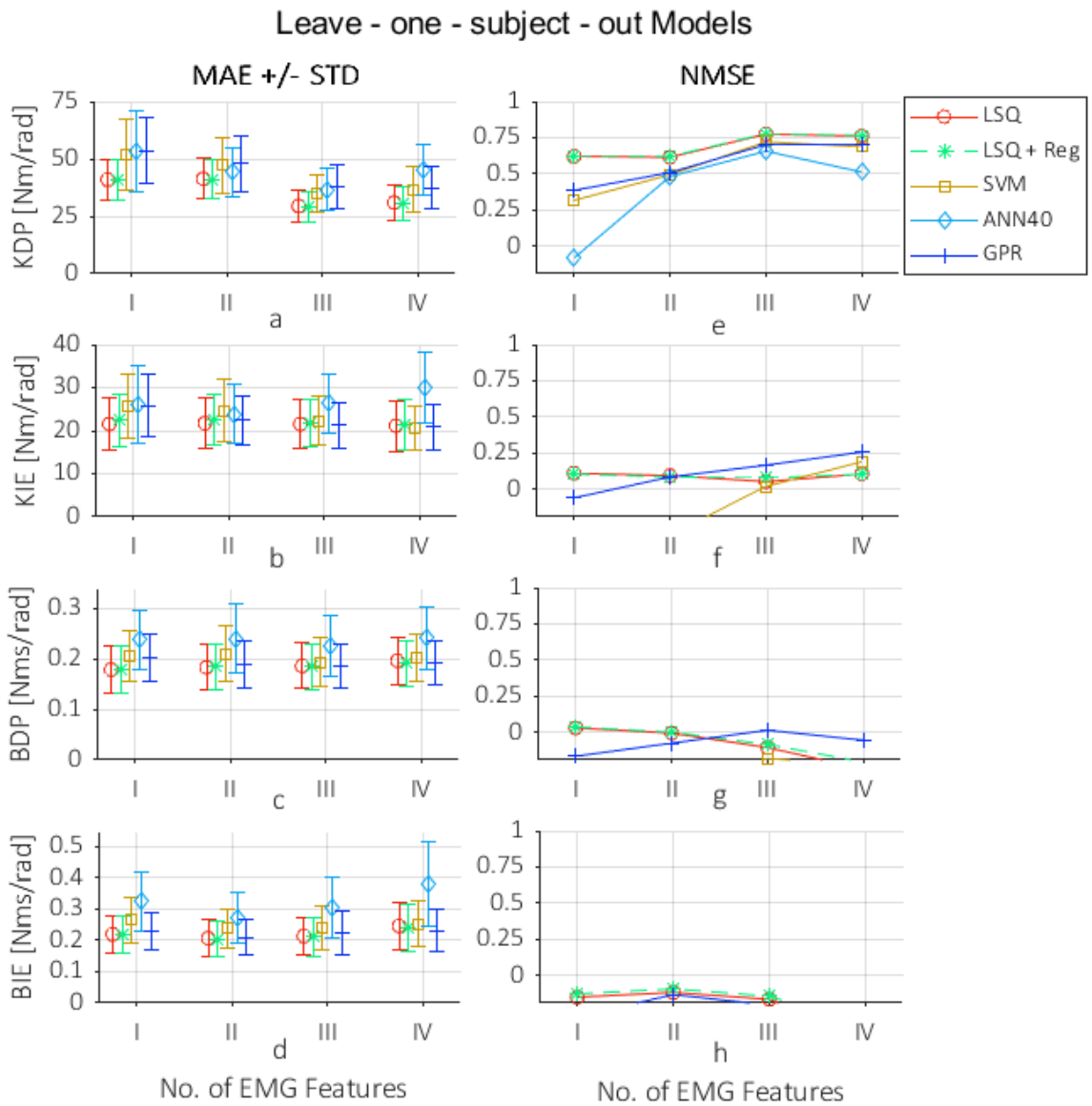
Figure 3-9. The MAE (a − d) and NMSE (e − h) performances of the leave-one-subject-out models for varied number of EMG feature inputs and regression models.

3.7 Discussion

This chapter presented the results of a novel experiment that quantified the multi-directional ankle impedance while subjects were standing and actively co-contracting the muscles of their lower extremity. The purpose of this study was to quantify the relationship between the level of muscle activation and the ankle impedance, described by the ankle stiffness and damping parameters, using regression modeling techniques. First, this study determined the linear correlation between each of the four muscles and the corresponding ankle impedance parameters. It was determined that less than 20% of the EMG to impedance parameter combinations showed a significant linear correlation.

To expand upon these results, additional regression modeling techniques were explored. First, ANN was used to generate 1) individual models for each subject and 2) an aggregated model containing data from the entire subject population. The model performance for both techniques showed average NMSE greater than 0.93 for the individual models and 0.87 for the aggregated model. These NMSE scores demonstrated that both model types could predict the ankle impedance for a given subject with high accuracy. However, when presented with EMG information from subjects not used during the model training, these models did not perform well.

Implications toward a subject-independent model were also investigated. Various regression models were tested to determine if they could predict ankle impedance using the EMG information of a subject not used in the training of the model. Factors such as the number of subjects included during the training process, EMG feature selection, and the regression algorithms were explored in this study. It was determined that model prediction improved when the data of more subjects was used to generate a model, with the highest prediction accuracy being a model size of 11 subjects. Additionally, using more features extracted from the EMG signals also improved model performance. Last, this study determined that simpler models, such a Least Squares linear regression with regularization, might be able to generalize better to new subject inputs.

The major advantage of generating a subject-independent model is that the ankle impedance could be predicted within a reasonable accuracy without needing to perform time-expensive experiments that require specialized equipment. In an ideal scenario, an accurate model could predict the ankle impedance in DP and IE, using only the EMG measurements. This idea has the

potential to determine a user's intent to improve the control of active prostheses. However, as shown by the results presented in this paper, there are still many challenges that need to be overcome to achieve this goal.

One limiting factor in the generalized model performance is that there is variability in both the ankle impedance and muscle activation levels across the subjects. As an example, the performance for the KIE, BDP, and BIE parameters from the leave-one-subject-out method showed low NMSE. A closer look showed that some subjects had damping parameters that increased with muscle activity, while others showed decreasing or constant trends. The different trends could make it difficult for the model to generalize across subjects. Additionally, this study was limited to exploring model performance using the data of only 12 subjects. A few questions pertaining to model accuracy improvements include: Will the model accuracy improve if more subjects are used during model training? How many subjects are needed for improvements?

Future implications will look to improve the generalization abilities for a subject-independent model that can relate lower extremity muscle activation. In addition, this study was performed during a stationary standing procedure, where muscles were co-contracted. Applications of the specific models generated by this study would lay the groundwork toward a more complex and realistic scenario, such as relating the muscle activity and ankle impedance dynamic walking and other time-varying maneuvers. With this goal in mind, the next chapter describes the next steps toward achieving this goal using a new experiment.

4 Variation of Ankle Impedance and Muscle Activity with the Center of Pressure during Standing

4.1 Motivation

The work presented in this dissertation thus far has focused on the study of ankle impedance while the lower extremity muscles were co-contracted to different activation levels. As the muscle activity changed, the corresponding ankle impedance also varied. However, during these studies, the mean ankle angle remained relatively constant while small perturbations were applied. Moving forward, the work presented in this chapter explores how both ankle impedance and muscle activity adapts to different mean ankle angles and ankle torques. For this experiment, the subjects were not asked to actively co-contract their muscles; but rather maintain a constant ankle torque while standing in various poses. The resulting muscle activity and impedance were determined while the subjects maintained their balance in the stationary pose. The subject's center of pressure (COP) location, with respect to the length of their foot, was used as a visual reference in order to sustain a constant ankle torque.

Previous work that has studied the ankle impedance as a function of the COP of the foot were focused on understanding how the body maintains an upright, stable posture. One study analyzed the ankle impedance while the subjects shifted their COP away from the neutral position during standing [66]. They determined that the ankle stiffness increased when the ankle angle moved away from the neutral position and when there was an active increase in ankle torque [66]. Another study determined that the ankle stiffness increased linearly as the COP location moved from the heel of the foot closer to the toes [67]. Furthermore, the muscle activity of the TA and GA muscles varied as perturbations were applied and the COP moved forward during standing.

Similar to the changing ankle impedance caused by standing sway, the ankle impedance also varies across the gait cycle [78], [79], [83]. Typically, the gait cycle is divided into two phases: 1) the stance phase, which includes the initial contact of the foot with the ground, mid-stance, and terminal stance, and 2) the swing phase, which is also divided into initial, mid, and terminal swing sub-phases. During straight walk, the ankle impedance typically has lower stiffness and damping parameters during the swing phase, but the parameters drastically increase throughout the stance

phase [79]. The purpose of this study was to explore the tonic muscle activity and the ankle impedance of unimpaired subjects while they stood in poses that resembled the stages within the stance phase of the gait cycle.

This chapter is organized as follows: Section 4.2 describes the experimental setup, procedure, and data acquisition techniques. Section 4.3 provides analytical explanations of the measured muscle activity, ankle kinematics, and ankle kinetic data. Section 4.4 describes the standing ankle impedance estimation technique, which was developed further from previous methods. Last, Section 4.5 explains how the results of this work are comparable to walking scenarios.

4.2   Experimental Study

A total of 15 male subjects were recruited for this study. All subjects had no self-reported previous musculoskeletal injuries and gave written consent to participate as approved by the Michigan Technological University Institutional Review Board (IRB). Table 4-1 includes the physiological data across the subject population; including the age, mass, height, and foot length.

Table 4-1. Subject physiological data for the standing experiment.

Age	Mass (kg)	Height (cm)	Foot Length (cm)
28.0 ± 4.3	79.0 ± 10.7	178.0 ± 7.7	26.5 ± 1.4

4.2.1   Set-up

The experimental setup used to determine the standing ankle impedance and measure lower extremity muscle activity was the same as the setup described in Chapter 3. A developed instrumented walkway consisting of motion capture cameras (8 – Optitrack 17W) and a force plate (Kistler 9260AA3) mounted on a vibrating platform were used. During an experiment, the subject stood with one foot on top of the force plate, and the vibrating platform applied perturbations to the ankle in both the sagittal (DP) and frontal (IE) anatomical planes. The motion capture cameras and force plate systems recorded data with sampling rates of 350 Hz.

Additionally, the experiment measured the muscle activity of five muscle that surround the ankle using wireless EMG sensors (Delsys Trigno wireless). The muscles selected for this study included the tibialis anterior (TA), peroneus longus (PL), soleus (SOL), gastrocnemius lateral (GAL),

and gastrocnemius medial (GAM). The muscles selected differed slightly from the procedure in Chapter 3 to include measurements from both heads of the gastrocnemius. While both the GAL and GAM muscles typically work together to plantarflex the ankle, this study aimed to investigate the contribution of each muscle head throughout the standing experiments. In addition, it was hypothesized that additional muscle data from the EMG activity could improve an EMG-ankle impedance model. All EMG data were recorded with a sampling rate of 2000 Hz.

4.2.2   Procedure

The experiment consisted of 12 trials, where subjects stood in one out of four poses. As shown in Figure 4-1, the four poses analyzed in the study were Flat Foot (FF), Midstance (MS), Post-Mid-Stance (MS+), and Terminal Stance (TS). These stationary standing poses varied the subject's ankle angle and COP of the foot, as shown by the red dot, and resembled different stages within the stance phase of walking. Three trials were performed for each pose, and the trials were selected in random order. The duration of each trial lasted 30 seconds, and adequate rest (> 1 min) was given in between each trial.
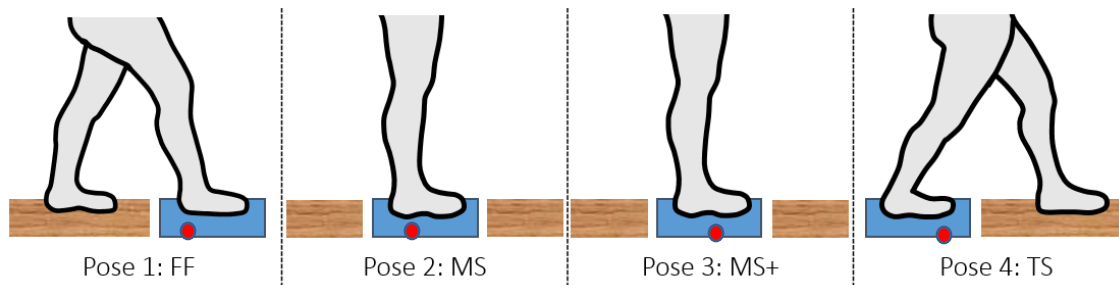
Figure 4-1. Four stationary poses that resembled stages within the stance phase of the gait cycle, including 1) Flatfoot (FF), 2) Mid-stance (MS), 3) Post-Mid-Stance (MS+), and 4) Terminal Stance (TS). The red dot represents the varying COP.

To maintain consistency across the trials, the foot location, COP position, and weight distribution between feet were observed. The placement of the subject's right foot was marked on the force plate to ensure that the foot was positioned in the same location for every trial. In addition, the stance length, defined by the anterior-posterior distance between the left and right feet, was determined to be 40% of the subject's height. For the FF and TS poses, the stance length of the subject determined the placement of the left foot with respect to the right foot on the force plate. Last, the subjects were provided with real-time feedback of their COP on a monitor. The feedback included the target COP location, actual COP location, and the subject's weight

distribution between their left and right feet. The target COP locations for the FF, MS, MS+, and TS poses were 30.6%, 40.5%, 53.0%, and 63.6% of the subject's foot length, respectively.

During each trial, the vibrating platform applied perturbations to the right foot, and the resulting ground reaction torques, ground reaction forces, ankle angles, and EMG activity were recorded. The perturbations were in the form of random pulse trains that varied in frequency (5 – 33 Hz) and axis of rotation (0 – 360°). In addition, the duration and the time in between pulse trains varied between 0.9 – 1.1 seconds. The use of random time durations and pauses were intended to prevent the subjects from predicting when the next perturbations would occur, which could cause overcompensation of their muscles. An example of the measured ankle torque and ankle angle for the TS pose in response to the pulse train perturbations in DP and IE directions is shown in Figure 4-2. This figure cropped the period of time in between pulse trains for visualization purposes.
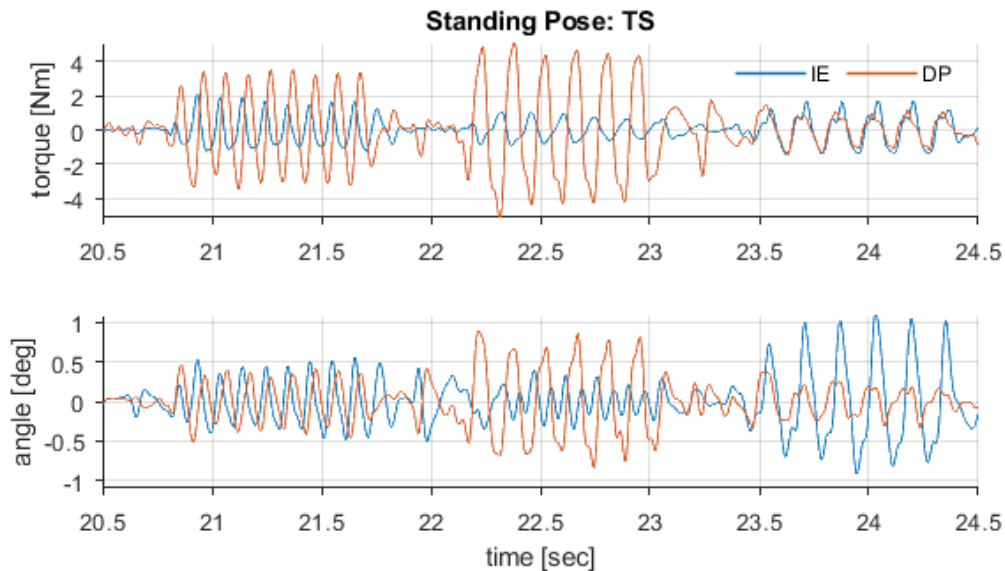
Figure 4-2. The (a) ankle torque and (b) ankle angle measurements from an example trial in IE (blue) and DP (red).

4.2.3   Data Acquisition

To estimate the ankle impedance, the ankle torque and ankle angle measurements were band-pass filtered between 3-35 Hz using a 5th order Butterworth filter. This filter was selected to remove the effects of the low-frequency ankle torque, due to the body sway, and higher-frequency measurement noise. For every pulse train, the first 0.8 seconds of data were selected from the start of the perturbation for the identification of ankle impedance. Additionally, the numerical

derivatives of the motion capture data were determined using the Savitzky-Golay filter, with a 5th order polynomial and 0.04-second windows. The ankle impedance estimation method is described in the following section.

In addition, the COP for each pose along the anterior-posterior direction (defined by the x-axis) was determined from the forces F_P^Y acting in the vertical direction (along $y-axis$) and the torques T_P^Z generated about the z-axis, which correspond to dorsi-plantarflexion (DP). These forces and torques were measured from the force plate, respectively, and are described in Eq. 4.1.

$$COP_x = (T_P^Z/F_P^Y - r_{P.heel}) /L_{foot}$$
4.1

where $r_{P,heel}$ is the distance from the heel to the center of the force plate and L_{foot} is the length of the subject's foot. This parameter was provided as feedback to the subject during each trial. The visual COP measurements ensured that each subject maintained a constant ankle torque within each of the four poses and that the torques remained consistent across repeated trials.

The EMG data were also divided into windows, corresponding to the beginning of a pulse train and the ankle torque and angle measurements. Similar to the previous chapters, each window of the EMG signals was bandpass filtered between 65 and 200 Hz using a 500th order FIR filter. Next, the EMG signals were z-score normalized within the subject to remove the mean and standardize the signal scale. Both time domain and frequency domain analyses were performed to understand how the muscle activity changed according to the standing pose.

4.3 EMG and Ankle Response vs. Standing Pose

The average COP positions across all subjects for the FF, MS, MS+, and TS standing poses were 28.1 ± 1.6%, 40.7 ± 1.2%, 52.7 ± 2.0%, and 64.9 ± 2.9% of the foot length, respectively, and were within the target COP positions of 30.6%, 40.5%, 53.0%, and 63.6%, respectively. Additionally, the small standard deviations of the COP showed that the trials were repeatable across all subjects.

As the COP position moved forward, the ankle angle and ankle torque in the DP direction increased, as shown in Figure 4-3a. Across all subjects, the ankle torque in DP, shown by the blue boxplots, monotonically increased with mean ankle torque values of 4.8 ± 3.1 Nm, 19.7 ± 3.3 Nm, 31.4 ± 6.0 Nm, 47.5 ± 8.9 Nm for the FF, MS, MS+, and TS poses, respectively. Additionally, the DP

ankle angle, represented by the orange boxplots, shows the ankle angle for each pose with respect to the angle of the ankle during neutral standing. The resulting average angles across the population were -11.9 ± 3.4° (FF), 0.54 ± 3.0° (MS), 1.8 ± 3.7° (MS+), and 10.8 ±2.8° (TS). For the MS and MS+ poses, the ankle angles remained relatively constant and close to the neutral angle, even though the torques increased. During MS+ pose, the subjects stood in the same position as the MS pose, but actively shifted their COP forward toward their toes.
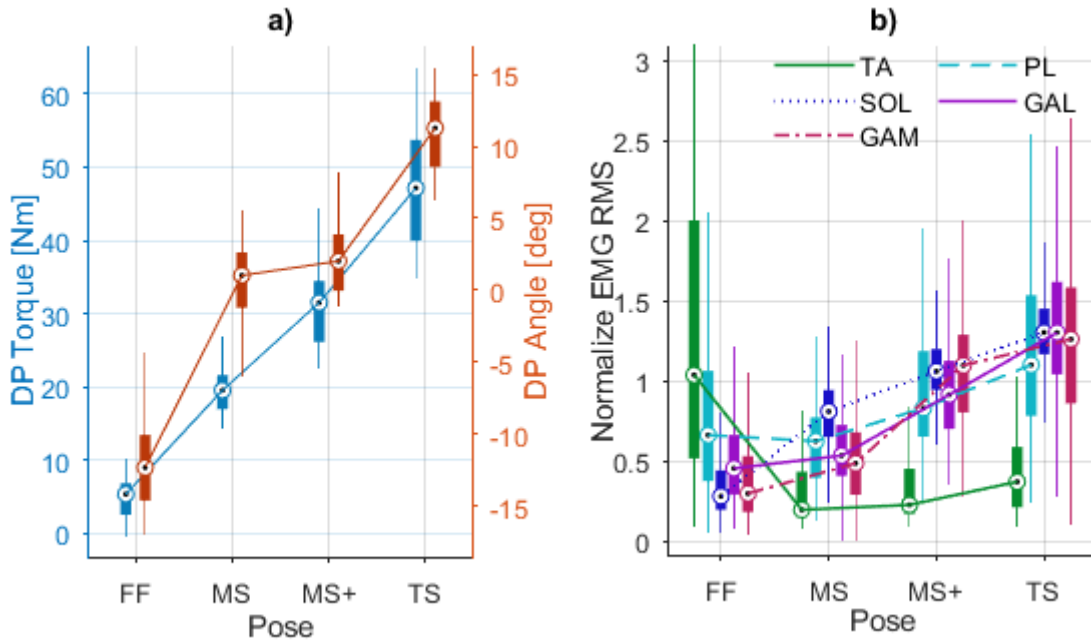
Figure 4-3. The boxplots of the (a) the average ankle angle (orange) and ankle torque (blue) in DP across subjects for each standing pose and (b) the normalized RMS of the EMG signals for the TA (green), PL (light blue), SOL (blue), GAL (purple), and GAM (red) muscles across all subjects.

Furthermore, Figure 4-3b shows the boxplots containing the RMS of the z-score normalized EMG signals for the TA, PL, SOL, GAL, and GAM muscles across all subjects. The SOL, GAL, and GAM muscles showed increasing trends as the COP was shifted forward for each pose. Additionally, the range of the muscle signals across subjects grew substantially as the COP moved toward the TS pose. The PL muscle contractions remained relatively constant for the FF and MS poses, and then increased as the COP moved forward for the MS+ and TS poses. Interestingly, the TA showed the opposite trend, where the highest TA measurements were recorded during the FF pose and became very small for the other three poses.

To further explore the differences in muscle activity across the poses, the average power spectral densities (PSD) of each muscle and subject were determined. All the pulse trains from a single subject and a single pose were selected. The Welch's power spectral density function was used to determine the PSD of the normalized EMG signals for each pose. The parameters selected for this method included a Hanning window with a size of 1000 samples and no overlap. Once the PSD was determined, the magnitude of the curve at 100 Hz was selected for analysis. This frequency was selected because of its large and consistent magnitude across all subjects. This process was repeated for each subject (15), pose (4), and muscle (5); resulting in a total of 300 samples from the magnitude at 100 Hz. All trials were multiplied by the average magnitude across the population to remain in units of volts.

Next, Figure 4-4 shows the average and standard deviation of the PSD magnitudes at 100 Hz, across the population. Similarly, the average amplitudes and standard deviations for each muscle followed similar trends to the RMS boxplots in Figure 4-3b. The TA muscle had the highest average magnitude for the FF pose. The PL muscle was also active during the FF pose, and reduced in activity for the MS pose. However, the PL then increased for the MS+ and TS poses. The average PSD for the other three muscles, including the SOL, GAL, and GAM, increased as the COP shifted forward.

A one-way Analysis of Variance (ANOVA) test was performed for each muscle to determine if significant differences (p-value < 0.01) existed across the four poses. Significant differences, denoted by the asterisk, were determined between the first pose (FF) of the TA muscle and all the other the MS, MS+ and TS poses (p-value < 0.001). Additionally, a significant difference was determined across all poses for the SOL muscle (p-value < 0.0001). Last, the PL, GAL, and GAM muscles showed some significant differences across the four poses.
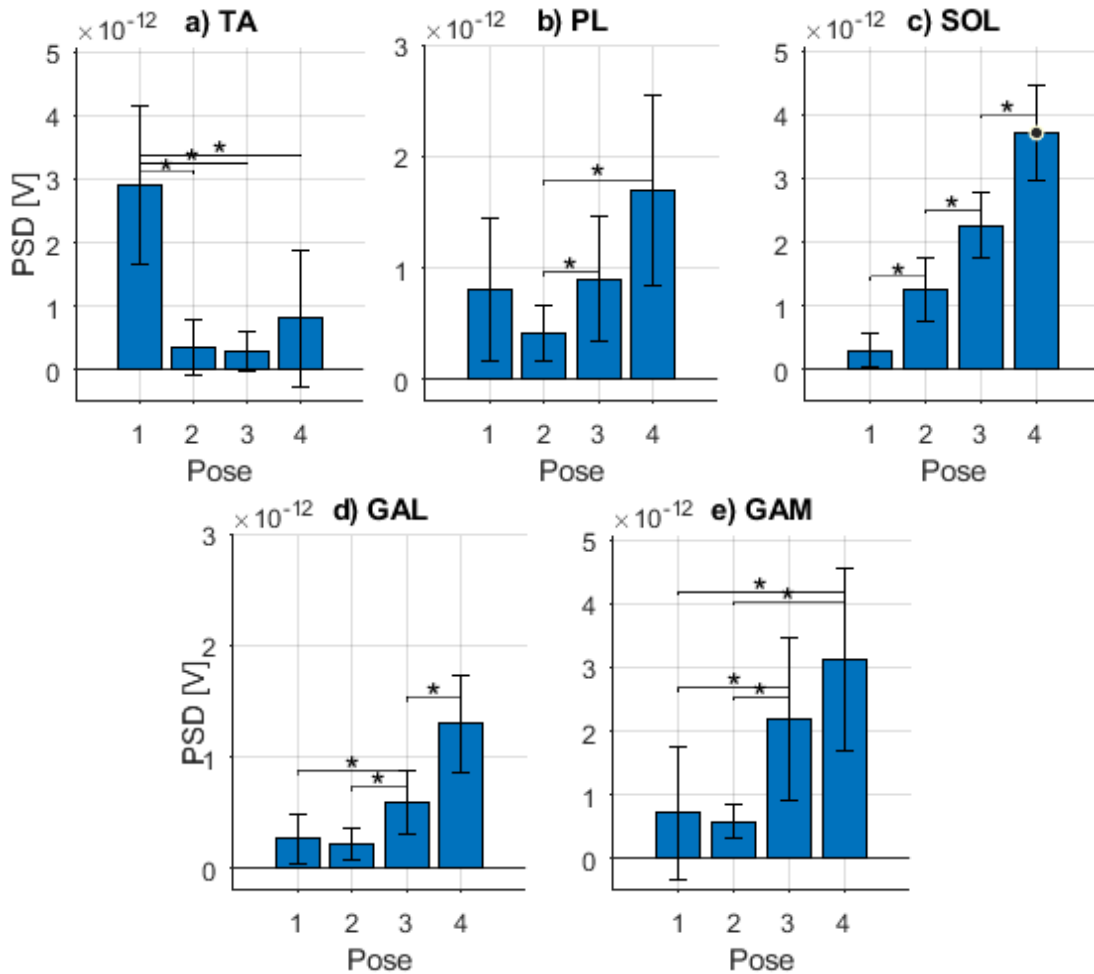
*Figure 4-4. Average PSD at 100 Hz across all subjects for the four poses: FF, MS, MS+, and TS. Significant different in EMG activity across poses (p < 0.01) are denoted by *.*

The EMG muscle activity presented in Figure 4-3 and Figure 4-4 resembled patterns similar to the muscle activation patterns across the gait cycle [143], [144]. During the early stance phase of the gait cycle, which corresponds to the FF pose, the TA muscle reported to have the highest amount of activity, followed by a continuous decrease in activity throughout the rest of the stance phase. Additionally, during the swing phase and early stance, the plantar flexor muscles (PL, SOL, GAL, and GAM) have very little activity, which is similar to the results presented in this chapter for the stationary poses. During the mid-stance and terminal phases of walking, which correspond to the MS, MS+, and TS poses, the activity of the plantar flexor muscles increased until the foot pushed off from the ground.

الـمنـارة للاستشارات

www.manaraa.com

4.4 Standing Ankle Impedance Estimation

To estimate the standing ankle impedance, the system identification technique was performed in two stages. First, the inertia of the force plate was determined using a dynamic model of the system. A test was performed with only the force plate module, where stochastic perturbations were applied to the force plate, and the resulting force plate angles, forces, and torques were recorded. The measured torques were used to fit a nonlinear model and to estimate the inertia of the vibrating force plate system.

Next, the resulting compensated external torques were used with the linear model of the ankle, where the predictors of this equation were ankle angle, ankle velocity, ankle acceleration, and the kinematics of the foot. The corresponding ankle impedance parameters, including the ankle stiffness and damping in DP and IE, were solved using least squares optimization method. A single impedance parameter was determined for each pose for the DP and IE directions. Additionally, for this study only the pulse trains aligned with DP or IE directions were selected to be used in the impedance estimation. Future work will look to quantify the anisotropic ankle impedance about all perturbation axes (0 - 360°).

Figure 4-5 shows the resulting average ankle stiffness, damping, inertia, and % VAF across all subjects for four standing poses. The stiffness in DP increased linearly as the COP shifted forward. Additionally, the standard deviation for both the DP and IE stiffness were relatively small across subjects. The other parameters, including stiffness in IE, and damping in DP and IE did not show an increasing trend with COP position. This is likely because the majority of the torque and angle changes were in the DP direction. Some of the damping and inertia parameters resulted in negative values, suggesting the presence of more complex ankle dynamics, including both the intrinsic (passive) and reflexive (active) components of the impedance.
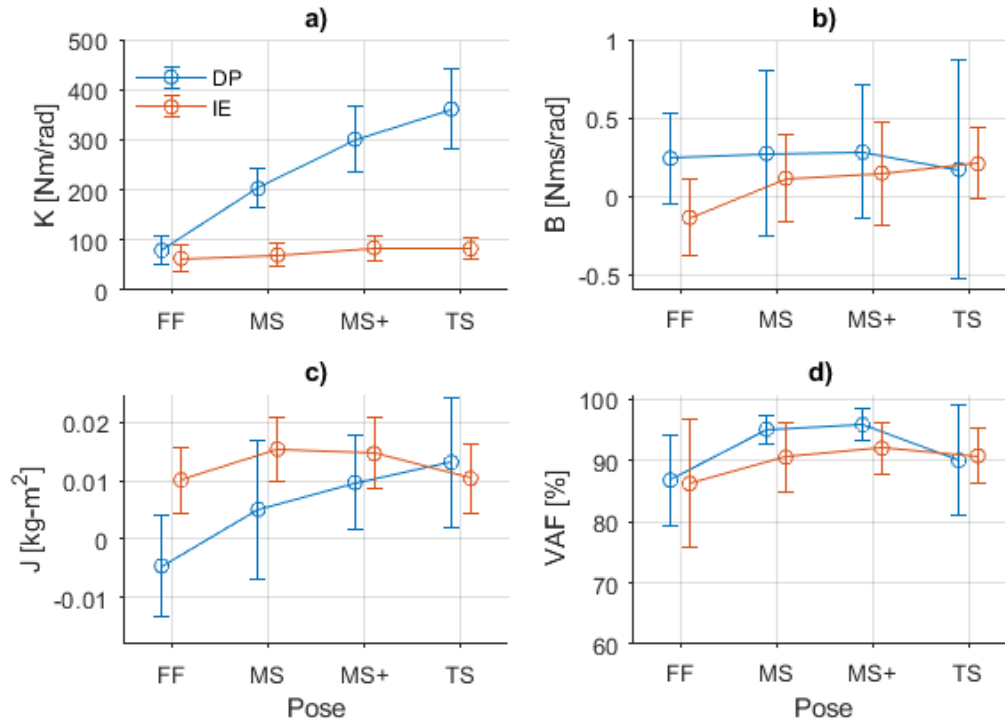
Figure 4-5. Average (± standard deviation) ankle a) stiffness, b) damping and c) inertia across four standing poses. The results in d) show the average VAF across all the 15 subjects.

Last, the VAF of the impedance estimation was high across the four poses, with average values for DP and IE of 86.6 ± 8.9%, 92.8 ± 4.0%, 93.9 ± 3.3%, and 90.4 ± 6.8% for the FF, MS, MS+, and TS poses, respectively. The VAF was slightly lower for the first pose (FF) for both the DP and IE estimates. The decrease in prediction accuracy could be because this pose was more difficult for the subject to maintain a constant COP. The less stable pose might have added variance to the ankle impedance estimation.

4.5 Discussion

The purpose of this study was to understand how the ankle impedance and muscle activity change during different standing poses, with varied ankle angles and angle torques. The stationary standing poses were selected to resemble the ankle angle during the stance phase of the gait cycle; including the early stance phase, where the foot comes in contact with the ground (FF), mid stance (MS), post mid stance (MS+), and terminal stance (TS) – just before the foot pushes off from the ground. The study determined that the ankle torque and ankle stiffness increased monotonically as the COP was shifted from the FF pose to the TS pose. In addition, the muscle activity of the TA,

PL, SOL, GAL, and GAM muscle significantly changed throughout difference poses. Interestingly, the muscle activity in each pose closely resembled the activation pattern during the stance phase of the gait cycle.

In this study, the COP moved along the anterior-posterior direction, in parallel to the sagittal plane. The resulting ankle torque and ankle impedance showed strong correlations in this direction. However, the resulting ankle impedance in IE remained relatively constant throughout the experiment. During the development of the experimental procedure, shifting the COP of the foot along the frontal plane during standing was found to be a difficult task for the subjects. It would not have been easily repeatable throughout the trials, so this study focused only on varying the COP in the anterior-posterior direction. Future work will look for more consistent and reproducible protocols to move the COP in the lateral directions and to understand how the ankle and lower extremity muscles behave.

Additionally, a model of the ankle impedance and EMG activity was not determined during this study. Future work will analyze the ankle impedance and EMG for the pulse train perturbations that perturbed a combination of the DP and IE ankle directions.

www.manaraa.com

5   Conclusion & Future Work

5.1   Overview

The presented work investigates the relationship between the lower extremity muscle activities to the mechanical impedance of the ankle. This relationship was studied about multiple degrees-of-freedom of the ankle in the sagittal, frontal, and transverse anatomical planes. Numerous regression modeling techniques relating the lower extremity muscle activity to multi-directional ankle impedance were studied. The resulting models may have the potential to improve a user's control of a robotic device, including powered ankle-foot prostheses, exoskeletons, orthoses, and other medical devices.

Four experiments were performed with able-bodied subjects to characterize the ankle impedance during activities with both non-loaded and loaded ankle. Additionally, these studies explored how the ankle impedance changes as a function of the co-contraction of agonistic and antagonistic muscles and as a function of tonic contractions during stationary standing poses.

Using regression and machine learning techniques, subject-dependent models, aggregate models, and subject-independent models were generated. The subject-dependent models resulted in the highest overall performance, followed by the aggregated model. These models could accurately predict ankle impedance when presented with the muscle activation measurements. These models were tested with information from the same subjects that were used to train. This work explored the capabilities of a subject-independent model. The results of the current study suggest the mechanical impedance of the ankle can be predicted using the corresponding lower extremity muscle activity.

5.2   Challenges

There were several challenges throughout the experiments. First, the methods for processing the EMG measurements assumed that the experiments were performed while the muscles did not fatigue throughout the trials. For all experiments, the subjects were required to rest in between trials to minimize the onset of fatigue; however, it is likely that some effects of fatigue occur. In addition, the effects caused by changes in the EMG signal over time were not

explored. All experiments were performed within the same day. It is unknown how the effects of EMG measurements from different testing days would affect the model prediction performance.

Additionally, in an effort to determine a subject-independent model a diverse population is likely needed. Using experimental data from both male and female subjects, with a range of ages, athletic abilities, and body sizes could improve generalizability. The subject populations recruited for the studies presented in this paper were limited to mostly male subjects with ages between 20-35 years.

5.3   Future Work

The models created throughout this study explained the relationship between muscle co-contraction and activation during stationary conditions. The goal of future work is to expand upon these results to create models for dynamic movements and maneuvers that result in the time-varying impedance of the ankle. Additionally, exploring ways to estimate ankle impedance using real-time EMG information would be useful for implementation in prostheses controllers.

Furthermore, all subjects within this experiment were able-bodied, with no previous musculoskeletal injuries. However, it is unknown how the residual muscles of an amputee would perform using a regression model similar to the ones developed in this work. Future work can look to expand these ideas for such applications.

6 Reference List

[1]   C. L. Brockett and G. J. Chapman, "Biomechanics of the ankle," *Orthop Trauma*, vol. 30, no. 3, pp. 232–238, Jun. 2016.

[2]   K. Ziegler-Graham, E. J. MacKenzie, P. L. Ephraim, T. G. Travison, and R. Brookmeyer, "Estimating the Prevalence of Limb Loss in the United States: 2005 to 2050," *Archives of Physical Medicine and Rehabilitation*, vol. 89, no. 3, pp. 422–429, Mar. 2008.

[3]   P. Manickum, S. Ramklass, and T. Madiba, "A five-year audit of lower limb amputations below the knee and rehabilitation outcomes: the Durban experience," *Journal of Endocrinology, Metabolism and Diabetes of South Africa*, pp. 1–5, Jan. 2019.

[4]   R. S. Gailey, C. R. Clark, and I. A. Gaunaurd, "REHABILITATION OF THE DIABETIC AMPUTEE," in *Levin and O'Neal's The Diabetic Foot*, Elsevier, 2008, pp. 547–561.

[5]   "Leg Amputation - an overview | ScienceDirect Topics." [Online]. Available: https://www.sciencedirect.com/topics/medicine-and-dentistry/leg-amputation. [Accessed: 02-Apr-2019].

[6]   Timothy R Dillingham, Liliana E. Pezzin, and Ellen J. MacKenzie, "Limb amputation and limb deficiency: epidemiology and recent trends in the United States," *Southern Medical Journal*, vol. 95, no. 8, p. 875+, Aug. 2002.

[7]   Douglas G. Smith, "Congenital Limb Deficiencies and Acquired Amputations in Childhood," *Amputee Coalition inMotion*, vol. 18, no. 1, Feb-2006.

[8]   N. H. Molen, "Energy/speed relation of below-knee amputees walking on a motor-driven treadmill," *Internationale Zeitschrift fr Angewandte Physiologie Einschlielich Arbeitsphysiologie*, vol. 31, no. 3, pp. 173–185, 1973.

[9]   M. R. Tucker *et al.*, "Control strategies for active lower extremity prosthetics and orthotics: a review," *Journal of NeuroEngineering and Rehabilitation*, vol. 12, no. 1, p. 1, Jan. 2015.

[10]   J. D. Ventura, A. D. Segal, G. K. Klute, and R. R. Neptune, "Compensatory mechanisms of transtibial amputees during circular turning," *Gait & Posture*, vol. 34, no. 3, pp. 307–312, Jul. 2011.

[11]   K. Parker, E. Hanada, and J. Adderson, "Gait variability and regularity of people with transtibial amputations," *Gait & Posture*, vol. 37, no. 2, pp. 269–273, Feb. 2013.

[12] N. Vanicek, S. Strike, L. McNaughton, and R. Polman, "Gait patterns in transtibial amputee fallers vs. non-fallers: Biomechanical differences during level walking," *Gait & Posture*, vol. 29, no. 3, pp. 415–420, Apr. 2009.

[13] A. D. Segal, M. S. Orendurff, J. M. Czerniecki, J. Schoen, and G. K. Klute, "Comparison of transtibial amputee and non-amputee biomechanics during a common turning task," *Gait & Posture*, vol. 33, no. 1, pp. 41–47, Jan. 2011.

[14] M. Goldfarb, B. E. Lawson, and A. H. Shultz, "Realizing the Promise of Robotic Leg Prostheses," *Science Translational Medicine*, vol. 5, no. 210, Nov. 2013.

[15] M. H. Ebrahimzadeh and S. Hariri, "Long-Term Outcomes of Unilateral Transtibial Amputations," *Military Medicine*, vol. 174, no. 6, pp. 593–597, Jun. 2009.

[16] A. M. Grabowski and S. D'Andrea, "Effects of a powered ankle-foot prosthesis on kinetic loading of the unaffected leg during level-ground walking," *Journal of NeuroEngineering and Rehabilitation*, vol. 10, no. 1, p. 49, Jun. 2013.

[17] R. D. Bellman, M. A. Holgate, and T. G. Sugar, "SPARKy 3: Design of an active robotic ankle prosthesis with two actuated degrees of freedom using regenerative kinetics," in *2008 2nd IEEE RAS EMBS International Conference on Biomedical Robotics and Biomechatronics*, 2008, pp. 511–516.

[18] "BiOM Ankle Foot System - Infinite Technologies Prosthetics," *Infinite Technologies Orthotics and Prosthetics*. .

[19] "Elan - Carbon, Feet, Hydraulic, Sandal Toe," *Endolite USA - Lower Limb Prosthetics*. [Online]. Available: https://www.endolite.com/products/elan. [Accessed: 24-Apr-2019].

[20] "PROPRIO FOOT®." [Online]. Available: https://www.ossur.com/about-ossur/news-from-ossur/2-uncategorised/66-proprio-foot. [Accessed: 24-Apr-2019].

[21] F. Sup, A. Bohara, and M. Goldfarb, "Design and Control of a Powered Transfemoral Prosthesis," *The International Journal of Robotics Research*, vol. 27, no. 2, pp. 263–273, Feb. 2008.

[22] S. Au, M. Berniker, and H. Herr, "Powered ankle-foot prosthesis to assist level-ground and stair-descent gaits," *Neural Networks*, vol. 21, no. 4, pp. 654–666, May 2008.

[23] A. E. Ferris, J. M. Aldridge, C. A. Rábago, and J. M. Wilken, "Evaluation of a Powered Ankle-Foot Prosthetic System During Walking," *Archives of Physical Medicine and Rehabilitation*, vol. 93, no. 11, pp. 1911–1918, Nov. 2012.

91

[24] L. Fradet, M. Alimusaj, F. Braatz, and S. I. Wolf, "Biomechanical analysis of ramp ambulation of transtibial amputees with an adaptive ankle foot system," *Gait & Posture*, vol. 32, no. 2, pp. 191–198, Jun. 2010.

[25] B. E. Lawson, H. A. Varol, A. Huff, E. Erdemir, and M. Goldfarb, "Control of Stair Ascent and Descent With a Powered Transfemoral Prosthesis," *IEEE Transactions on Neural Systems and Rehabilitation Engineering*, vol. 21, no. 3, pp. 466–473, May 2013.

[26] S. K. Au, J. Weber, and H. Herr, "Powered Ankle–Foot Prosthesis Improves Walking Metabolic Economy," *IEEE Transactions on Robotics*, vol. 25, no. 1, pp. 51–66, Feb. 2009.

[27] E. M. Ficanha, M. Rastgaar, B. Moridian, and N. Mahmoudian, "Ankle angles during step turn and straight walk: Implications for the design of a steerable ankle-foot prosthetic robot," in *ASME 2013 Dynamic Systems and Control Conference*, 2013.

[28] B. C. Glaister, J. A. Schoen, M. S. Orendurff, and G. K. Klute, "Mechanical Behavior of the Human Ankle in the Transverse Plane While Turning," *IEEE Transactions on Neural Systems and Rehabilitation Engineering*, vol. 15, no. 4, pp. 552–559, Dec. 2007.

[29] B. C. Glaister, G. C. Bernatz, G. K. Klute, and M. S. Orendurff, "Video task analysis of turning during activities of daily living," *Gait & Posture*, vol. 25, no. 2, pp. 289–294, Feb. 2007.

[30] E. Ficanha, M. R. Aagaah, and K. R. Kaufman, "Cable-Driven Two Degrees-of-Freedom Ankle–Foot Prosthesis," *Journal of Medical Devices*, vol. 10, no. 3, 2016.

[31] E. M. Ficanha, G. A. Ribeiro, H. Dallali, and M. Rastgaar, "Design and Preliminary evaluation of a Two DOFs cable-Driven ankle–Foot Prosthesis with active Dorsiflexion–Plantarflexion and inversion–eversion," *Frontiers in bioengineering and biotechnology*, vol. 4, p. 36, 2016.

[32] N. M. Olson and G. K. Klute, "Design of a Transtibial Prosthesis With Active Transverse Plane Control," *Journal of Medical Devices*, vol. 9, no. 4, Aug. 2015.

[33] N. Hogan, "The mechanics of multi-joint posture and movement control," *Biol. Cybern.*, vol. 52, no. 5, pp. 315–331, Sep. 1985.

[34] Clifford R. Wheeless, III, *Wheeless' Textbook of Orthopaedics*. Durham, NC: Data Trace Internet Publishing, LLC, 2016.

[35] C. J. Nester, A. F. Findlow, P. Bowker, and P. D. Bowden, "Transverse Plane Motion at the Ankle Joint," *Foot Ankle Int.*, vol. 24, no. 2, pp. 164–168, Feb. 2003.

[36] V. Santilli *et al.*, "Peroneus Longus Muscle Activation Pattern during Gait Cycle in Athletes Affected by Functional Ankle Instability: A Surface Electromyographic Study," *Am J Sports Med*, vol. 33, no. 8, pp. 1183–1187, Aug. 2005.

[37] I. Di Giulio, C. N. Maganaris, V. Baltzopoulos, and I. D. Loram, "The proprioceptive and agonist roles of gastrocnemius, soleus and tibialis anterior muscles in maintaining human upright posture," *J Physiol*, vol. 587, no. Pt 10, pp. 2399–2416, May 2009.

[38] I. W. Hunter and R. E. Kearney, "Dynamics of human ankle stiffness: Variation with mean ankle torque," *Journal of Biomechanics*, vol. 15, no. 10, pp. 747–752, Jan. 1982.

[39] R. E. Kearney and I. W. Hunter, "Dynamics of human ankle stiffness: Variation with displacement amplitude," *Journal of Biomechanics*, vol. 15, no. 10, pp. 753–756, Jan. 1982.

[40] P. L. Weiss, R. E. Kearney, and I. W. Hunter, "Position dependence of ankle joint dynamics— I. Passive mechanics," *Journal of Biomechanics*, vol. 19, no. 9, pp. 727–735, Jan. 1986.

[41] P. L. Weiss, I. W. Hunter, and R. E. Kearney, "Human ankle joint stiffness over the full range of muscle activation levels," *Journal of Biomechanics*, vol. 21, no. 7, pp. 539–544, Jan. 1988.

[42] P. L. Weiss, R. E. Kearney, and I. W. Hunter, "Position dependence of ankle joint dynamics— II. Active mechanics," *Journal of Biomechanics*, vol. 19, no. 9, pp. 737–751, Jan. 1986.

[43] T. Sinkjaer, E. Toft, S. Andreassen, and B. C. Hornemann, "Muscle stiffness in human ankle dorsiflexors: intrinsic and reflex components," *Journal of Neurophysiology*, vol. 60, no. 3, pp. 1110–1121, Sep. 1988.

[44] R. E. Kearney, R. B. Stein, and L. Parameswaran, "Identification of intrinsic and reflex contributions to human ankle stiffness dynamics," *IEEE Transactions on Biomedical Engineering*, vol. 44, no. 6, pp. 493–504, Jun. 1997.

[45] R. E. Kearney and I. W. Hunter, "System identification of human stretch reflex dynamics: Tibialis anterior," *Exp Brain Res*, vol. 56, no. 1, pp. 40–49, Aug. 1984.

[46] R. E. Kearney and I. W. Hunter, "System identification of human triceps surae stretch reflex dynamics," *Experimental Brain Research*, vol. 51, no. 1, Jun. 1983.

[47] H. Lee, P. Ho, M. A. Rastgaar, H. I. Krebs, and N. Hogan, "Multivariable static ankle mechanical impedance with relaxed muscles," *Journal of biomechanics*, vol. 44, no. 10, pp. 1901–1908, 2011.

[48] H. Lee, P. Ho, M. Rastgaar, H. I. Krebs, and N. Hogan, "Multivariable static ankle mechanical impedance with active muscles," *IEEE Transactions on Neural Systems and Rehabilitation Engineering*, vol. 22, no. 1, pp. 44–52, 2014.

[49] H. Lee, H. I. Krebs, and N. Hogan, "Multivariable Dynamic Ankle Mechanical Impedance With Relaxed Muscles," *IEEE Transactions on Neural Systems and Rehabilitation Engineering*, vol. 22, no. 6, pp. 1104–1114, Nov. 2014.

[50] H. Lee, H. I. Krebs, and N. Hogan, "Multivariable Dynamic Ankle Mechanical Impedance With Active Muscles," *IEEE Transactions on Neural Systems and Rehabilitation Engineering*, vol. 22, no. 5, pp. 971–981, Sep. 2014.

[51] E. M. Ficanha and M. Rastgaar, "Stochastic Estimation of Human Ankle Mechanical Impedance in Lateral/Medial Rotation," presented at the ASME 2014 Dynamic Systems and Control Conference, San Antonio, Texas, USA, 2014, vol. 2.

[52] E. M. Ficanha, G. A. Ribeiro, and M. Rastgaar, "Mechanical impedance of the non-loaded lower leg with relaxed muscles in the transverse plane," *Frontiers in bioengineering and biotechnology*, vol. 3, p. 198, 2015.

[53] M. Rastgaar, H. Lee, E. Ficanha, P. Ho, H. I. Krebs, and N. Hogan, "Multi-directional dynamic mechanical impedance of the human ankle; A key to anthropomorphism in lower extremity assistive robots," in *Neuro-Robotics*, Springer, 2014, pp. 157–178.

[54] H. Lee, S. Wang, and N. Hogan, "Relationship between ankle stiffness structure and muscle activation," in *2012 Annual International Conference of the IEEE Engineering in Medicine and Biology Society*, 2012, pp. 4879–4882.

[55] D. A. Winter, A. E. Patla, F. Prince, M. Ishac, and K. Gielo-Perczak, "Stiffness Control of Balance in Quiet Standing," *Journal of Neurophysiology*, vol. 80, no. 3, pp. 1211–1221, Sep. 1998.

[56] P. G. Morasso and V. Sanguineti, "Ankle muscle stiffness alone cannot stabilize balance during quiet standing," *Journal of Neurophysiology*, vol. 88, no. 4, pp. 2157–2162, 2002.

[57] R. C. Fitzpatrick, J. L. Taylor, and D. I. McCloskey, "Ankle stiffness of standing humans in response to imperceptible perturbation: reflex and task-dependent components.," *The Journal of Physiology*, vol. 454, no. 1, pp. 533–547, 1992.

[58] H. van der Kooij, S. Donker, M. de Vrijer, and F. van der Helm, "Identification of human balance control in standing," in *Systems, Man and Cybernetics, 2004 IEEE international conference on*, 2004, vol. 3, pp. 2535–2541.

[59] H. Zhang, M. A. Nussbaum, and M. J. Agnew, "A new method to assess passive and active ankle stiffness during quiet upright stance," *Journal of Electromyography and Kinesiology*, vol. 25, no. 6, pp. 937–943, 2015.

[60] M. Casadio, P. G. Morasso, and V. Sanguineti, "Direct measurement of ankle stiffness during quiet standing: implications for control modelling and clinical application," *Gait & posture*, vol. 21, no. 4, pp. 410–424, 2005.

[61] I. D. Loram and M. Lakie, "Direct measurement of human ankle stiffness during quiet standing: the intrinsic mechanical stiffness is insufficient for stability," *The Journal of Physiology*, vol. 545, no. 3, pp. 1041–1053, 2002.

[62] I. D. Loram and M. Lakie, "Human balancing of an inverted pendulum: position control by small, ballistic-like, throw and catch movements," *The Journal of Physiology*, vol. 540, no. 3, pp. 1111–1124, 2002.

[63] I. D. Loram, C. N. Maganaris, and M. Lakie, "Paradoxical muscle movement in human standing," *The Journal of physiology*, vol. 556, no. 3, pp. 683–689, 2004.

[64] M. Vlutters, T. A. Boonstra, A. C. Schouten, and H. van der Kooij, "Direct measurement of the intrinsic ankle stiffness during standing," *Journal of biomechanics*, vol. 48, no. 7, pp. 1258–1263, 2015.

[65] T. M. Vieira, D. Farina, and I. D. Loram, "EMG and Posture in Its Narrowest Sense," *Surface Electromyography: Physiology, Engineering, and Applications*, pp. 408–439, 2016.

[66] T. E. Sakanaka, J. Gill, M. D. Lakie, and R. F. Reynolds, "Intrinsic ankle stiffness during standing increases with ankle torque and passive stretch of the Achilles tendon," *PloS one*, vol. 13, no. 3, 2018.

[67] P. Amiri and R. E. Kearney, "Ankle intrinsic stiffness changes with postural sway," *Journal of Biomechanics*, vol. 85, pp. 50–58, Mar. 2019.

[68] S. M. Zinder, K. P. Granata, D. A. Padua, and B. M. Gansneder, "Validity and reliability of a new in vivo ankle stiffness measurement device," *Journal of Biomechanics*, vol. 40, no. 2, pp. 463–467, Jan. 2007.

[69] L. Konradsen, M. Voigt, and C. Hojsgaard, "Ankle Inversion Injuries: The Role of the Dynamic Defense Mechanism," *Am J Sports Med*, vol. 25, no. 1, pp. 54–58, Jan. 1997.

[70] A. Saripalli and S. Wilson, "Dynamic Ankle Stability and Ankle Orientation," presented at the 7th Symposium Footwear Biomechanics, 2005.

[71] Y.-J. Lee, J.-N. Liang, B. Chen, M. Ganesan, and A. S. Aruin, "Standing on wedges modifies side-specific postural control in the presence of lateral external perturbations," *Journal of Electromyography and Kinesiology*, vol. 36, pp. 16–24, 2017.

[72] E. M. Ficanha, G. A. Ribeiro, and M. Rastgaar, "Design and evaluation of a 2-dof instrumented platform for estimation of the ankle mechanical impedance in the sagittal and frontal planes," *IEEE/ASME Transactions on Mechatronics*, vol. 21, no. 5, pp. 2531–2542, 2016.

[73] E. Ficanha, "Anthropomorphic robotic ankle-foot prosthesis with active dorsiflexion-plantarflexion and inversion-eversion," 2015.

[74] E. M. Ficanha, G. Ribeiro, and M. R. Aagaah, "Instrumented walkway for estimation of the ankle impedance in dorsiflexion-plantarflexion and inversion-eversion during standing and walking," in *ASME 2015 Dynamic Systems and Control Conference*, 2015.

[75] E. M. Ficanha, G. Ribeiro, and M. R. Aagaah, "Validation of an Instrumented Walkway Designed for Estimation of the Ankle Impedance in Sagittal and Frontal Planes," in *ASME 2016 Dynamic Systems and Control Conference*, 2016.

[76] G. A. Ribeiro, E. Ficanha, L. Knop, and M. Rastgaar, "Impedance of the Human Ankle During Standing for Posture Control," in *2018 Design of Medical Devices Conference*, 2018.

[77] H. Lee and N. Hogan, "Investigation of human ankle mechanical impedance during locomotion using a wearable ankle robot," in *2013 IEEE International Conference on Robotics and Automation*, 2013, pp. 2651–2656.

[78] E. J. Rouse, L. J. Hargrove, E. J. Perreault, and T. A. Kuiken, "Estimation of Human Ankle Impedance During the Stance Phase of Walking," *IEEE Transactions on Neural Systems and Rehabilitation Engineering*, vol. 22, no. 4, pp. 870–878, Jul. 2014.

[79] H. Lee, E. J. Rouse, and H. I. Krebs, "Summary of Human Ankle Mechanical Impedance During Walking," *IEEE Journal of Translational Engineering in Health and Medicine*, vol. 4, pp. 1–7, 2016.

[80] E. M. Ficanha, G. A. Ribeiro, L. Knop, and M. Rastgaar, "Time-varying human ankle impedance in the sagittal and frontal planes during stance phase of walking," in *Robotics and Automation (ICRA), 2017 IEEE International Conference on*, 2017, pp. 6658–6664.

[81] E. M. Ficanha, G. A. Ribeiro, L. Knop, and M. Rastgaar, "Time-varying impedance of the human ankle in the sagittal and frontal planes during straight walk and turning steps," in *Rehabilitation Robotics (ICORR), 2017 International Conference on*, 2017, pp. 1413–1418.

[82] A. L. Shorter and E. J. Rouse, "Mechanical Impedance of the Ankle During the Terminal Stance Phase of Walking," *IEEE Transactions on Neural Systems and Rehabilitation Engineering*, vol. 26, no. 1, pp. 135–143, Jan. 2018.

[83] E. Ficanha, G. Ribeiro, L. Knop, and M. Rastgaar, "Estimation of the Two Degrees-of-Freedom Time-Varying Impedance of the Human Ankle," *J. Med. Devices*, vol. 12, no. 1, Jan. 2018.

[84] R. Merletti and P. Parker, *Electromyography: Physiology, Engineering, and Non-Invasive Applications*. Hoboken, New Jersey: Wiley-IEEE Press, 2004.

[85] C. Disselhorst-Klug, T. Schmitz-Rode, and G. Rau, "Surface electromyography and muscle force: Limits in sEMG–force relationship and new approaches for applications," *Clinical Biomechanics*, vol. 24, no. 3, pp. 225–235, Mar. 2009.

[86] R. A. Garnett, M. J. O'Donovan, J. A. Stephens, and A. Taylor, "Motor unit organization of human medial gastrocnemius.," *The Journal of Physiology*, vol. 287, no. 1, pp. 33–43, 1979.

[87] T. Moritani and M. Muro, "Motor unit activity and surface electromyogram power spectrum during increasing force of contraction," *European Journal of Applied Physiology and Occupational Physiology*, vol. 56, no. 3, pp. 260–265, May 1987.

[88] H. S. Milner-Brown and R. B. Stein, "The relation between the surface electromyogram and muscular force.," *The Journal of Physiology*, vol. 246, no. 3, pp. 549–569, 1975.

[89] T. Moritani, M. Muro, and A. Nagata, "Intramuscular and surface electromyogram changes during muscle fatigue," *Journal of Applied Physiology*, vol. 60, no. 4, pp. 1179–1185, Apr. 1986.

[90] T. Moritani, M. Muro, A. Kijima, F. A. Gaffney, and D. Parsons, "Electromechanical changes during electrically induced and maximal voluntary contractions: Surface and intramuscular EMG responses during sustained maximal voluntary contraction," *Experimental Neurology*, vol. 88, no. 3, pp. 484–499, Jun. 1985.

[91] C. J. De Luca, "The Use of Surface Electromyography in Biomechanics," *Journal of Applied Biomechanics*, vol. 13, no. 2, pp. 135–163, May 1997.

[92] J. R. Potvin and S. H. M. Brown, "Less is more: high pass filtering, to remove up to 99% of the surface EMG signal power, improves EMG-based biceps brachii muscle force estimates," *Journal of Electromyography and Kinesiology*, vol. 14, no. 3, pp. 389–399, Jun. 2004.

[93] J. Hashemi, E. Morin, P. Mousavi, and K. Hashtrudi-Zaad, "Surface EMG force modeling with joint angle based calibration," *Journal of Electromyography and Kinesiology*, vol. 23, no. 2, pp. 416–424, Apr. 2013.

[94] K. N. An, W. P. Cooney, E. Y. Chao, L. J. Askew, and J. R. Daube, "Determination of forces in extensor pollicis longus and flexor pollicis longus of the thumb," *Journal of Applied Physiology*, vol. 54, no. 3, pp. 714–719, Mar. 1983.

[95] E. A. Clancy and N. Hogan, "Relating agonist-antagonist electromyograms to joint torque during isometric, quasi-isotonic, nonfatiguing contractions," *IEEE Transactions on Biomedical Engineering*, vol. 44, no. 10, pp. 1024–1028, Oct. 1997.

[96] J.-J. Luh, G.-C. Chang, C.-K. Cheng, J.-S. Lai, and T.-S. Kuo, "Isokinetic elbow joint torques estimation from surface EMG and joint kinematic data: using an artificial neural network model," *Journal of Electromyography and Kinesiology*, vol. 9, no. 3, pp. 173–183, Apr. 1999.

[97] E. P. Doheny, M. M. Lowery, D. P. FitzPatrick, and M. J. O'Malley, "Effect of elbow joint angle on force–EMG relationships in human elbow flexor and extensor muscles," *Journal of Electromyography and Kinesiology*, vol. 18, no. 5, pp. 760–770, Oct. 2008.

[98] E. A. Clancy, L. Liu, P. Liu, and D. V. Z. Moyer, "Identification of Constant-Posture EMG–Torque Relationship About the Elbow Using Nonlinear Dynamic Models," *IEEE Transactions on Biomedical Engineering*, vol. 59, no. 1, pp. 205–212, Jan. 2012.

[99] C. DaSalla, J. Kim, and Y. Koike, "Robot Control Using Electromyography (EMG) Signals of the Wrist," *Applied Bionics and Biomechanics*, vol. 2, no. 2, pp. 97–102, 2005.

[100] N. P. Reddy and V. Gupta, "Toward direct biocontrol using surface EMG signals: Control of finger and wrist joint models," *Medical Engineering & Physics*, vol. 29, no. 3, pp. 398–403, Apr. 2007.

[101] E. N. Kamavuako, E. J. Scheme, and K. B. Englehart, "Wrist torque estimation during simultaneous and continuously changing movements: surface vs. untargeted intramuscular EMG," *Journal of Neurophysiology*, vol. 109, no. 11, pp. 2658–2665, Mar. 2013.

[102] S. L. Kilbreath and S. C. Gandevia, "Neural and biomechanical specializations of human thumb muscles revealed by matching weights and grasping objects.," *The Journal of Physiology*, vol. 472, no. 1, pp. 537–556, Dec. 1993.

[103] W. F. Genadry, R. E. Kearney, and I. W. Hunter, "Dynamic relationship between EMG and torque at the human ankle: Variation with contraction level and modulation," *Med. Biol. Eng. Comput.*, vol. 26, no. 5, pp. 489–496, Sep. 1988.

[104] M. A. Golkar and R. E. Kearney, "Closed-loop identification of the dynamic relation between surface EMG and torque at the human ankle," *IFAC-PapersOnLine*, vol. 48, no. 28, pp. 263–268, Jan. 2015.

[105] M. M. Ardestani *et al.*, "Human lower extremity joint moment prediction: A wavelet neural network approach," *Expert Systems with Applications*, vol. 41, no. 9, pp. 4422–4433, Jul. 2014.

[106] C. Dai, S. Martel, F. Martel, D. Rancourt, and E. A. Clancy, "Single-trial estimation of quasi-static EMG-to-joint-mechanical-impedance relationship over a range of joint torques," *Journal of Electromyography and Kinesiology*, vol. 45, pp. 18–25, Apr. 2019.

[107] M. A. Golkar, E. Sobhani Tehrani, and R. E. Kearney, "Linear Parameter Varying Identification of Dynamic Joint Stiffness during Time-Varying Voluntary Contractions," *Front. Comput. Neurosci.*, vol. 11, 2017.

[108] H. Dallali, L. Knop, L. Castelino, E. Ficanha, and M. Rastgaar, "Using lower extremity muscle activity to obtain human ankle impedance in the external–internal direction," *International Journal of Intelligent Robotics and Applications*, vol. 2, no. 1, pp. 29–42, 2018.

[109] H. Dallali, L. Knop, L. Castelino, E. Ficanha, and M. Rastgaar, "Estimating the multivariable human ankle impedance in dorsi-plantarflexion and inversion-eversion directions using EMG signals and artificial neural networks," *International Journal of Intelligent Robotics and Applications*, vol. 1, no. 1, pp. 19–31, 2017.

[110] L. N. Knop, G. A. Ribeiro, E. M. Ficanha, and M. Rastgaar, "Estimating the Relationship Between Multivariable Standing Ankle Impedance and Lower Extremity Muscle Activation," in *2018 7th IEEE International Conference on Biomedical Robotics and Biomechatronics (Biorob)*, 2018, pp. 285–290.

[111] L. N. Knop, G. A. Ribeiro, and M. Rastgaar, "Towards a Generalized Model of Multivariable Ankle Impedance during Standing based on the Lower Extremity Muscle EMG," presented at the 2019 Design of Medical Devices, Minneapolis, Minnesota, USA, 2019.

[112] C. Castellini *et al.*, "Proceedings of the first workshop on Peripheral Machine Interfaces: going beyond traditional surface electromyography," *Front. Neurorobot.*, vol. 8, 2014.

[113] R. Gopura, D. S. V. Bandara, J. M. P. Gunasekara, and T. S. S. Jayawardane, "Recent trends in EMG-Based control methods for assistive robots," in *Electrodiagnosis in new frontiers of clinical research*, IntechOpen, 2013.

[114] K. Englehart and B. Hudgins, "A robust, real-time control scheme for multifunction myoelectric control," *IEEE Trans. Biomed. Eng.*, vol. 50, no. 7, pp. 848–854, Jul. 2003.

[115] F. Zhang and H. Huang, "Source Selection for Real-Time User Intent Recognition Toward Volitional Control of Artificial Legs," *IEEE Journal of Biomedical and Health Informatics*, vol. 17, no. 5, pp. 907–914, Sep. 2013.

[116] Yonghong Huang, K. B. Englehart, B. Hudgins, and A. D. C. Chan, "A Gaussian mixture model based classification scheme for myoelectric control of powered upper limb prostheses," *IEEE Transactions on Biomedical Engineering*, vol. 52, no. 11, pp. 1801–1811, Nov. 2005.

[117] G. Li, A. E. Schultz, and T. A. Kuiken, "Quantifying Pattern Recognition—Based Myoelectric Control of Multifunctional Transradial Prostheses," *IEEE Transactions on Neural Systems and Rehabilitation Engineering*, vol. 18, no. 2, pp. 185–192, Apr. 2010.

[118] D. Farina *et al.*, "The Extraction of Neural Information from the Surface EMG for the Control of Upper-Limb Prostheses: Emerging Avenues and Challenges," *IEEE Transactions on Neural Systems and Rehabilitation Engineering*, vol. 22, no. 4, pp. 797–809, Jul. 2014.

[119] P. Zhou *et al.*, "Decoding a New Neural–Machine Interface for Control of Artificial Limbs," *Journal of Neurophysiology*, vol. 98, no. 5, pp. 2974–2982, Nov. 2007.

[120] T. A. Kuiken *et al.*, "Targeted Muscle Reinnervation for Real-time Myoelectric Control of Multifunction Artificial Arms," *JAMA*, vol. 301, no. 6, pp. 619–628, Feb. 2009.

[121] H. Huang, T. A. Kuiken, and R. D. Lipschutz, "A Strategy for Identifying Locomotion Modes Using Surface Electromyography," *IEEE Transactions on Biomedical Engineering*, vol. 56, no. 1, pp. 65–73, Jan. 2009.

[122] L. Peeraer, B. Aeyels, and G. Van der Perre, "Development of EMG-based mode and intent recognition algorithms for a computer-controlled above-knee prosthesis," *Journal of Biomedical Engineering*, vol. 12, no. 3, pp. 178–182, May 1990.

[123] Dewen Jin, Ruihong Zhang, Jichuan Zhang, Rencheng Wang, and W. A. Gruver, "An intelligent above-knee prosthesis with EMG-based terrain identification," in *2000 IEEE International Conference on Systems, Man and Cybernetics.*, 2000, vol. 3, pp. 1859–1864 vol.3.

[124] G. A. Ribeiro and M. Rastgaar, "Prediction of Ground Profile for Lower-Leg Prosthesis Control Using a Visual-Inertial System," in *2018 Design of Medical Devices Conference*, 2018.

[125] L. Resnik, H. (Helen) Huang, A. Winslow, D. L. Crouch, F. Zhang, and N. Wolk, "Evaluation of EMG pattern recognition for upper limb prosthesis control: a case study in comparison with direct myoelectric control," *Journal of NeuroEngineering and Rehabilitation*, vol. 15, no. 1, p. 23, Mar. 2018.

[126] J. Wang, O. A. Kannape, and H. M. Herr, "Proportional EMG control of ankle plantar flexion in a powered transtibial prosthesis," in *2013 IEEE 13th International Conference on Rehabilitation Robotics (ICORR)*, 2013, pp. 1–5.

[127] D. P. Ferris, K. E. Gordon, G. S. Sawicki, and A. Peethambaran, "An improved powered ankle–foot orthosis using proportional myoelectric control," *Gait & Posture*, vol. 23, no. 4, pp. 425–428, Jun. 2006.

[128] S. Huang and H. Huang, "Voluntary Control of Residual Antagonistic Muscles in Transtibial Amputees: Reciprocal Activation, Coactivation, and Implications for Direct Neural Control of Powered Lower Limb Prostheses," *IEEE Transactions on Neural Systems and Rehabilitation Engineering*, vol. 27, no. 1, pp. 85–95, Jan. 2019.

[129] D. L. Crouch and H. Huang, "Lumped-parameter electromyogram-driven musculoskeletal hand model: A potential platform for real-time prosthesis control," *Journal of Biomechanics*, vol. 49, no. 16, pp. 3901–3907, Dec. 2016.

[130] L. H. Smith, T. A. Kuiken, and L. J. Hargrove, "Linear regression using intramuscular EMG for simultaneous myoelectric control of a wrist and hand system," in *2015 7th International IEEE/EMBS Conference on Neural Engineering (NER)*, 2015, pp. 619–622.

[131] L. H. Smith, T. A. Kuiken, and L. J. Hargrove, "Use of probabilistic weights to enhance linear regression myoelectric control," *J. Neural Eng.*, vol. 12, no. 6, Dec. 2015.

[132] L. H. Smith, T. A. Kuiken, and L. J. Hargrove, "Evaluation of Linear Regression Simultaneous Myoelectric Control Using Intramuscular EMG," *IEEE Transactions on Biomedical Engineering*, vol. 63, no. 4, pp. 737–746, Apr. 2016.

[133] A. Roy *et al.*, "Robot-Aided Neurorehabilitation: A Novel Robot for Ankle Rehabilitation," *IEEE Transactions on Robotics*, vol. 25, no. 3, pp. 569–582, Jun. 2009.

[134] J. J. Palazzolo, "Robotic technology to aid and assess recovery and learning in stroke patients," Thesis, Massachusetts Institute of Technology, 2005.

[135] C. M. Bishop, *Pattern recognition and machine learning*. New York: Springer, 2006.

[136] L. Pan, D. L. Crouch, and H. Huang, "Myoelectric Control Based on a Generic Musculoskeletal Model: Toward a Multi-User Neural-Machine Interface," *IEEE Transactions on Neural Systems and Rehabilitation Engineering*, vol. 26, no. 7, pp. 1435–1442, Jul. 2018.

[137] G. A. Ribeiro, L. N. Knop, and M. Rastgaar, "Correlation Between Ankle Impedance and EMG Signals," in *International Conference on NeuroRehabilitation*, 2018, pp. 627–631.

[138] C. J. De Luca, "Surface Electromyography: Detection and Recording," *Delsys Incorporated*, vol. 10, p. 2011, 2002.

[139] C. R. Winby, P. Gerus, T. B. Kirk, and D. G. Lloyd, "Correlation between EMG-based co-activation measures and medial and lateral compartment loads of the knee during gait," *Clinical Biomechanics*, vol. 28, no. 9, pp. 1014–1019, Nov. 2013.

[140] B. Hudgins, P. Parker, and R. N. Scott, "A new strategy for multifunction myoelectric control," *IEEE Transactions on Biomedical Engineering*, vol. 40, no. 1, pp. 82–94, Jan. 1993.

[141] M. Zardoshti-Kermani, B. C. Wheeler, K. Badie, and R. M. Hashemi, "EMG feature evaluation for movement control of upper extremity prostheses," *IEEE Transactions on Rehabilitation Engineering*, vol. 3, no. 4, pp. 324–333, Dec. 1995.

[142] D. Tkach, H. Huang, and T. A. Kuiken, "Study of stability of time-domain features for electromyographic pattern recognition," p. 13, 2010.

[143] H. Lee and N. Hogan, "Time-Varying Ankle Mechanical Impedance During Human Locomotion," *IEEE Transactions on Neural Systems and Rehabilitation Engineering*, vol. 23, no. 5, pp. 755–764, Sep. 2015.

[144] A. Schmitz, A. Silder, B. Heiderscheit, J. Mahoney, and D. G. Thelen, "Differences in lower-extremity muscular activation during walking between healthy older and young adults," *Journal of Electromyography and Kinesiology*, vol. 19, no. 6, pp. 1085–1091, Dec. 2009.